POLYTECHNIC UNIVERSITY OF TURIN

Degree course in Mechatronic Engineering

Master of Science Thesis

GaN-Based Half-Bridge Converter Assessment for Capacitive Wireless Power Transfer System

Advisor:

Prof. Solimene Luigi

Prof. Musumeci Salvatore

Candidate:

Zannella Amedeo Giovanni

Academic Year 2024/2025

Turin

Summary

This thesis work focused on the design, implementation, and evaluation of a Capacitive Wireless Power Transfer (CPT) system, with the specific goal of realizing an innovative charging device. The project is situated within the broader context of the evolution of Wireless Power Transfer (WPT), recognizing CPT as a promising and versatile solution capable of overcoming the intrinsic limitations of traditional wired charging.

The research journey began with a theoretical exploration of into the fundamental principles of WPT. The different types of wireless technologies are analyzed (near-field and far-field, with a particular focus on Inductive Power Transfer - IPT and Capacitive Power Transfer - CPT) and their applications. Specific attention was dedicated to the structure of CPT systems, examining in detail the essential functional blocks such as inverters, rectifiers, compensation circuits, and for CPT, capacitive couplers. This initial phase provided the necessary conceptual foundations for subsequent design.

The core of the practical work involved the conceptualization and design of a CPT-based charging solution. A process was undertaken that included:

- **Analytical Calculations:** Theoretical calculations were performed to define the optimal system parameters. These calculations specifically concerned:

    o The determination of capacitive coupling elements, fundamental for power transmission through the electric field.

    o The definition of the circuit's resonant frequencies, crucial for maximizing power transfer efficiency.

    o The quantification of power transfer capabilities in relation to different system parameters. These preliminary calculations were essential for establishing design specifications and for guiding subsequent choices.

- **Power Converter Selection and Design:** Based on the analytical calculations, an half-bridge converter was selected and designed. The choice of this topology was dictated by its proven effectiveness in high-frequency power conversion applications. To optimize performance, the decision was made to employ semiconductor technology based on Gallium Nitride (GaN). Although the thesis focuses on the design work, the choice of GaN was motivated by its intrinsic high-speed switching capabilities, reduced parasitic capacitances, and the absence of the body diode reverse recovery issue, which allow for higher efficiencies and reduced dead times – critical factors for high-frequency CPT system operation. The design process included optimizing switching timings and managing dead times to maximize the overall converter efficiency.

- **Simulation and Validation:** Once the detailed design phase was completed, simulations of the proposed CPT system were conducted. These simulations were fundamental for:

    o Validating the theoretical calculations performed previously.

    o Evaluating the key operational performance of the system, including:

        ▪ The power transfer efficiency as a function of different coupling distances.

        ▪ The analysis of critical voltage and current waveforms within the resonant circuit, to identify any peaks or anomalies.

        ▪ The quantification of power losses and the verification of the overall system stability under different operating conditions.

    o A crucial aspect of the simulations was also the selection of commercial components that could be practically implemented in a future prototype, guiding the choice of components with appropriate specifications.

The results obtained from these simulations demonstrated the high efficiency and performance achieved through the design. They provided a clear validation of the calculated parameters and designed components, highlighting the practical feasibility and robust operation of the analyzed CPT charging device.

Contents

Chapter I

Introduction

1.1 Wireless Power Transfer

In recent years, the growing interest in Wireless Power Transfer (WPT) systems has spurred the development of innovative technologies with applications ranging from consumer electronics to electric vehicles. Wireless Power Transmission (WPT), or wireless energy transmission, represents a significant step forward in the energy distribution sector.

This technology enables the transmission of energy from a power source to an electrical load without the use of cables, thereby overcoming the limitations of traditional wired systems.

The first research on wireless energy transmission dates back to the late 19th century, thanks to Nikola Tesla, one of the greatest innovators of the modern era. Tesla was among the pioneers in seeking to develop a system capable of transmitting electrical energy wirelessly, using the Earth and the atmosphere as conductors. His experiments paved the way for modern WPT, despite being limited by the technologies available at the time.

His visionary and futuristic ideas, though never fully realized, contributed to laying the groundwork for the progress of technologies, experiments, and the implementation of current systems developed for WPT. [1]

In general, a wireless power system consists of a transmitter that transmits energy towards a receiver designed to receive it. Energy is therefore transferred wirelessly through various technologies (induction, laser, radio waves, microwaves, etc.). Unlike traditional methods that rely on a flow of electrons within a metallic conductor, WPT utilizes electromagnetic fields to transfer energy through space.
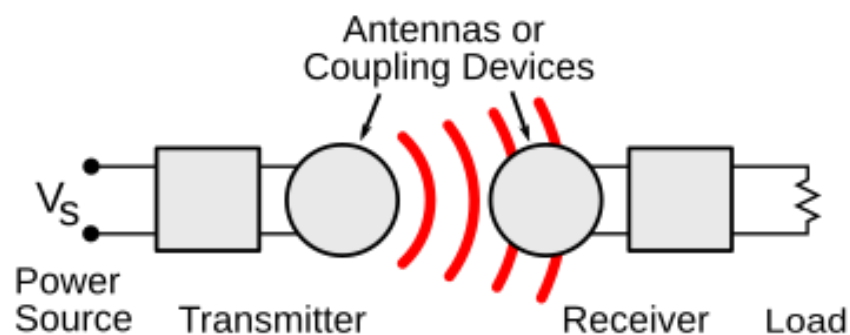

Figure 1: Basic scheme of wireless power transmission

Based on the range of action and the specific application, two charging modes are distinguished:

- **Short-range charging:** Commonly used for charging devices such as smartphones, smartwatches, and electric vehicles, it relies on electromagnetic induction, similar to that used in wireless chargers.
- **Long-range transmission:** This technology, still under development, aims to transmit energy over greater distances, using radio waves, microwaves, or laser beams.

1.2 Applications of Wireless Power Transfer

The WPT, thanks to its adaptability, finds application in different fields including:

Automotive

This offers the possibility of charging electric vehicles, both **statically** and **dynamically**, optimizing charging operations (e.g., for scooter sharing services).

Figure 2: WPT for charging vehicle

Aerospace

This enables the charging of lunar robots, collecting solar light in space and converting it into electrical energy for transmission to Earth.
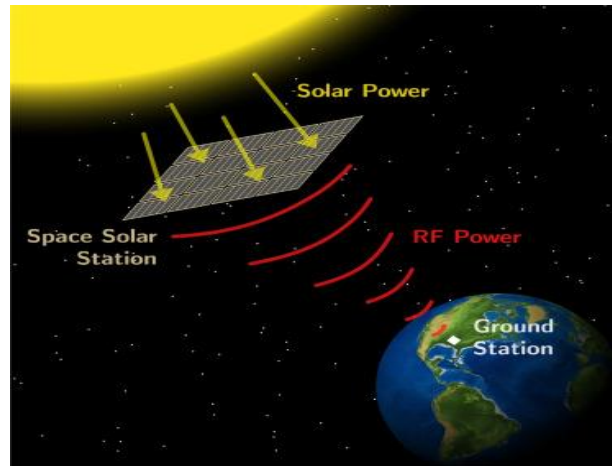

Figure 3: WPT aerospace transmission

Distribution

This ensures the transmission of energy to remote and hard-to-reach areas that are difficult to connect with cables.

Industry

This allows for the autonomous charging of robots and IoT sensors, reducing downtime and maintenance costs, and optimizing workspace management.

Smart Home

This enables the simultaneous charging of multiple devices and home appliances.

Figure 4: WPT for home wireless transmission

Medical

This enables the charging of biosensors and implanted devices, allowing for patient data collection without the need for surgical intervention. [2]
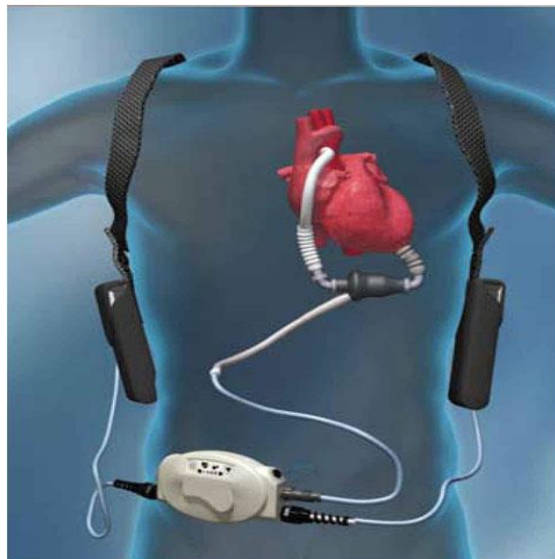

Figure 5: WPT for intrabody transmission

Wireless Power Transmission represents one of the most promising technologies for the near future, with the potential to revolutionize how we power electronic devices and electric vehicles. Research in this field could pave the way for a future where energy is distributed more efficiently and without the limitations imposed by cables in terms of cost, energy loss, and environmental impact. Challenges remain, but the opportunities far outweigh the obstacles.

1.3 Thesis objective

This thesis aims to design a capacitive wireless power transmission system, by analyzing and evaluating the performance of GaN-based half-bridge converters, using an approach that combines theoretical modeling, numerical simulations, and experimental validation.

Specifically, the following aspects will be addressed:

- Design of compensation networks to maximize energy efficiency
- Analysis of results with respect to power conversion and transfer
- Determination of the real components and comparison of the results with the theoretical study

Chapter 2

Structure of Wireless Power Transfer

2.1 Far-field and Near-field Power Transfer

As already introduced, Wireless Power Transmission (WPT) is a process that enables the wireless transfer of electrical energy from a source to a receiver device. This technology is currently under development and study, but it is already widely used for transmitting energy to small devices such as smartphones and smartwatches, or for charging electric vehicles.

Considering the latter aspect, it's worth noting that in some parts of the world, road sections are emerging that allow cars to charge directly while in motion. An exemplary experiment took place in Detroit, where the first wireless electric road in the United States was launched. The section is approximately 400 meters long, where the technology utilizes inductive charging coils that allow vehicles equipped with a receiver to charge their batteries while driving or parked [5].

Now, let's focus on the fundamental principles underlying this technology.

Wireless power transmission is typically divided into two categories based on the method of energy transfer: Far-field transmission and Near-field transmission.

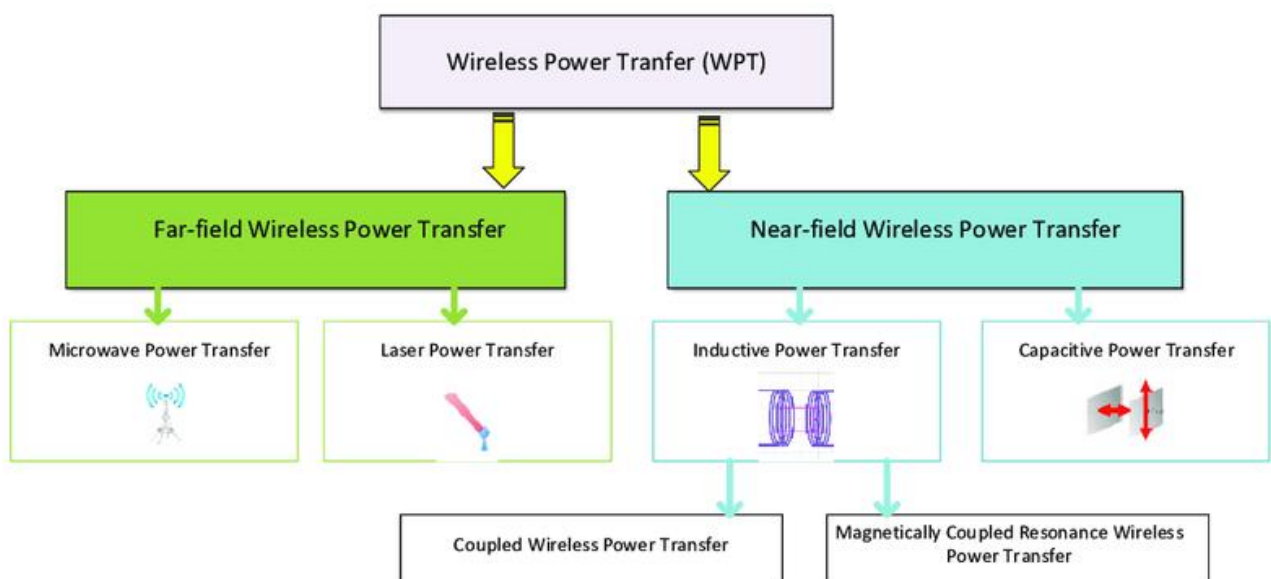A detailed classification is presented in the following Figure.

Figure 6 : WPT Classification

Regarding Far-field transmission, this method utilizes an electromagnetic wave in the form of a radio frequency signal. The transmitter radiates energy using the electric field generated by the wave, and specifically, this can be transported via microwaves or lasers.

In the first case, the operating principle of this solution is based on using microwave devices to radiate a signal as a radio wave, in the frequency range of 300 MHz to 300 GHz, through an appropriate antenna. At the receiver, which is also an antenna, the energy stored in the wave's electric field is transferred to the load. A significant advantage of this type of transmission is the high transmitted power (from tens to hundreds of Watts depending on the application), excellent environmental adaptability, and great flexibility in transmitting and receiving signals. Due to these factors, this type of energy transmission is used when there is a need to power devices located over long distances from each other and operating in various weather conditions. However, a significant limitation in the use of this technology is the very low transmission efficiency, which does not exceed 10%, and the necessity of using very large transmitters (antennas).

To compensate for this disadvantage, greater attention is being paid to energy transmission via a laser beam. This method uses highly concentrated laser light directed at the energy receiver to achieve the maximum possible transmission efficiency over very long distances. The new wireless laser charging system consists of a transmitter and a receiver. The former can be placed in a room, while the latter can be integrated into electronic devices. When the transmitter and receiver are in line of sight, a laser cavity forms between them in the air, or free space, allowing light energy to be transmitted. The transmitter is an optical power source that uses a fiber amplifier doped with a rare earth element, erbium, and produces an infrared light beam with a central wavelength of 1550 nm. The receiving unit includes a retroreflector (a passive optical system), a photovoltaic cell that converts the optical signal into electrical energy, and an LED that lights up when power is delivered. This small receiver, currently measuring 1 cm x 1 cm, could be easily integrated into devices and sensors [6].

A negative aspect of long-range transmission that should not be underestimated concerns the safeguarding of people exposed to microwaves in the surrounding environment, potentially violating the limits of human-tolerable radiofrequency (**RF**) exposure. The following Figure shows the Maximum Permissible Exposure (**MPE**) levels specified in the **IEEE C95.1-2005 standard** [7]. It should be noted that the MPE level from 2 to 100 GHz is 10 W/m², which translates into rather large antennas even for modest power reception. This MPE level is also more stringent than the previous level in the 1999 edition, which specified 100 W/m² at 15 GHz and above.
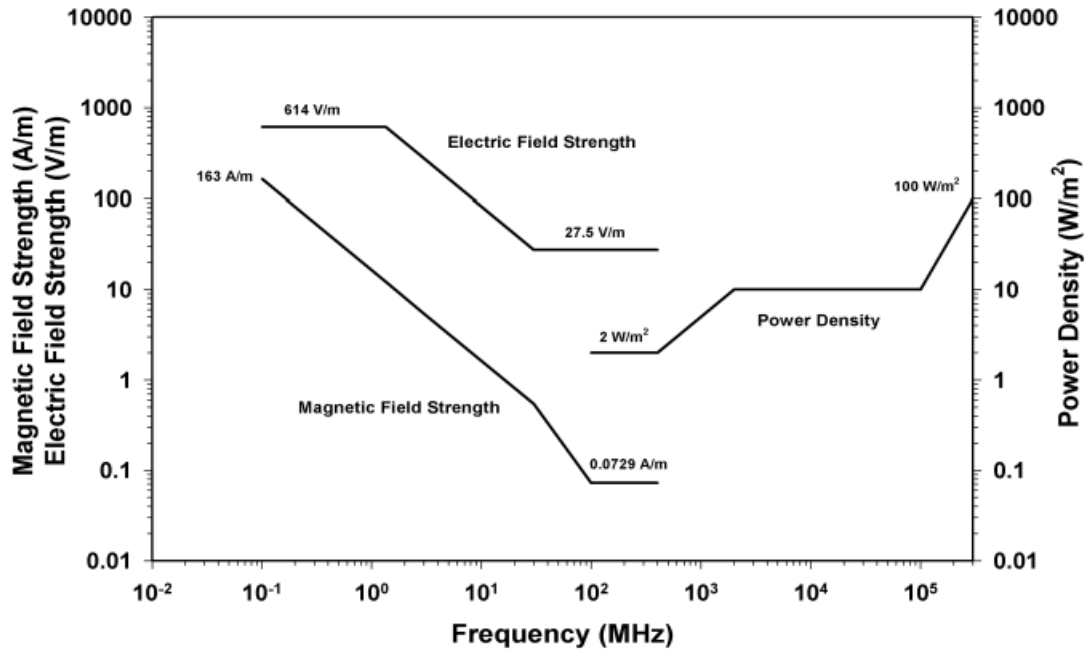
Figure 7 : Safety limits for wave in WTP

Conversely, for moderate power requirements (from a few Watts to hundreds of Watts) and potential distances (from 0 to a few meters), a short-range wireless system operating below 100 MHz achieves higher efficiency with a less stringent RF exposure limit. The distances involved in this case are significantly reduced.

2.2 Inductive Power Transfer

Power can be transferred via a magnetic field or an electric field.

In the first case, we speak of inductive power transmission (**IPT**), while in the second, it is capacitive power transmission (**CPT**).

Regarding wireless transmission via a magnetic field, both the transmitter and receiver are composed of two coils. The operating principle is that of an air-core transformer, albeit with lower coupling, as indicated in the following Figure.
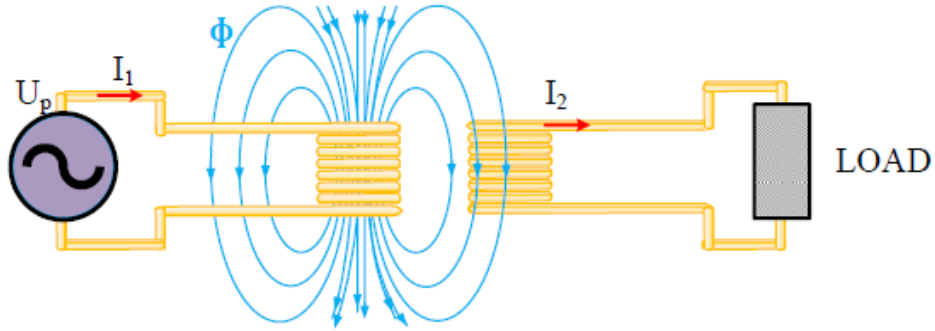
8

Figure 8 : Inductive Power Transfer scheme

By applying an alternating voltage Up with amplitude U0 [V~] and frequency F [Hz] to the primary coil N1 (where N is the number of turns in the primary winding) of the transformer, a current intensity I [A] will flow through it, capable of generating a time-varying magnetic field Φ [T]. Thanks to the phenomenon of electromagnetic induction, a current and an electromotive force (f.e.m.) [V] will be induced in the secondary coil N2. The magnetic field flux is calculated as:

$$\phi = B \cdot S \tag{1}$$

where the magnetic induction lines B are considered perpendicular to the surface S traversed by the magnetic flux, and the magnetic field is homogeneous. In accordance with Faraday's law, the value of the induced electromotive force E is equal to the product of the number of turns of the secondary winding and the derivative of the magnetic flux with respect to time.

$$F.e.m. = -N_2 \cdot \frac{d\phi}{dt} = -N_2 \cdot S \cdot \frac{dB}{dt} \tag{2}$$

Assuming that losses in the windings are negligible, it is also possible to assume that the voltages across windings N1 and N2 are equal to the electromotive forces. Therefore, the effective voltage values can be calculated as :

$$U_{rms} = k \cdot \pi \cdot \sqrt{2} \cdot f \cdot N \cdot B_m \cdot S \qquad (3)$$

where the voltage value is expressed as the RMS (Root Mean Square) value, k represents the coupling coefficient, and Bm is the amplitude of the magnetic flux density.

The transmitted power can be expressed as follows:

$$P_{out} = V_1 \cdot I_1 \cdot k^2 \cdot Q_2 \qquad (4)$$

In this configuration, power transfer can be seen as the apparent input power (VA) multiplied by the square of the magnetic coupling coefficient (k2) and by the electrical quality factor (Q2) of the secondary circuit, which is the load.

It's important to note that power transfer does not directly depend on the angular frequency (ω), as ω is already accounted for in the voltage applied to the primary winding input (N1). It is therefore possible to increase the transferred power by increasing the product of the number of turns and the current (N·I) or the frequency at the primary, staying within the Volt-Ampere (VA) limits; otherwise, a compensation circuit is needed, which will be discussed in the section on Capacitive Power Transfer [8].

The operating frequency range for this solution is in the Kilohertz order, while typical distances between transmitter and receiver do not exceed 40 mm. Transmitted powers range from a few Watts to a few Kilowatts.

It has been demonstrated that as the distance between the transmitter and receiver increases from 20 to 100 mm, the inductive coupling value reduces from 0.6 to 0.1, as shown in Figure 9, while the transmission efficiency drops from 80% to 40%, as shown in the Figure 10.
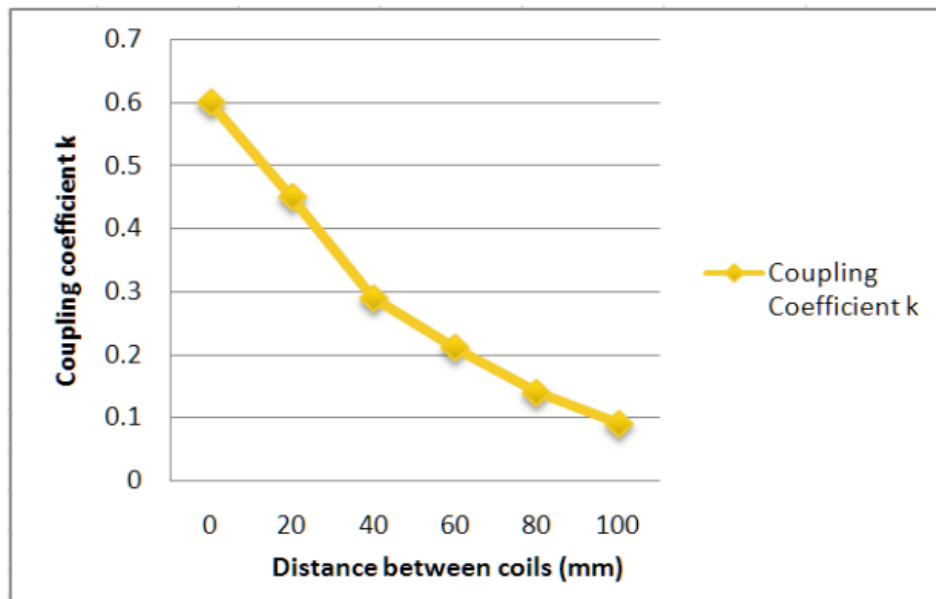
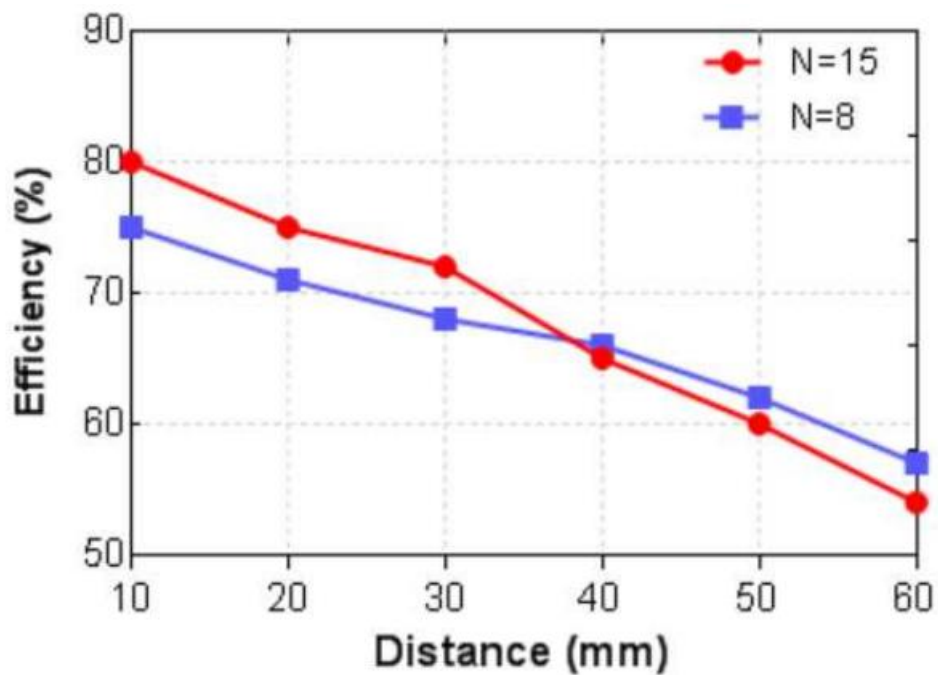Figure 9 : variation of the coupling coefficient as the distance varies

Figure 10 : variation of efficiency as the distance varies, with N being
the number of turns in the winding.

As can be observed in Figure 10, efficiency is directly proportional to the number of windings and inversely proportional to the distance between the two coils. The shape of the coils is also of fundamental importance for power transfer. This is because different shapes generate different fluxes and magnetic fields, and if these are not stable, the correct energy transfer would not be achieved. Some studies have shown that a planar spiral coil without any core has better coupling efficiency compared to a rounded winding, and even possesses lower resistance. A rectangular planar spiral coil, as shown in Figure 11, has been implemented for an electric car battery charging system due to its tolerance to misalignments [9]. This latter aspect is also relevant in the design of a wireless inductive system, as a limitation in equipment efficiency is its strong sensitivity to misalignments between the transmitter and receiver coils. Maximum coupling is indeed achieved with perfect coil alignment.
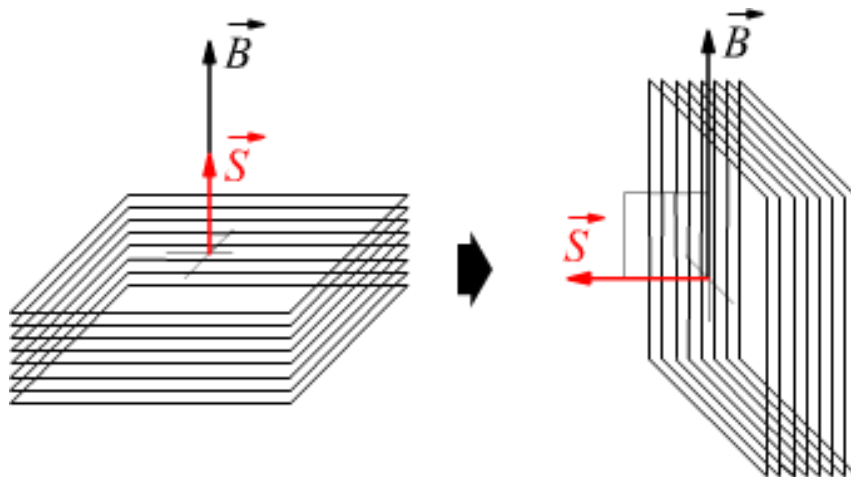

Figure 11 : Rectangular coil with planar spiral

2.3 Capacitive Power Transfer

The last block of Figure 6 shows how wireless power transfer can also be achieved through capacitive coupling.
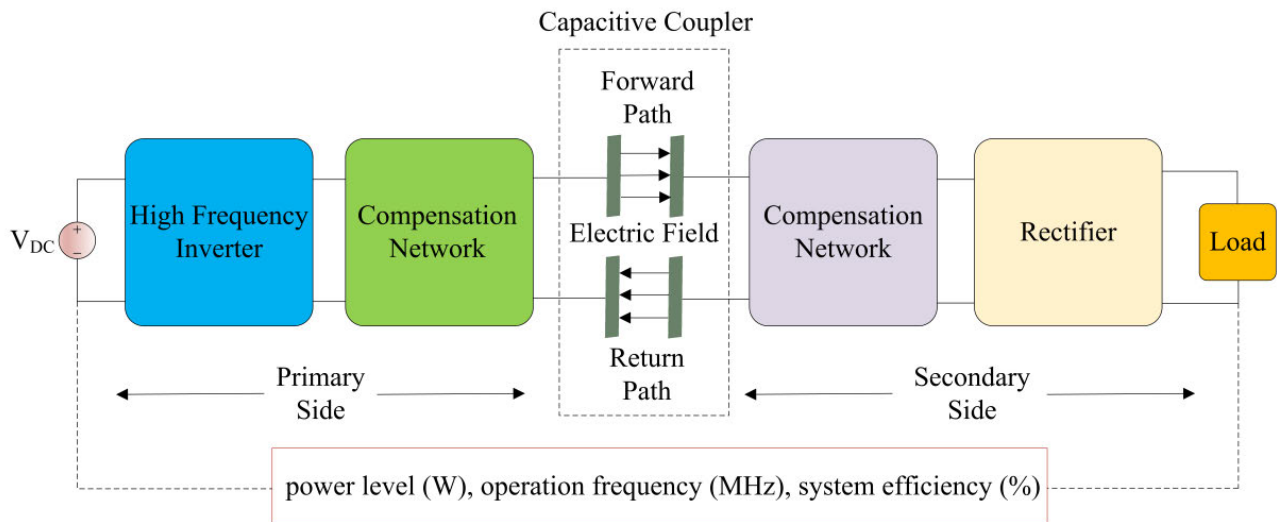
The basic scheme of the system is as follows:

Figure 12 : Capacitive Power Transfer scheme

Capacitive Wireless Power Transfer (CWPT) has established itself as a promising technology due to several advantages, including lower electromagnetic interference (EMI) emissions compared to inductive transfer systems.

This aspect is particularly relevant in applications requiring high electromagnetic compatibility (EMC), such as medical devices or power supply systems for sensitive electronics. Unlike IPT systems, which generate strong magnetic fields potentially harmful to other nearby electronic devices, CWPT uses electric fields confined between metallic plates, significantly reducing radiated interference and improving compatibility with EMC standards.

A further advantage of CWPT is its greater tolerance to misalignments between the transmitter and receiver compared to its inductive counterpart.

In CWPT systems, the capacitive coupling between the transmitting and receiving plates is less affected by variations in their relative position, allowing for greater flexibility in device placement and a more versatile design for mobile or time-varying applications [3].

However, this methodology presents some inherent limitations, such as low coupling capacitance, high voltage stress on the metallic plates, and reduced efficiency at high frequencies. These aspects necessitate careful design and the adoption of advanced solutions to improve system performance.

The operating principle of CWPT is based on the use of alternating electric fields to transfer energy across a capacitive interface, typically consisting of metallic plates. The system is divided into two main sections: primary and secondary.

The primary section includes a high-frequency inverter (in the MHz range) and a compensation network, while the secondary section includes a second compensation network, a rectifier, and the load.

Capacitive coupling, a fundamental element of the system, is achieved through a four-plate structure, a design choice that favors energy transfer and reduces equipment size. Due to the limited size of the metallic plates and the low permittivity of air, coupling capacitances tend to have a very low value, leading to a large coupling impedance. Therefore, the latter is generally much greater than the load impedance. For this reason, compensation networks are implemented, designed to increase the voltage across the capacitive coupling on the primary side and to reduce it on the secondary side. Thanks to this aspect, compensation provides greater power transfer and efficiency.

Another fundamental aspect for CWPT is the need to operate at high switching frequencies for conversion, with the aim of achieving better power transmission efficiency.

The integration of GaN devices with advanced compensation networks, such as LCL and CLLC configurations, allows for a reduction in energy losses, voltage ripple, and stress on passive components.

This approach helps to overcome the main challenges of CWPT, such as managing high switching frequencies, reducing the size of magnetic components, and improving the system's thermal behavior.

2.3.1 Inverter and Rectifier

Let's now analyze the various parts of the system in detail, starting with the conversion section. The first conversion takes place on the primary side, which, for a charging circuit, we will call the transmitter side. High-frequency power converters are essential parts of a CPT system, designed to convert a low-frequency or direct current (DC) input into a high-frequency source on the transmitting side, and vice versa on the receiving side. High-frequency inverters are divided into two categories: Full-bridge and Half-bridge. In the former case, the inverter is composed of four identical MOSFETs (M1, M2, M3, M4), controlled by voltages $V_{c1}, V_{c2}, V_{c3}, V_{c4}$ respectively, as shown in the schematic represented in the Figure.
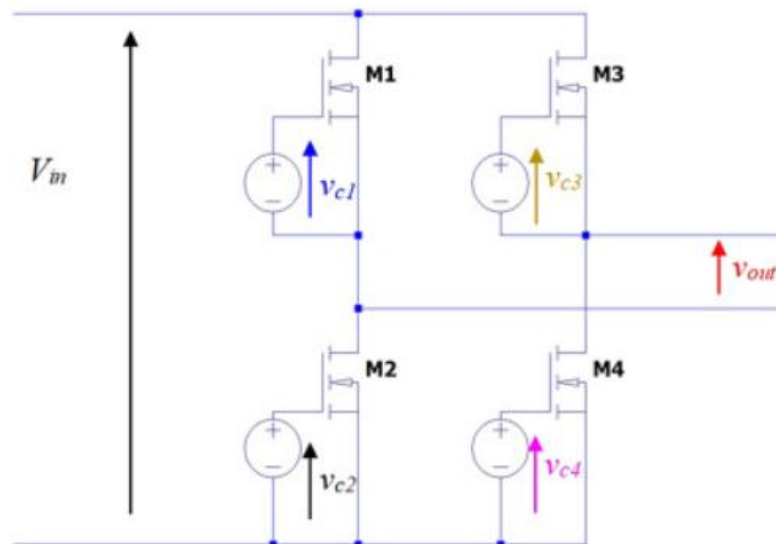
Figure 13 : Inverter Full-Bridge

V_{in} is the input voltage of the inverter, while the output presents a square alternating voltage V_{out} with period $T = 1/F_0$ [s], where F_0 is the operating frequency of the WPT system.

The conversion is performed by the opening and closing of the MOSFETs, which behave like switches, controlled by the drain-source voltages. When the control signal is high, the MOSFET acts as a closed switch, whereas when the signal is low, it acts as an open switch.

A wireless transmission system using a full-bridge inverter configuration can achieve a transmitted power on the order of 2.50 kW with an efficiency of 89% for a distance of 150 mm between the capacitor plates.

On the other hand, a voltage half-bridge converter is structurally equivalent to a full-bridge but uses only two MOSFETs, with the other two replaced by a capacitance or inductance. Compared to the full-bridge where the four MOSFETs were arranged in two parallel pairs, in the half-bridge, only two are in series, as shown in the following Figure.
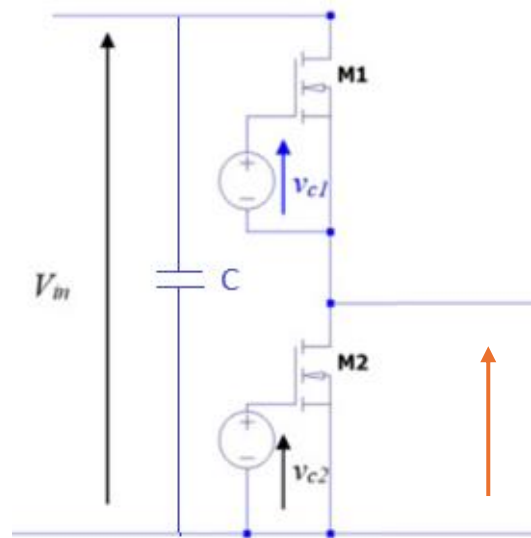

Figure 14 : Inverter Half-Bridge

The MOSFETs are still driven by the two voltages and provide an output voltage that is also square-shaped. To obtain an alternating output with a specific frequency, the two MOSFETs are triggered alternately to ensure the output current and voltage flow first in one direction and then in the other [10].

Being a simpler configuration, it benefits from easier management of the switching pulses for the MOSFETs compared to the full-bridge, although its use is limited to conversion for lower powers. Indeed, for wireless transmission, maximum powers typically reach only a few hundred Watts with an efficiency of 88%.

To maintain this simplified configuration while increasing transmission efficiency, silicon semiconductor devices, such as the previously mentioned MOSFETs, have been replaced over the years by semiconductor devices with a larger band gap between the conduction and valence bands, known as Wide-Bandgap (WBG) devices.

With these devices, the band gap shifts from 0.7-1.5 electron Volt (eV) to values exceeding 2 eV. Furthermore, the material from which they are made changes, with Gallium Nitride (GaN) transistors being of particular interest. Thanks to their high switching speed (MHz-GHz) and superior thermal management, they allow for lower conversion losses and reduced use of dissipation components, thereby improving performance in terms of power density [11].

These aspects make WBG-based conversion systems compact, robust, and efficient, with lower conversion losses, finding wide application in high-frequency, high-voltage, and high-power contexts, such as hybrid or electric vehicles, or in powering electric motors.

In the second part of our wireless transmission system, the conversion performed is from an alternating current (AC) signal to a direct current (DC) signal. The circuits designed for this conversion are rectifier circuits. These also play an equally important role in wireless systems to deliver voltage to the load. Similar to inverters, rectifiers can also be configured as Full-bridge or Half-bridge.

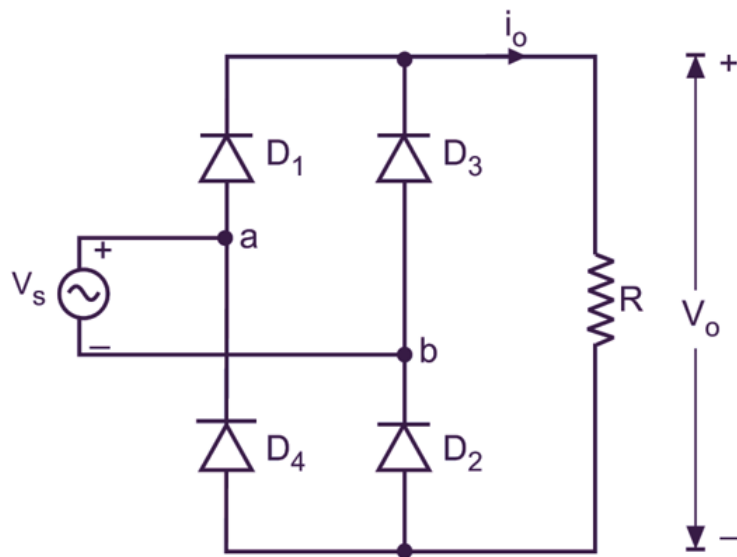The first configuration is shown in the following Figure.

Figure 15: Full-bridge rectifier

During normal operation, two diodes are in the ON mode and two in the OFF mode, ensuring that only the positive half-wave of the alternating input signal is output. The same happens for the negative half-wave by switching the conduction of the diodes. We note how the rectifier uses passive components like diodes for power conversion. Although this presents a limitation for high-frequency operation due to the capacitive effect of the diodes, which creates resonance issues, it makes its application less complex. Furthermore, this full-bridge configuration supports power transfers for both small and larger coupling distances.

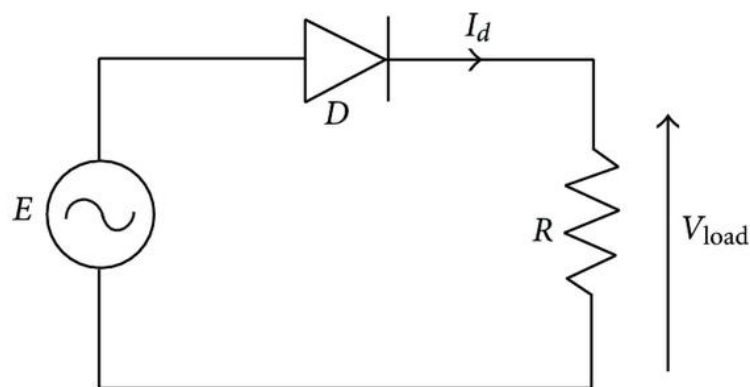Another rectifier topology is the half-bridge, as shown in the Figure.

Figure 16: Half-bridge rectifier

Unlike the full-bridge, the half-bridge rectifier utilizes the conduction of only one diode. During the positive half-wave of the alternating signal, the diode is ON, transferring the signal to the output. For the negative half-wave, however, the diode remains OFF, delivering no voltage to the load. Although the half-bridge rectifier requires fewer components and has lower power losses than the full-bridge, it presents an output voltage that is half that of the full-bridge, which can limit its high-power applications.

 Another delicate aspect is a higher output ripple, which may require larger smoothing filters compared to the full-bridge. The choice between one configuration and the other depends on the design specifications and the application to be realized. Nevertheless, the full-bridge rectifier generally offers greater reliability in terms of transmitted power, output voltage, and efficiency, at the expense of greater complexity and cost.

2.3.2 Compensation Circuit

Let's now focus our attention on a fundamental part of the CWPT system: the compensation section, present on both the transmitter and receiver sides. Depending on the type of compensation, the system's power, efficiency, and frequency-varying behavior change. A good compensation circuit should indeed be able to apply optimal voltage values to the capacitor's metallic plates for proper power transfer, achieve a high coupling coefficient (Kc), and a suitable load ratio (α) to maximize efficiency. Compensation circuits are divided into two types: resonant and non-resonant. The former are used with high-frequency power converters or the previously mentioned full-bridge inverters, utilizing auxiliary components such as inductors and capacitors. Non-resonant circuits are achieved through pulse-width modulation (PWM) converters.

Power transmission in a CWPT circuit is made possible by the capacitive coupling of two plates, one on the transmitter side and one on the receiver side, thus creating a separation. When connected to an AC source, the capacitor's reactance decreases as the frequency increases. At a certain frequency, the capacitive reactance equals that of the equivalent series inductance, causing the capacitor to behave resistively. This frequency is known as self-resonance and is in the order of a few MHzTo achieve resonance at much lower frequencies, a compensation network is connected to the capacitive interface.

Operating at such high frequencies, converter efficiency is usually low due to switching losses. In the case of inverters, we refer to hard-switching, with losses that vary with the square of the input voltage. To overcome this phenomenon, the CWPT system is made resonant; the compensation circuit creates a resonance with the capacitive interface at a frequency lower than the self-resonant frequency. This leads to the advantage that the inverter can perform zero-voltage switching (ZVS), meaning there is no voltage drop across the switches.

When it comes to CWPT systems, there are various factors and systems to consider when discussing compensation. The most common ones are analyzed below.

Series Inductance Compensation

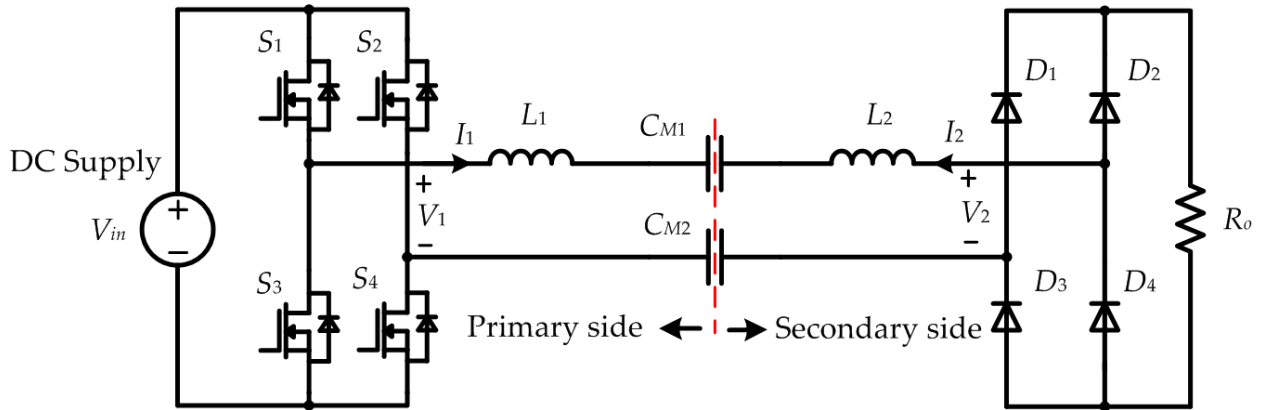This is the simplest form of compensation and is shown in the following Figure.

Figure 17: CWPT circuit with inductive compensation only

In Figure 17, the two inductors, L1 and L2, are used on both the primary and secondary sides to compensate for the two capacitances CM1 and CM2. Their value determines the resonant frequency and, consequently, the value of the inductors. Typically, to reduce the inductance size, the switching frequency is very high. In practical applications, to reduce secondary-side complexity, the two inductors can be combined into one and placed on the primary side. Furthermore, to increase the system's power level, the full-bridge inverter can be upgraded to a three-phase inverter, requiring the addition of an extra inductor for the third output.

The advantage of this compensation is its simplicity and its applicability for both high and low power systems. On the other hand, particular attention must be paid to the size of the inductance and its sensitivity to parameter variations. Especially in scenarios involving long distances and high powers, the inductors must be sufficiently large to ensure resonance.

LC Compensation

The main challenge of capacitive power transfer arises from the conflict between the relatively small coupling capacitance and the system's power requirements. Therefore, to increase the equivalent coupling capacitance, it is possible to insert capacitances in parallel, resulting in a double-sided LC compensation circuit as shown in the Figure.
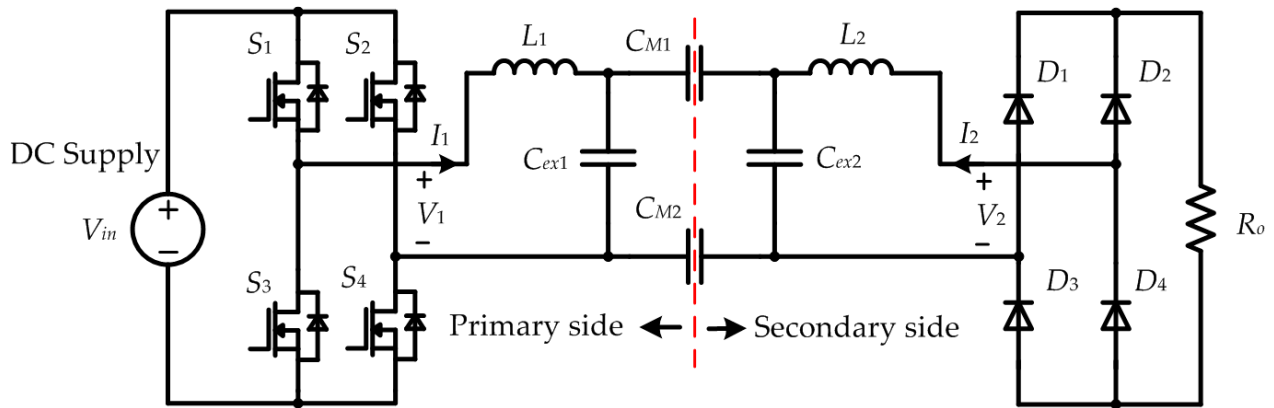
Figure 18: CWPT circuit with LC compensation

In the figure, the parallel capacitances C_{ex1} and C_{ex2} have a higher value than the coupling capacitances C_{M1} and C_{M2} for power transmission, dominating the equivalent capacitance of the network. The inductances L_1 and L_2 create resonance with the aforementioned capacitances in the primary and secondary circuits. In this case, since the capacitive value of the circuit has increased, the inductive value is lower.

The coupling coefficient and the resonant frequency are given by the following equations, respectively:

$$k_c = \frac{C_M}{\sqrt{C_{ex1} \cdot C_{ex2}}} \qquad (5)$$

$$\omega = \frac{1}{\sqrt{L \cdot C}} \qquad (6)$$

where C is the parallel capacitance.

The advantage of this compensation network is its feasibility for long-distance and high-power applications. The resonance in the system is insensitive to misalignments in the capacitive coupling, and since the latter is lower than the parallel capacitances, their variation does not affect the circuit's behavior.

Conversely, it must be emphasized that the transmitted power is inversely proportional to the capacitive coupling coefficient and that the latter increases with increasing distance, at the expense of decreasing efficiency. On the other hand, higher power means higher voltage and stress on the components used. For this reason, controlling the voltage drop across the inductor is of interest, as it can reach several kV and thus may not guarantee safe system operation.

LCLC Compensation

To overcome the limitations presented by the previous configuration, a double LC branch can be employed for compensation, as shown in the Figure.
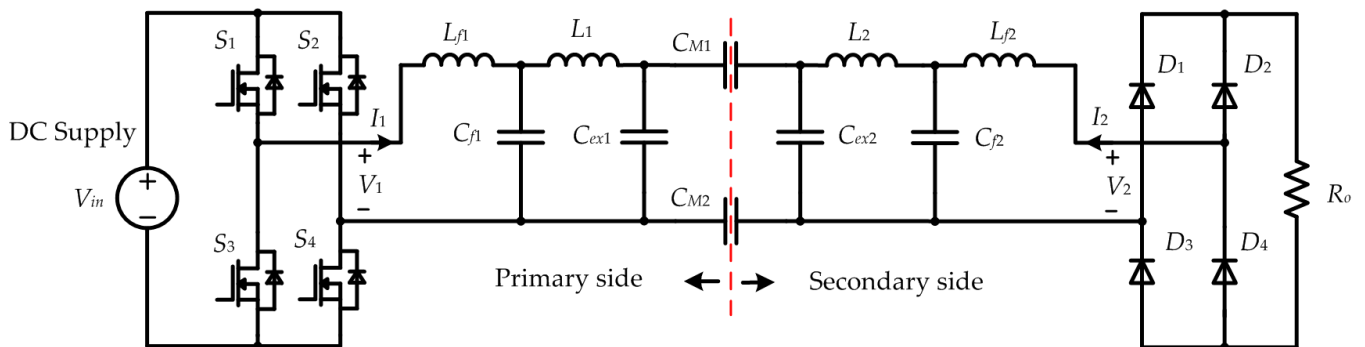

Figure 19: CWPT circuit with LCLC compensation

As can be seen from Figure 19, the first LC block remains unchanged compared to the previous configuration, while the second block, composed of inductance L_{f1} and capacitance C_{f1}, converts voltage V_1 into a current source for the resonant circuits, and the same occurs on the secondary side with voltage V_2. In this case, multiple resonances are indeed present; for example, capacitance C_{f1} can resonate with both inductance L_{f1} and L_1, which are used to increase the voltage in the capacitive coupling and thus achieve more transmitted power. If previously the transmitted power was inversely proportional to the coupling coefficient, now it is directly proportional and can be varied through component design without altering the capacitive coupling. Therefore, it is possible to maintain a high coupling coefficient for efficiency considerations while satisfying power requirements.

The disadvantage of the double-sided LCLC compensation circuit is its complexity. Since there are eight passive components in the circuit, the system's cost and weight increase. Furthermore, more components can cause additional power losses in the circuit, which may reduce system efficiency.

2.3.3 Capacitive Coupler

Let's now focus our attention on the fundamental part of the circuit where power transfer actually occurs. While for an IPT circuit, transfer was achieved through the use of inductors, in this case, capacitive coupling is utilized, as already mentioned in previous descriptions. This is determined by multiple metallic plates used to create electric fields for power transfer. There is a coupling for each pair of plates, and various implementation structures exist to define different models for varying transmission performances, which will be discussed in this section.

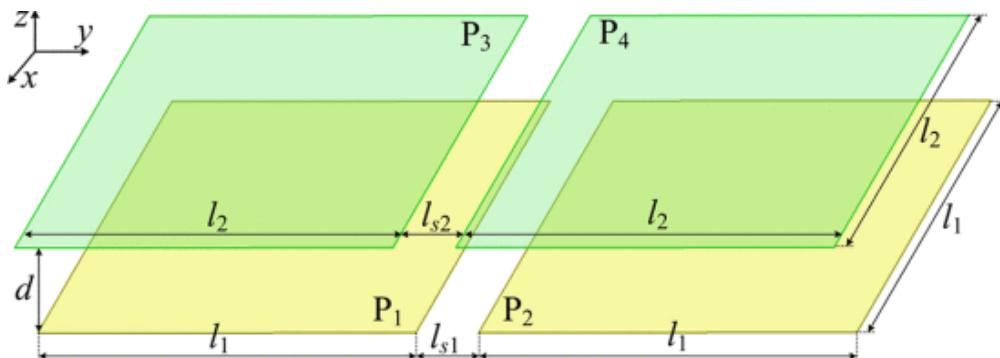Normally, the topology involves four plates, as shown in the Figure.

Figure 20: Structure of capacitive coupling plates

In Figure 20, plates P_1 and P_2 are positioned on the primary side as the transmitter, while plates P_3 and P_4 are positioned on the secondary side as the power receiver.

As is known, a capacitor is a device typically consisting of two conductors, called plates (or armatures), separated by an insulating material called a dielectric. When a voltage is applied across the two conductors, electric charges accumulate on the plates, one charging positively and the other negatively, thereby generating a potential difference and an electric field between them.

By keeping the charge on the two plates constant, the overall effect is to store electrical potential energy, giving rise to the concept of capacitance, which can be used for various applications. Power transfer in this case is therefore not via a magnetic field, but rather an electric field, which is directly proportional to the voltage applied to the plates and also depends on their structure. As shown in Figure 20, the plates or armatures have structural characteristics such as their size and the distance between them.

The electric field and capacitance vary based on these two aspects. Specifically, the formula:

$$E = \frac{\sigma}{\varepsilon} \qquad (7)$$

expresses the electric field, where σ indicates the charge density (C/m^2) on the plates and ε is the dielectric constant (C^2/Nm^2) of the medium between the two.

The electric field can also be expressed based on the potential difference on the two plates:

$$E = \frac{\Delta V}{d} \qquad (8)$$

where d is the distance between them.

It is observed that as the distance between the plates increases, the electric field's intensity, and thus the transmitted power, decreases. The latter varies depending on the models used for capacitive coupling, which are described in the next section.

Two Plate Structure

In a CPT system, to have a coupling, at least two plates must be used, defining a unipolar structure as shown in Figure 21.
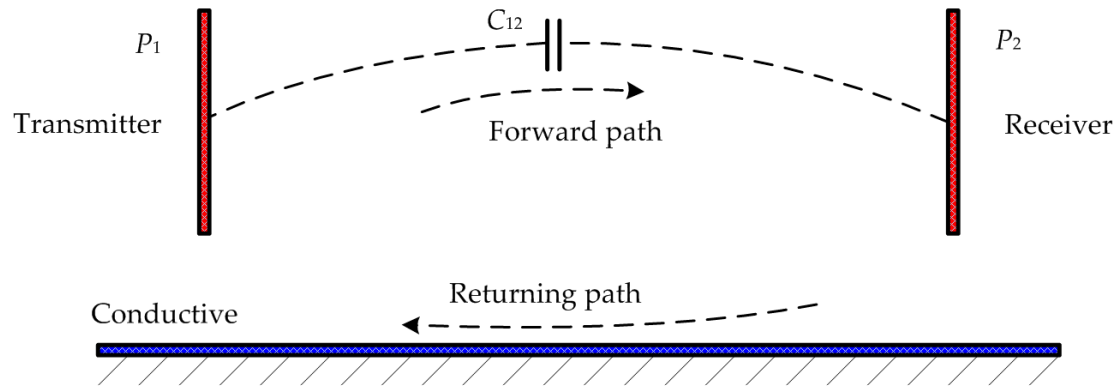

Figure 21 : Two-plate capacitive coupling structure

The mutual capacitance between the two plates provides the path for current flow (*Forward path*) to the load, while a conductive path allows the circuit to close back to the transmitter (*Returning path*).

The structure shown in Figure 21 can be used in both short- and long-distance applications. It's important to note that the size of the plates can differ, especially in an asymmetric coupling structure.

The conductive path can be realized via a metal-to-metal connection, resulting in a quasi-wireless CPT system. For instance, a receiving terminal can be directly connected to ground. In high-speed train propulsion applications, the metal wheels can be used as a return path, which can replace the conventional pantograph and improve system reliability.

Furthermore, since ground access is easy in most applications, and there are usually parasitic capacitances between the plates and the ground, the latter is often used as the conductive return path. For example, receiving terminals can be floating with respect to ground, and the parasitic capacitance can then be utilized to transfer power. In the electric vehicle charging scenario, the parasitic capacitance between the vehicle chassis and the ground is used to conduct current. The advantage of this structure is its simplicity and good tolerance to misalignments, except when an LCLC circuit is used for compensation.

Parallel Four-Plate Structure

The parallel four-plate structure is the most common way to realize a capacitive coupler, also referred to as a bipolar structure, which includes two pairs of metallic plates as shown in Figure 22. It is called this because the two pairs of plates are arranged in parallel.

Considering vehicle charging applications, the transmitter plates P_1 and P_2 are positioned on the ground side in the same horizontal plane, and the receiver plates P_3 and P_4 are positioned on the vehicle side and also in the same horizontal plane. Therefore, this structure can also be called a horizontal four-plate structure.
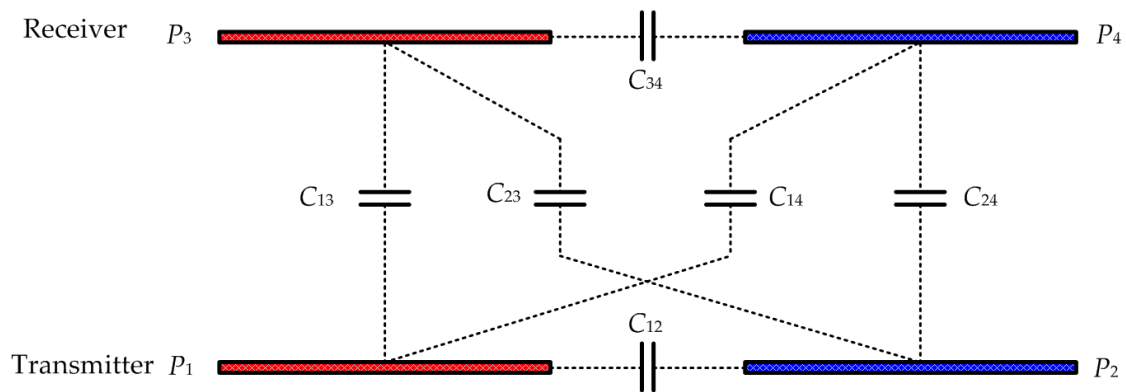

Figure 22 : Four-plate capacitive coupling structure

In Figure 22, there is a coupling capacitance between each pair of plates, resulting in a total of six capacitances, in which C_{13} and C_{24} are defined as main coupling capacitances; C_{14} and C_{23} are defined as cross-coupling capacitances; and C_{12} and C_{34} are defined as self-coupling capacitances.

Unlike the conventional coupling model, this six-capacitance model is more effective and accurate. Usually, when the plates are well-aligned and the distance between them is short, the main couplings dominate the capacitive model, and the others can be neglected to simplify circuit analysis. However, when the plates are misaligned and the distance between the plates is long, the cross-couplings are relatively large and must be considered in the circuit analysis.

Since the six-capacitance model is very complicated, an equivalent circuit as shown in Figure 23 can be used.
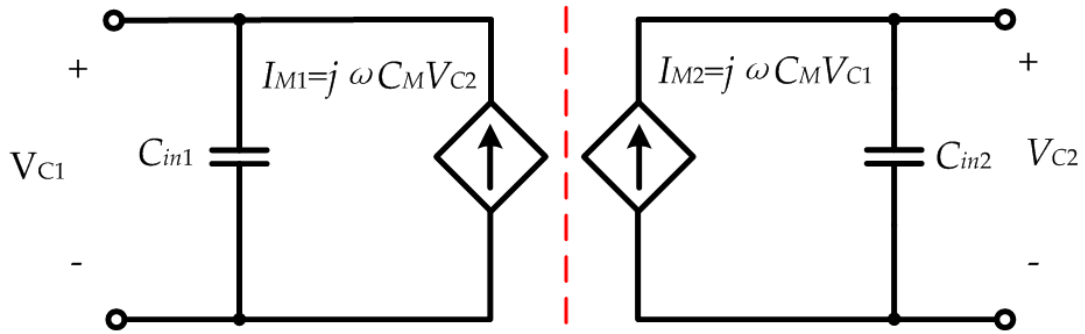

Figure 23 : Equivalent circuit of 4-plate capacitive coupling

The capacity relationship between Figure 22 and Figure 23 is as follows:

$$\begin{cases} C_M = \frac{C_{12}C_{34}-C_{14}C_{23}}{C_{12}+C_{34}+C_{14}+C_{23}} \\ C_{in1} = \frac{(C_{13}+C_{14})\cdot(C_{23}+C_{24})}{C_{12}+C_{34}+C_{14}+C_{23}} + C_{12} \\ C_{in2} = \frac{(C_{13}+C_{23})\cdot(C_{14}+C_{24})}{C_{12}+C_{34}+C_{14}+C_{23}} + C_{34} \end{cases} \qquad (9)$$

It is shown that the mutual capacitance C_M is determined by the main and cross-coupling capacitances, while the capacitances C_{in1} and C_{in2} are related to the self-couplings. In this parallel four-plate structure, the capacitances C_{12} and C_{34} are usually very small, which limits the self-capacitances. Therefore, it is necessary to connect external capacitors to the circuit to increase the equivalent self-capacitances.

Furthermore, this parallel structure is sensitive to angular misalignment. For example, when there is a 90° angular displacement between the transmitter and receiver, the system's power can drop to zero, which limits its application scope.

Stacked Four-Plate Structure

To increase the self-capacitances and eliminate the need for external capacitances, the primary plates P_1 and P_2 are positioned close to each other. Simultaneously, the distance between the secondary plates P_3 and P_4 is also reduced, as shown in Figure 24.
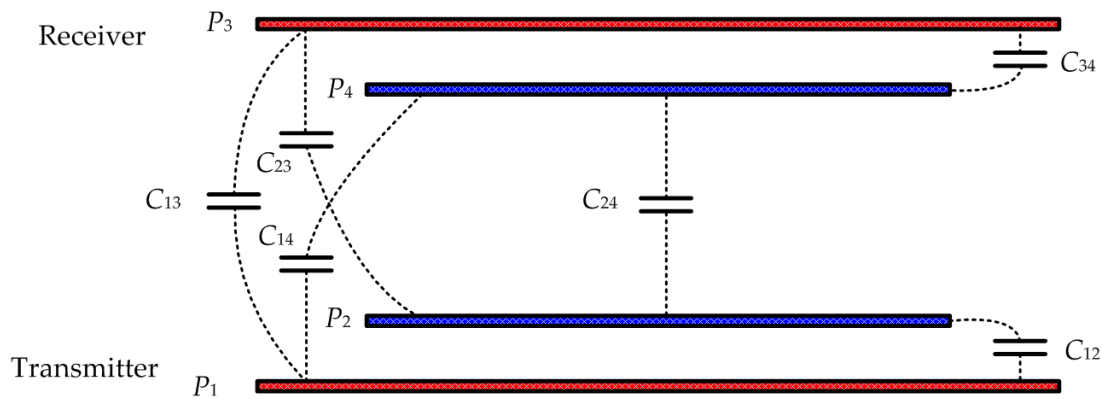

Figure 24: 4 stacked plate structure

Compared to the parallel four-plate structure, since plates P_2 and P_4 are inserted between P_1 and P_3, this model is much more compact. Furthermore, because all plates are centrally aligned, it is less sensitive to angular misalignment.

However, a limitation of this model is its relatively small mutual capacitance. As the coupler is more compact, the cross-coupling capacitances C_{14} and C_{23} are increased. According to Equation (9), the equivalent mutual capacitance CM is therefore reduced. Another important characteristic is the voltage stress between the plates on the same side. In the scenario of long-distance power transfer, the voltage stress between adjacent plates is usually very high; therefore, reliable insulation should be applied to the surface of the plates.

Compared to IPT systems, recent CWPT technology still has a long way to mature, and there are some limitations to overcome: low power density, low efficiency, and strong magnetic field emissions, which will be explained below.

First of all, in an IPT system, a 450 mm x 450 mm inductive coupler can achieve a power transfer of 7.7 kW for vehicle charging applications, resulting in a power density of 38.0 kW/m².

However, in a CWPT system, when the capacitive coupler size is 914 mm x 914 mm, it can achieve a power transfer of 1.87 kW for vehicle charging applications, which means the power density is only 2.2 kW/m². Therefore, in long-distance applications, the power density of a CWPT system is shown to be much lower than that of an IPT system. This is due to the fact that the coupling capacitance is usually in the pF range when the transfer distance is in the range of hundreds of mm. According to power analysis, for a given capacitive coupler, the effective method to increase power density is to increase the plate voltage and the switching frequency. Therefore, in future research, the topology and parameters of the compensation circuit can be optimized to further increase the plate voltage, and the insulation between them must be improved. Additionally, the switching frequency can be increased to the tens of MHz level to achieve high power.

Secondly, in an IPT system, magnetic fields can be easily shielded by ferrite and aluminum plates, and stray fields in the surrounding area can be reduced below the safety level. For example, the safe range of a 3.5 kW IPT system is approximately 200 mm from the coupler. However, electric field emission in a CWPT system is difficult to shield, because electric fields can easily pass through metallic material. Since a CWPT system usually requires high voltages on the plates to transfer power, neither the parallel four-plate nor the stacked four-plate capacitive coupler can reduce the electric field. [12]

Chapter 3

Design and engineering of a charging device with wireless capacitive transfer power technology.

In this chapter, the design of a wireless charging system for a mobile device, such as a smartphone, is addressed, utilizing Capacitive Power Transfer (CPT) technology.

The circuit under consideration is the following.
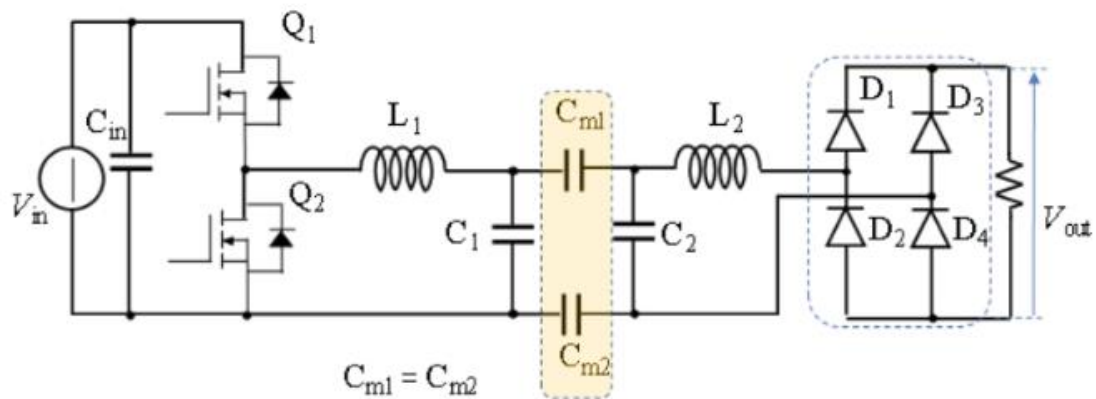

Figure 25 : CPT charging system circuit diagram

As can be seen, the configuration is very similar to those introduced in the previous chapter. The two parts of the circuit are composed, on one side, of the transmission part, which is the charger, while the secondary part represents the receiving part, or the device to be charged. These will be analyzed separately, as shown in the Figures.
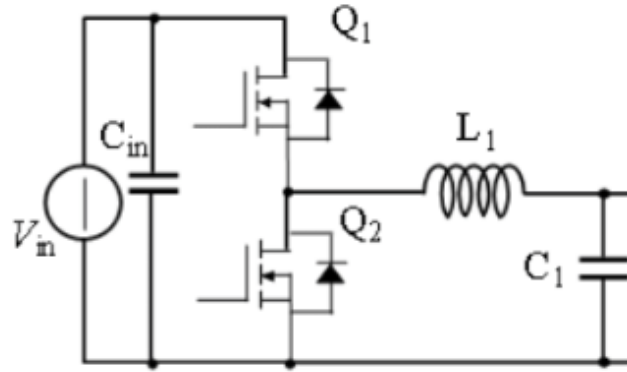
Figure 26 : CPT charging system circuit diagram

The charger-side circuit is composed of the inverter, chosen in a Half-Bridge configuration, and an LC compensation network. These design choices were made based on their simplicity and, specifically regarding the inverter, for better management of MOSFET pulses and its suitability for handling small powers.
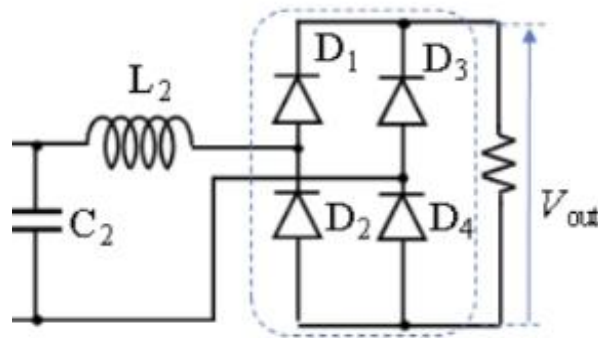
Figure 27 : Receiver side circuit

The device-side circuit consists of the dual of the compensation network and the rectifier, which in this case is a Full-bridge.

Power transfer is achieved through the coupling of the charger and the device. These are considered as the plates of a capacitor with air as the dielectric. The coupling capacitance is schematized by two capacitors of equal capacitance, C_{m1} and C_{m2}, the first in the forward path, and the second in the return path of the circuit.

The behavior of the circuit is studied with respect to voltages and currents, but primarily in terms of frequency, understanding how it affects the alternating values of the quantities and the variation of inductive and capacitive reactance.

It's possible to approximate to the first harmonic for calculating the quantities involved to simplify computation. The equivalent circuit of the one in Figure 25 is as follows.

Figure 28 : Equivalent circuit of CPT charging system

The circuit is considered without the use of the two converters. Indeed, on the transmitter side, the voltage provided by the inverter is repre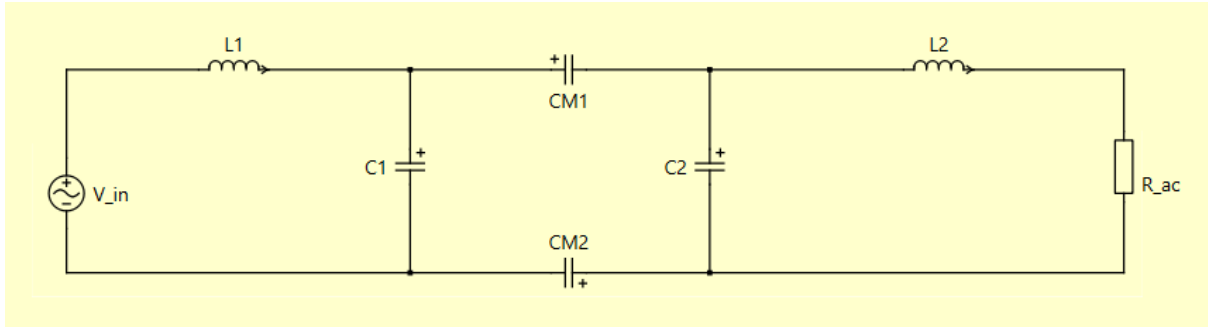sented by the alternating generator V_in, which is assumed to supply an effective voltage of 5.5 V. On the receiver side, the equivalent resistance at the input terminals of the rectifier, R_ac, is still considered in the alternating current (AC) regime.

The components are sized by imposing the following design considerations:

The coupling capacitance is calculated based on a structural decision regarding the dimensions of the plates and the distance between them. We hypothesize square plates with sides of 5cm x 5cm at a distance of 1mm.

The value of the capacitance between them is given by the formula:

$$C_M = \frac{8.875 \cdot 10^{-12} \cdot l^2}{d} \cdot \left(1 + 2.34 \cdot \left(\frac{d}{l}\right)^{0.891}\right) \qquad (10)$$

where the calculation is performed by applying a corrective factor in parentheses.

This computational value is halved for the reason explained above.

The two parallel capacitors, C_1 and C_2, for the resonant circuit are equal to each other, and their value will be subject to further observations and evaluations regarding the behavior of important parameters such as the voltage across the inductors, the transmitted power, and the operating frequency.

Once these two values are established, it is possible to calculate the series resonant inductances using the formulas:

$$L_1 = \frac{1}{\omega^2 \cdot C_1} \tag{11}$$

$$L_2 = \frac{1}{\omega^2 \cdot C_2} \tag{12}$$

For the inductances, the two values are also equal since the values of the two capacitances are equal. By expressing omega as 2πf, we notice the dependence on frequency for the value of the inductances and, consequently, for the resonance of the compensation circuit.

The equivalent resistance seen at the rectifier's terminals accounts for the load resistance and the AC domain. It can be calculated according to:

$$R_{ac} = \frac{8 \cdot R_{load}}{\pi^2} \tag{13}$$

It is of particular importance to analyze the circuit in terms of transmitted power based on the components described above, and to study the circuit to determine the voltage across the equivalent resistance R_ac and the current flowing through it, thus providing the power indication.

In sinusoidal steady-state, the circuit study is performed by representing inductances and capacitances in terms of capacitive and inductive reactance to define the circuit's impedances.

Starting from the equivalent resistance, the series impedance with inductor L_2 is equal to:

$$\overline{z_A} = R_{ac} + jX_{L_2} \tag{14}$$

It is of particular importance to analyze the circuit in terms of transmitted power based on the components described above, and to study the circuit to determine the voltage across the equivalent resistance R_ac and the current flowing through it, thus providing the power indication.

In sinusoidal steady-state, the circuit study is performed by representing inductances and capacitances in terms of capacitive and inductive reactance to define the circuit's impedances.

Starting from the equivalent resistance, the series impedance with inductor L_2 is equal to:

$$\bar{z}_B = \frac{jX_{C_2} \cdot \bar{z}_A}{jX_{C_2} + \bar{z}_A} \tag{15}$$

where X_{C2} is the capacitive reactance.

Similarly, the impedances given by the series with the coupling capacitance C_M and the parallel with C_1 are found respectively:

$$\bar{z}_D = \bar{z}_B + jX_{C_M} \tag{16}$$

$$\bar{z}_E = \frac{jX_{C_1} \cdot \bar{z}_D}{jX_{C_1} + \bar{z}_D} \tag{17}$$

The equivalent impedance seen by the AC generator is the last series with the inductor L_1.

$$\bar{z}_{eq} = \bar{z}_E + jX_{L_1} \tag{18}$$

The circuit then reduces to the following:
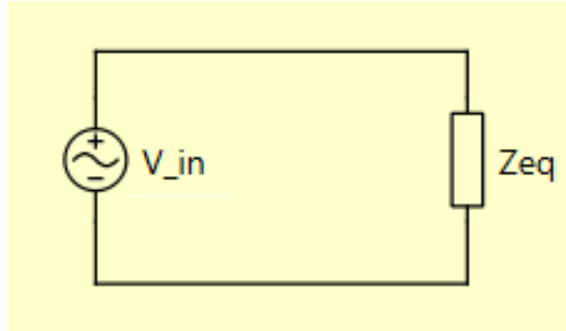
Figure 29 : Equivalent circuit for calculating voltage and current

It is therefore possible to obtain the total current of the circuit, that is, the current absorbed at the input of the system.

$$\bar{I}_{in} = \frac{\bar{V}_{in}}{\bar{Z}_{eq}} \tag{19}$$

The value of $\bar{V}_{in}$ is the first harmonic voltage of the square wave output from the Half-bridge converter, and its analytical value is as follows:

$$\bar{V}_{in} = \frac{2 \cdot U_{in}}{\pi} \tag{20}$$

where U_{in} is the DC input voltage of the converter.

Once these two values are obtained, the current in the plate branch and the current in the equivalent load can be derived through simple dividers, which will be respectively:

$$\bar{I}_{cm} = \bar{I}_{in} \frac{jX_{C_1}}{jX_{C_1} + \bar{z}_D} \tag{21}$$

$$\bar{I}_l = \bar{I}_{cm} \frac{jX_{C_2}}{jX_{C_2} + \bar{z_A}} \tag{22}$$

The current in the load allows us to calculate the voltage across the equivalent load.

$$\bar{V}_l = R_{ac} \cdot \bar{I}_l \tag{23}$$

This theoretical treatment for the calculation of the quantities involved is practically developed through a Matlab script for the execution of the calculations.

The code is given in the Appendix A.

The calculations were performed considering a power transfer of 10W between the plates and a DC output voltage from the rectifier of 5V. This allowed for the derivation of the load resistance (R_load) necessary to determine the equivalent resistance seen by the rectifier, R_ac.

From Formula (10), a coupling capacitance C_M value of 23.7780 pF was calculated. This is the total capacitance value between the two plates for which power transfer occurs.

As indicated in the equivalent circuit, this is represented by the two capacitances C_{M1} and C_{M2}, each assuming half of the total value:

C_{M1} = 11.8890 pF

C_{M2} = 11.8890 pF

As previously mentioned, for the values of capacitances C_1 and C_2, it's necessary to consider the operating frequency and, particularly, the peak voltage across the series inductor. The optimal capacitance value that minimizes the inductive voltage peak, where power transfer is maximized, is sought.

Considering capacitance values in the range of 100pF – 1nF, the following trends for transmitted power and voltage across the inductor are obtained:
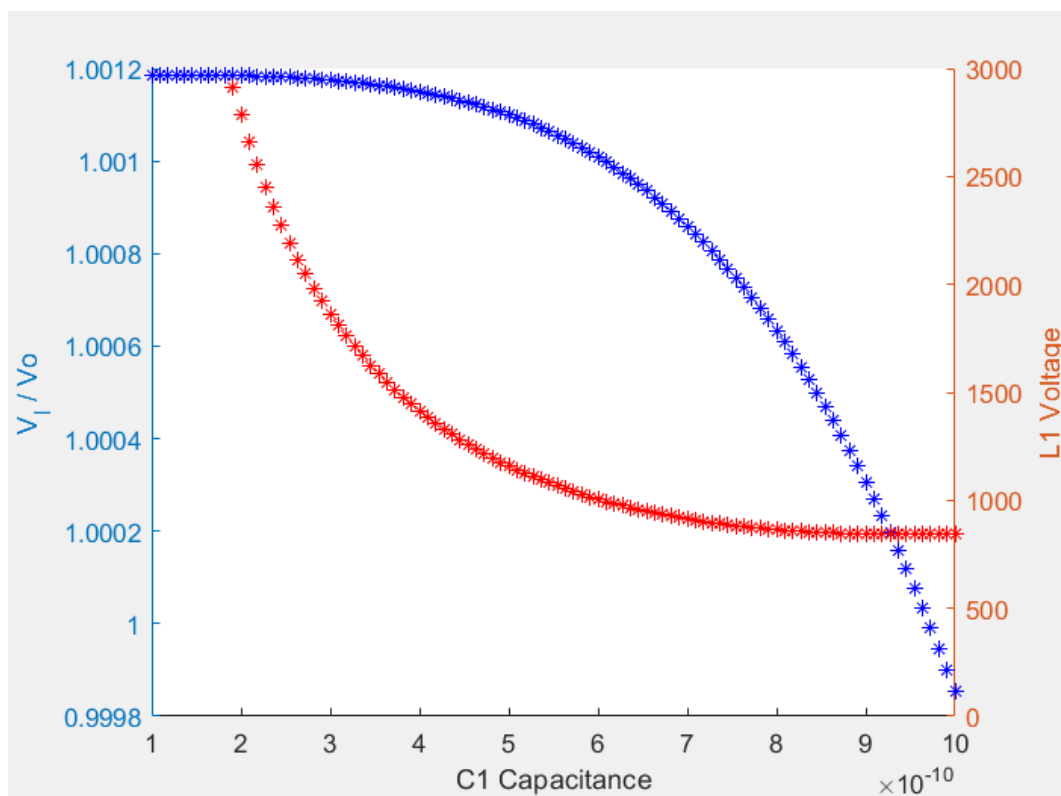
Figure 30 : Trend of transmitted power and voltage on the inductor

In the Figure 30, the blue curve indicates the power transfer, while the red curve shows the voltage variation across the inductor. It's notable that in the section where power remains constant and at its maximum transfer, the voltage is approximately 3 kV, which is an unacceptable value.

Simultaneously, for the minimum voltage value (around 900 V), the transmitted power value decreases drastically.

If the range shifts to values between 10 nF – 100 nF, the following trends are observed.
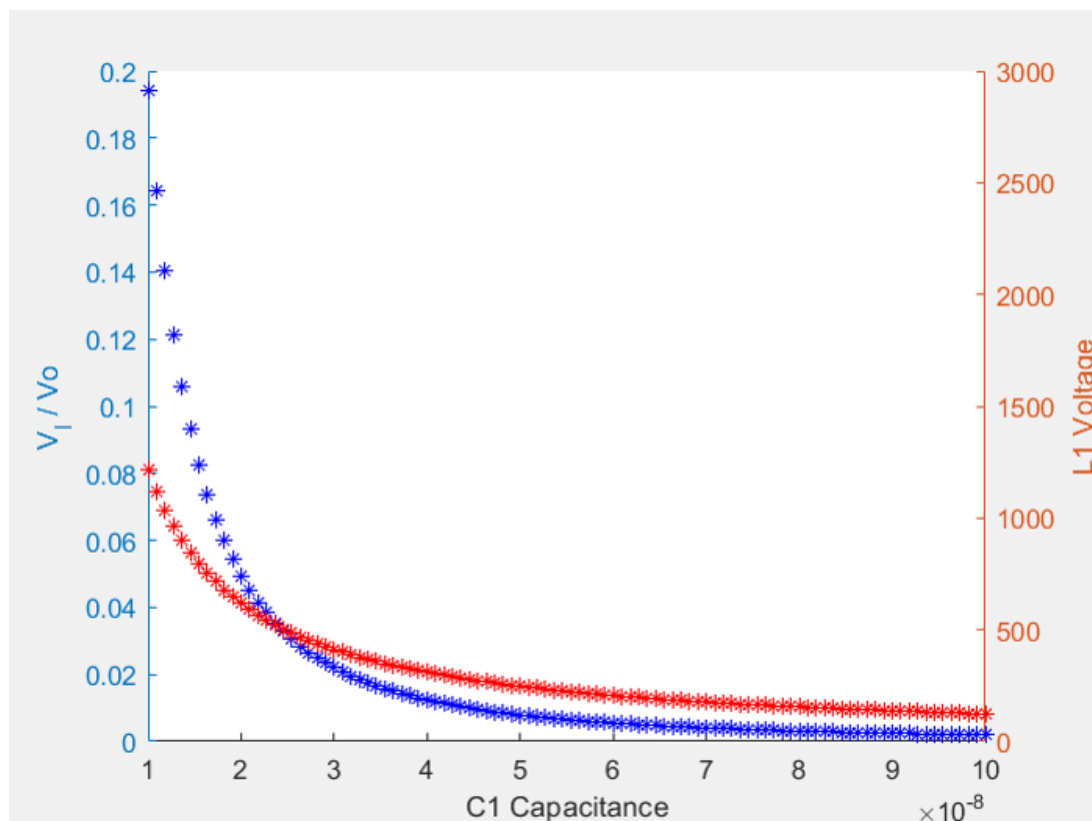
Figure 31 : Trend of transmitted power and voltage on the inductor

In this case, even with a low voltage across the inductor, there is no power transfer, as evidenced by the rapid decrease of the power curve to zero.

The right compromise between the two variables is achieved for a capacitance range of 600µF – 4nF, yielding the following trends.
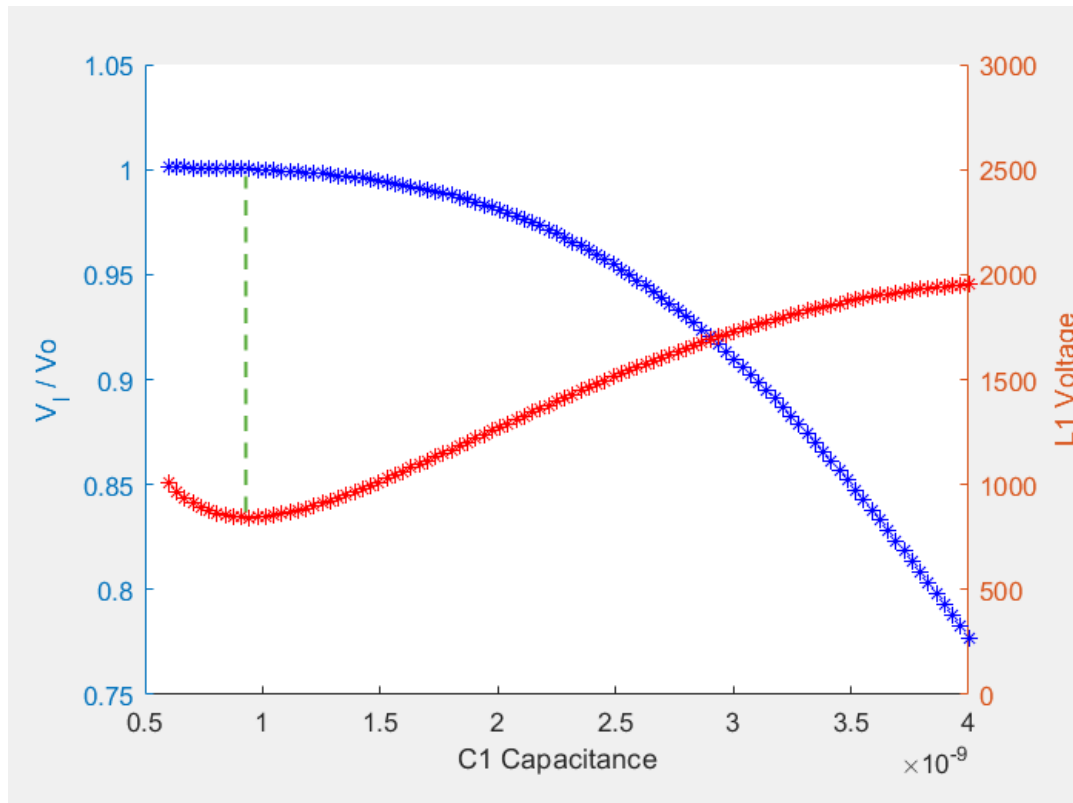
Figure 32 : Trend of transmitted power and voltage on the inductor

In this case, it's possible to observe that for a voltage drop across the inductor of approximately 900 V, we are in the correct power transfer range, as indicated by the dashed line.

These results are obtained considering an operating frequency of 1 MHz

Specifically, for the last case, the capacitance value C_1 considered is 943.43 pF, and the resulting inductance value from the formula (11) is 26.84 µH.

The minimum value of the voltage curve across the inductor is 843.25 V.

Using the same procedure, it's possible to derive the values of inductances, capacitances, and voltages as the operating frequency changes. The results are shown in Table 1.

5cm x 5cm plates				
Fsw (MHz)	C1 (pF)	L1 (µH)	V_{L1} peak(V)	V_{C1} peak (V)
1	943,43	26,84	843.25	837,961
2	662,62	9,55	599,35	594,071
3	535,35	5,15	491,34	486,101
4	464,64	3,41	426,91	421,648
5	412,12	2,46	383	377,770
6	369,69	1,9	350,77	345,617
6.68	363,63	1,56	332,78	327,432

Table 1 : Capacitance and inductance values as the frequency varies

It's noted from the values that as the operating frequency increases, the parameter values decrease. This justifies the consideration made in Chapter I, where it was indicated that higher frequencies lead to greater efficiency and power transfer. Indeed, the peak voltage value at a frequency of 6.68 MHz is significantly lower than the initial one.

The trend of the resonant capacitance, frequency and voltage values on the inductor L_1 is shown in the following graph.
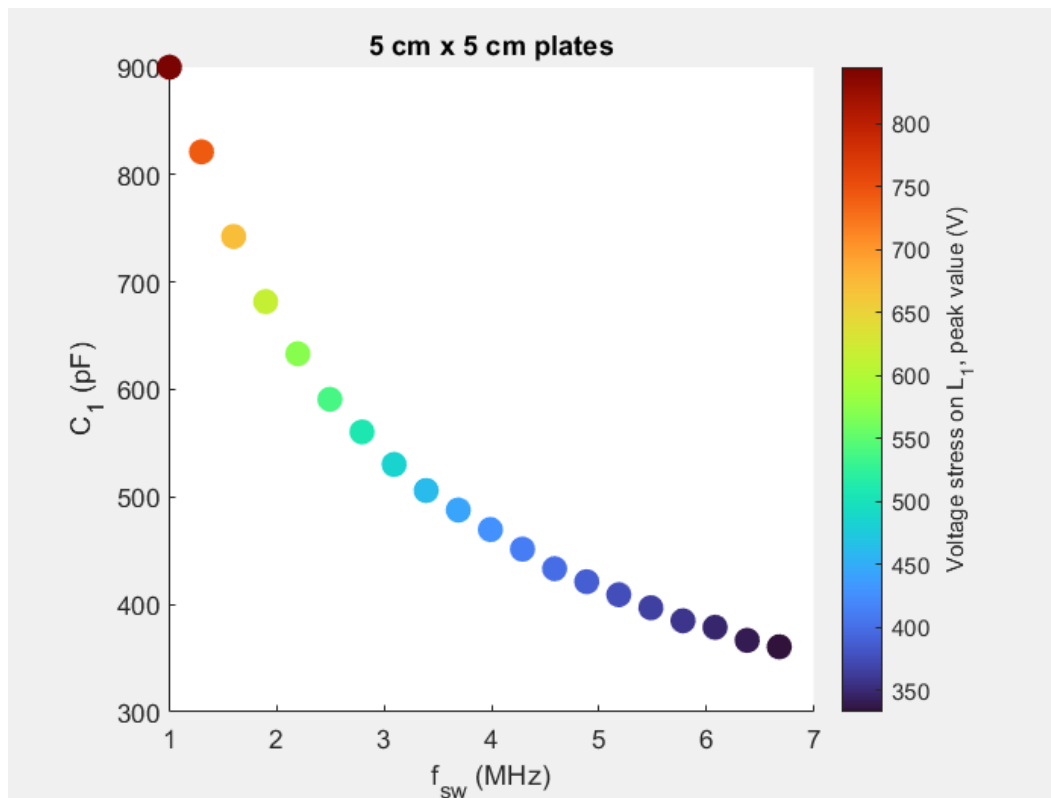
Figure 33 : Trend of the resonant capacitance respect frequency and voltage on L1

The figure clearly shows how as the frequency increases the values of C_1 and the voltage across L_1 decrease, observing a logarithmic trend in the results.

Chapter 4

Simulation of the theoretical circuit and results

The theoretical results obtained from the component calculations are simulated using the PLECS simulation software.

The first simulation involves observing the behavior of the voltage across the inductor. The circuit in the simulation is still the equivalent one, not considering the converters.
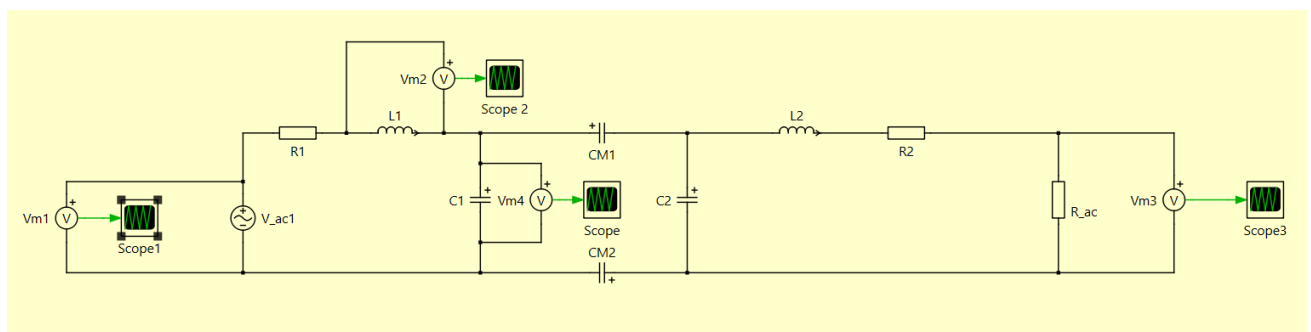
Figure 34 : Simulated circuit without converters

Note that compared to the circuit considered for theoretical calculation, two resistors have been inserted in series with the inductors to achieve higher impedance and limit the current. These are considered in the practical calculation of impedances in the MATLAB script.

Through Scopes, it's possible to visualize the waveforms of interest. Specifically, we observe the AC-side alternating voltage, the peak voltage across inductor L_1, and the voltage across the equivalent resistance seen before the rectifier.
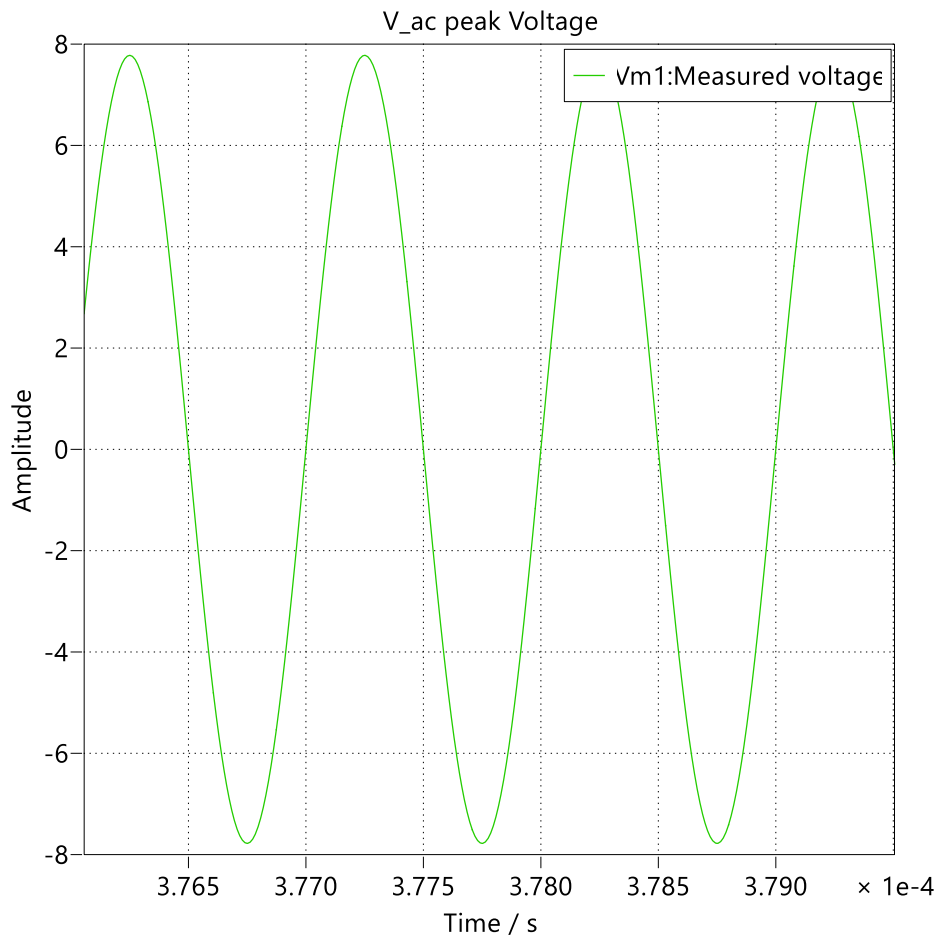
Figure 35 : Input Voltage of the circuit thanks' AC generator

The waveform in the Figure 35 represents the alternating voltage value on the transmitter side. The sine wave's value is higher than the 5.5V supposed in the theoretical formulation. This is because, during the simulation phase, the peak value is used, not the RMS (effective) value. Therefore, the value is 7.77 V, as shown by the following simulation result.

Data

Name		Cursor 1	Cursor 2	Delta		Max	RMS
Time		0.00037725	0.000378355	1.105e-06	🔒		
∨ V_ac peak Voltage	☑						
Vm1:Measured voltage	☑	7.77817	6.14596	-1.63221		7.77817	5.68857

Figure 36 : Input voltage AC value

Respect to this input voltage it is of interest to observe the behavior and the value of the voltage at the ends of the inductor by comparing it with the theoretical one in Table 1.
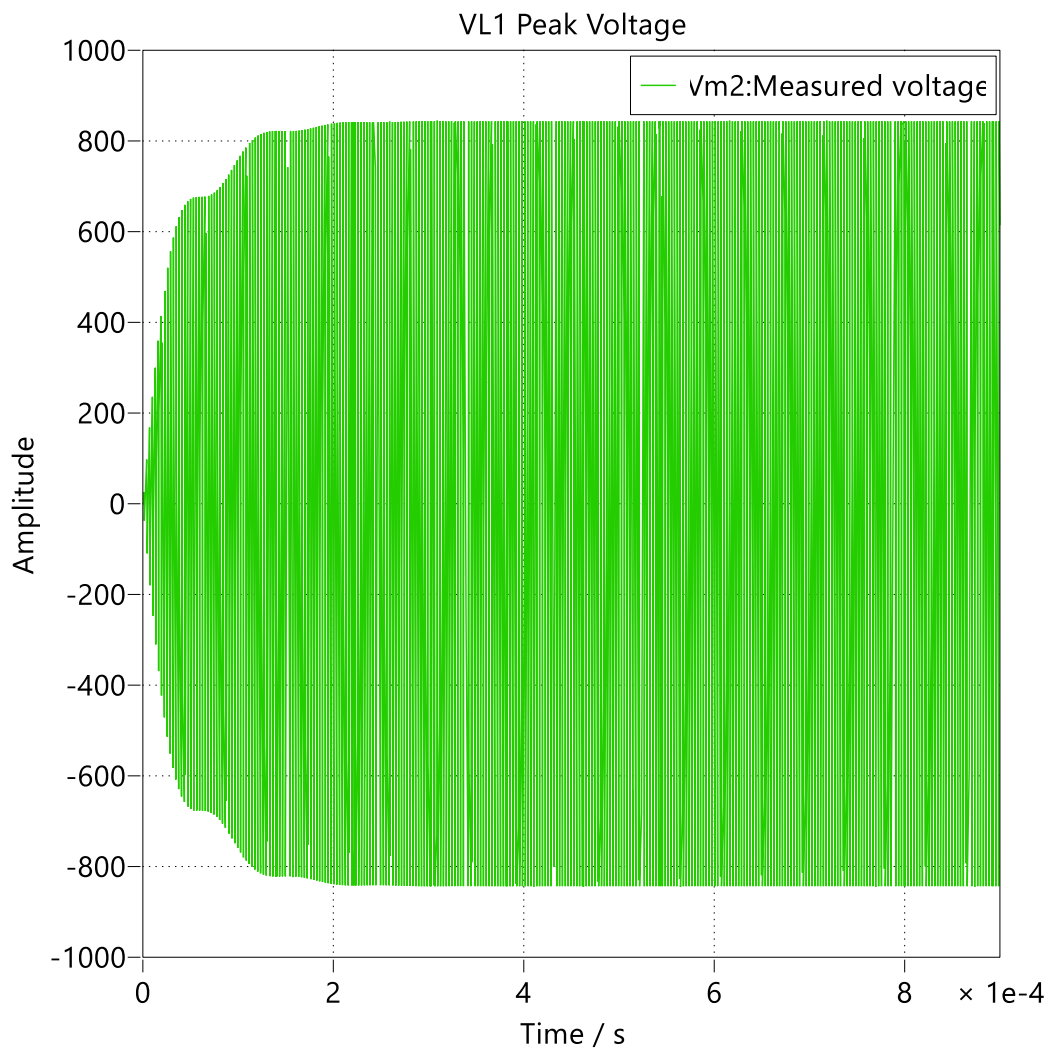
Figure 37 : Peak Voltage on L_1

It's observed how the voltage is initially zero. As the inductor begins to store energy in the form of a magnetic field, the voltage grows until it stabilizes in a steady-state condition, having the following waveform and value.
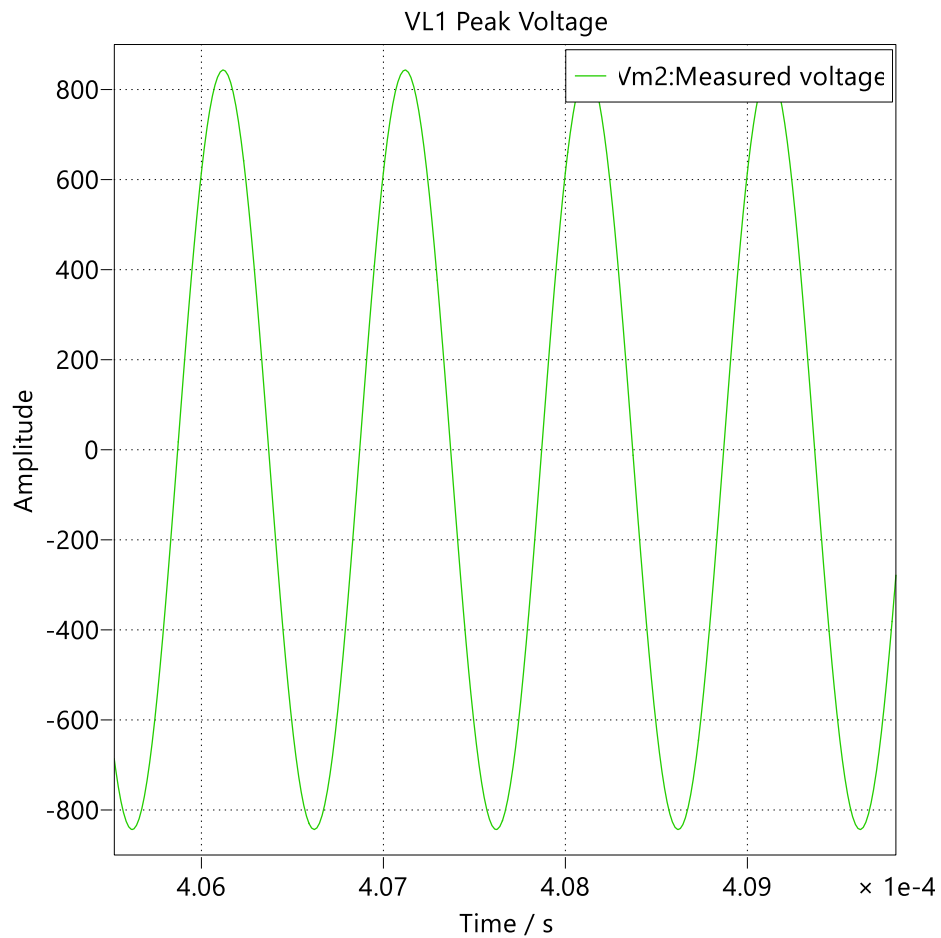
Figure 38 : Zoom on the Peak Voltage on L$_1$

Name		Cursor 1	Cursor 2	Delta		Max	RMS
Time		0.000407119	0.000408384	1.265e-06	🔓		
∨ VL1 Peak Voltage	☑						
Vm2:Measured voltage ∿	☑	843.341	-75.8096	-919.151		843.347	593.126

Figure 39 : Value of the Peak Voltage on L$_1$

As can be seen from the Figures, the voltage waveform is sinusoidal, considering a frequency of 1 MHz The peak value is 843.34 V, which reflects what was obtained from the theoretical calculation and is visible in the Table 1.

45

The same circuit is also simulated for the maximum considered frequency of 6.68MHz.
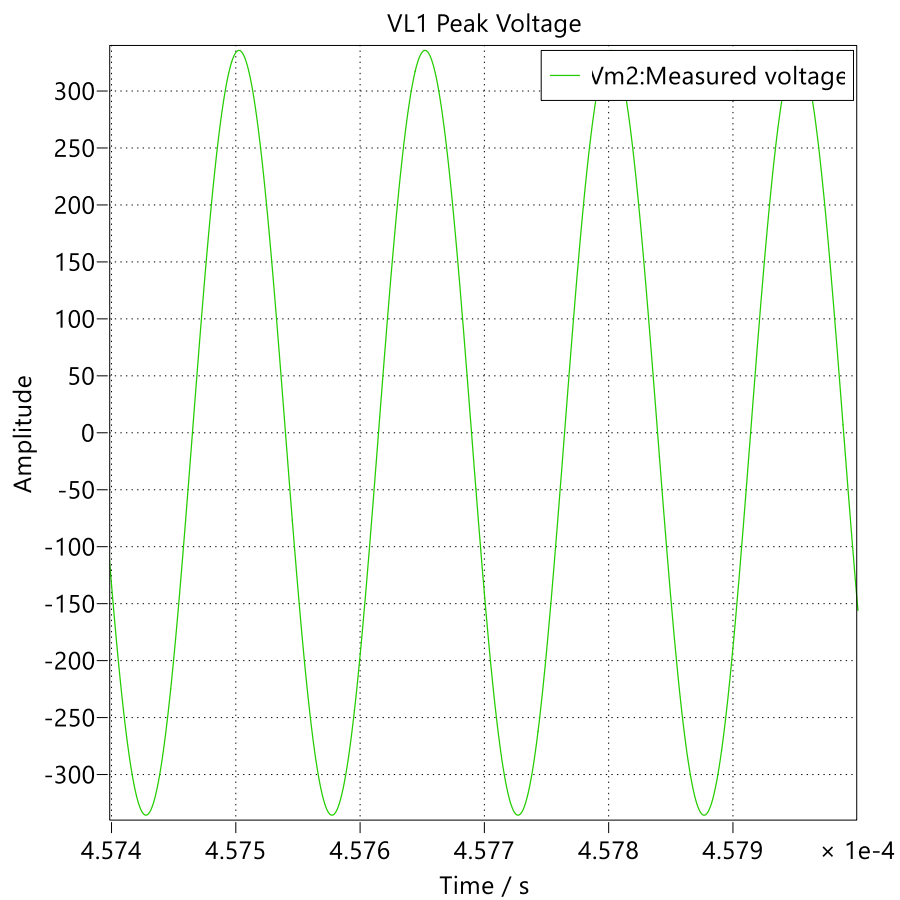
Figure 40 : Peak Voltage on L_1 at maximum frequency

Data						
Name		Cursor 1	Cursor 2	Delta	Max	RMS
Time		0.000407119	0.000408384	1.265e-06		
∨ VL1 Peak Voltage	☑					
Vm2:Measured voltage ☑		-310.466	256.152	566.618	335.703	237.027

Figure 41 : Value of the Peak Voltage on L_1 at maximum frequency

As can be seen from the simulation data, the peak voltage across the inductor is 335.70 V, which also in this case is near to the theoretical computation.

The Table 1 also indicates the voltage value across capacitor C_1. Its value does not deviate significantly from that of the inductor, thus the resonance condition is met, and it's observed that thanks to this resonance, the voltage across the coupling capacitances is much lower.

From the simulation, the values are found to be the same as the theoretical computation, as seen in the Figure.
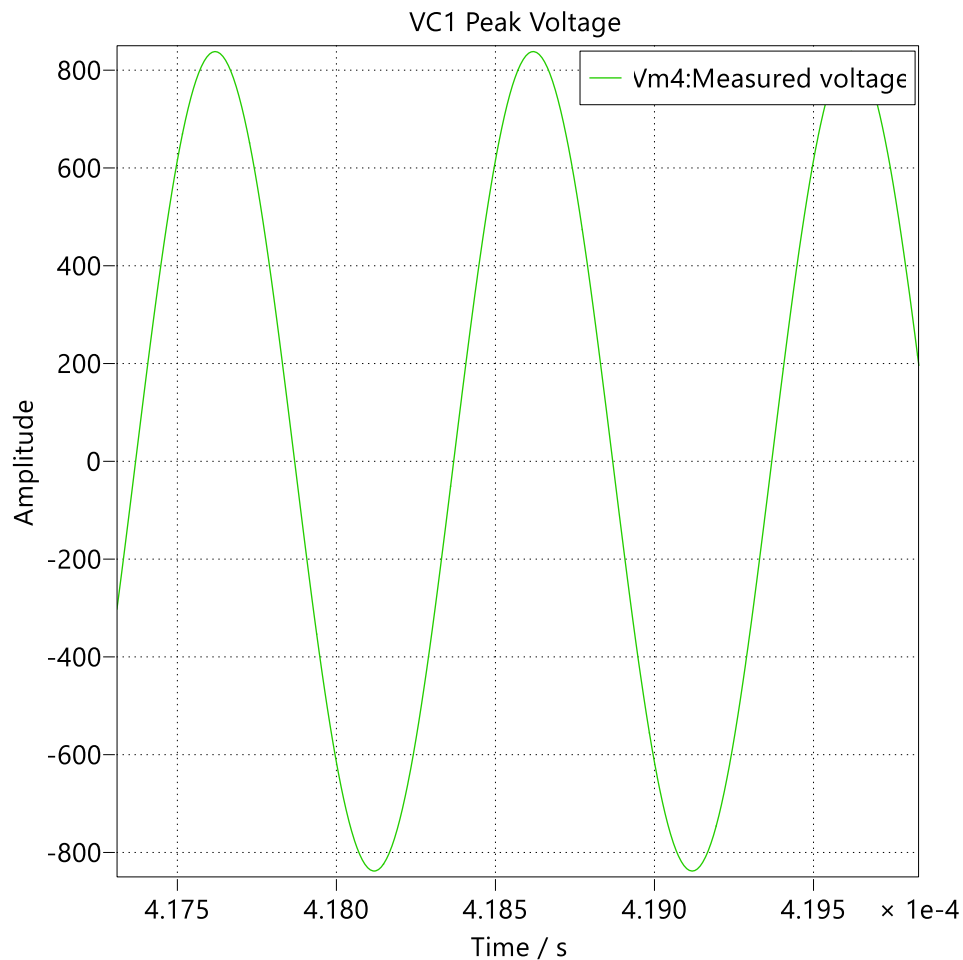
Figure 42 : Peak Voltage on C_1

Data					
Name	Cursor 1	Cursor 2	Delta	Max	RMS
Time	0.000417618	0.00041899	1.372e-06		
⌄ VC1 Peak Voltage					
Vm4:Measured voltage	838.014	-578.663	-1416.68	838.02	575.299

Figure 43 : Value of the Peak Voltage on C_1

Regarding the voltage across the equivalent resistance on the load side, a voltage of 5V was set. From the simulation, the following is obtained:
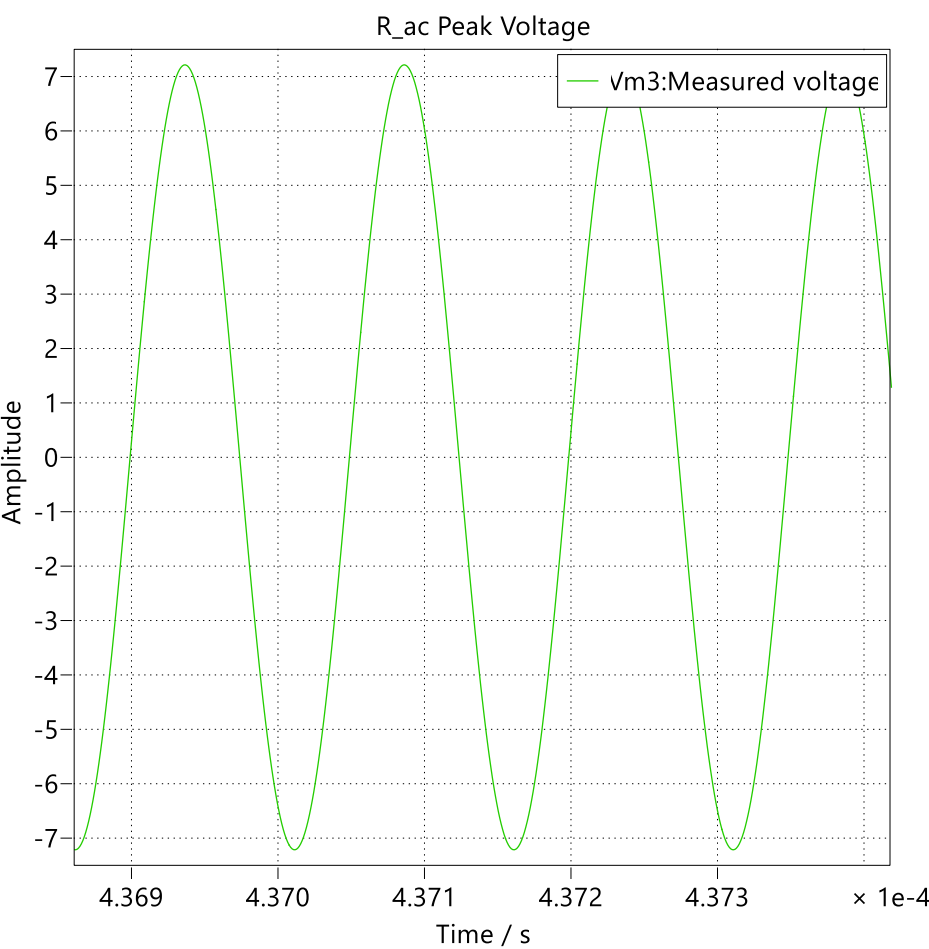
Figure 44 : Peak Voltage on the resistor R_ac

Name	Cursor 1	Cursor 2	Delta	Max	RMS
Time	0.000437086	0.000437236	1.49701e-07		
∨ R_ac Peak Voltage					
Vm3:Measured voltage	7.21418	7.21418	-2.39808e-14	7.21418	5.10083

Figure 45 : Value of Voltage on the resistor R_ac

The waveform is still sinusoidal as we are considering the voltage before the rectifier. Similar to the input voltage, the 5 V obtained are considered RMS (effective), as can be seen from the output data (5.1 V rms), while the peak value is 7.21 V. These results are consistent with the assumptions made during the calculation phase.

Besides the peak voltage across the inductor, what's of greater interest is also observing the amount of power transferred between the transmitter and the receiver. During the design and calculation phase, a power value P_0 of 10 Watts was established.

In the simulation, the power transferred to the equivalent load R_ac is observed to be as shown in the Figure:
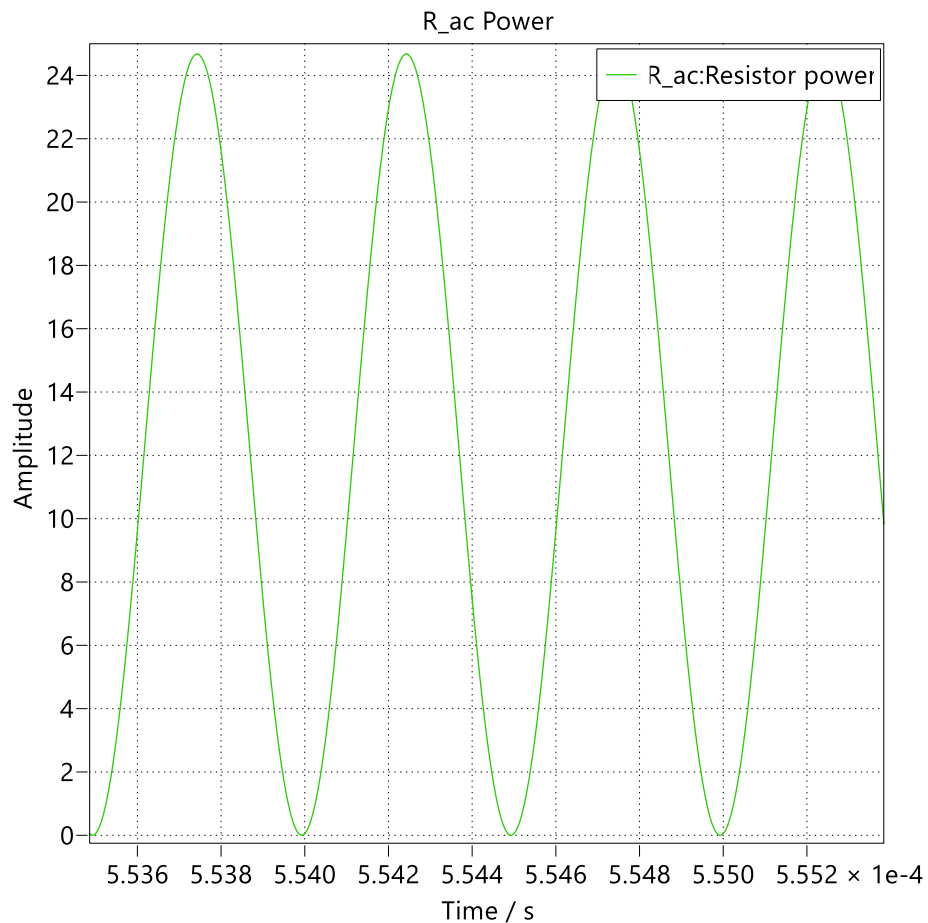
Figure 46 : Power transmitted on the resistor R_ac

It's observed that since this is a sinusoidal power, it presents a peak value and an average value, the latter being of interest for our discussion. The results are indicated in the Figure:

Data

Name		Cursor 1	Cursor 2	Delta	Max	Mean	RMS
Time		0.000554242	0.000554744	5.02e-07	🔒		
⌄ R_ac Power	☑						
R_ac:Resistor power	∿ ☑ 24.678		24.6769	-0.00109948	24.6784	12.3884	15.1624

Figure 47 : Value of Power transmitted on the resistor R_ac

The average value of transferred power is approximately 12 Watts, slightly higher than the design value but acceptable considering an equivalent circuit.

The circuit in Figure 28, as previously analyzed, is an equivalent circuit for calculating components according to design specifications. The complete circuit that requires a more in-depth discussion is the one in Figure 25, which includes the two converters. The circuit in the simulation is the following:
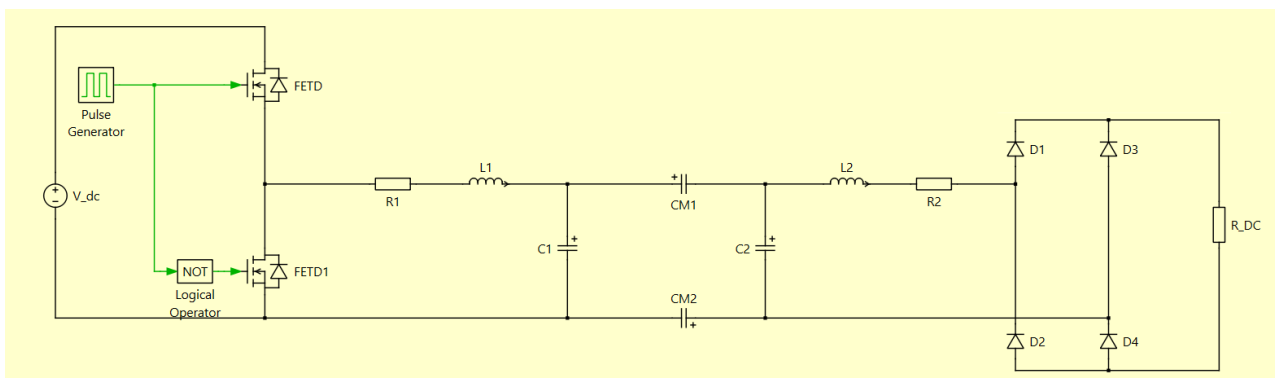
Figure 48 : Complete circuit with converters

In the circuit of the Figure 48, the input voltage is no longer approximated by an alternating generator but is the DC value calculated according the inverse of formula (20).

This voltage is the input to the inverter in a Half-Bridge configuration. The two MOSFETs, which operate as switches, are driven by a pulse train with a frequency equal to the desired output voltage frequency from the converter. To ensure the alternating opening and closing of the two transistors, the second pulse train is negated relative to the first.

The inverter's output voltage is shown in the following Figure:
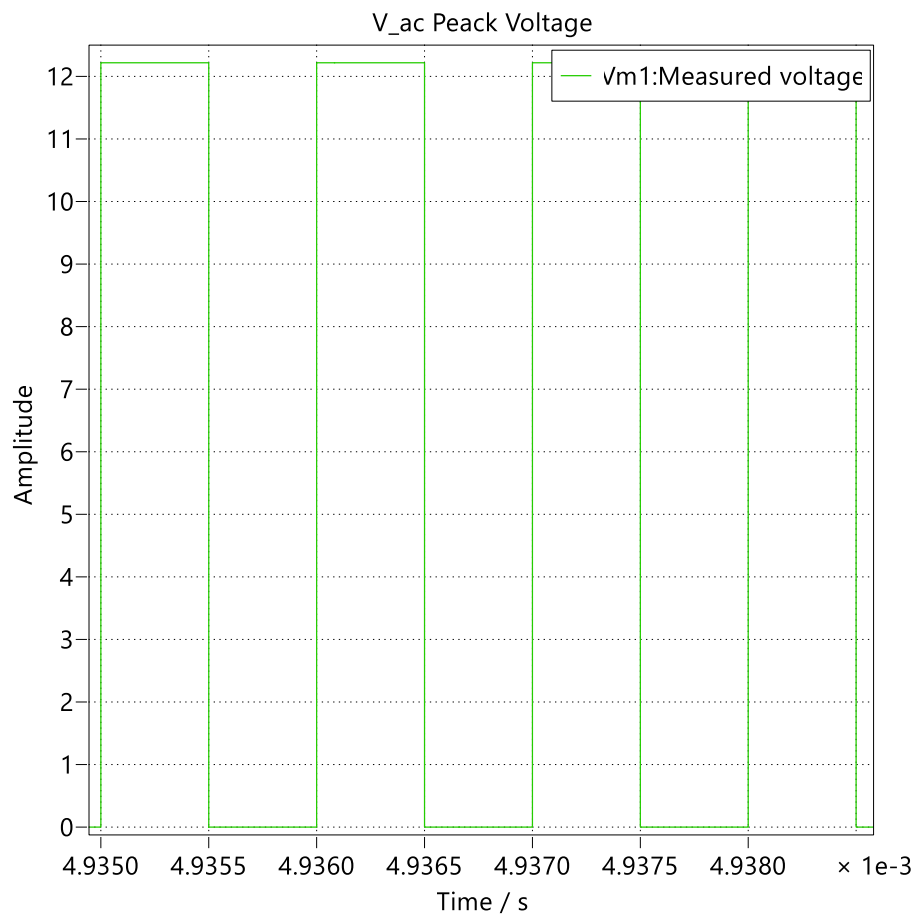
Figure 49 : Output voltage of the Half-Bridge inverter

Name	Cursor 1	Cursor 2	Max	Mean	RMS
Time	0.00493602	0.00493702			
˅ V_ac Peack Voltage ☑					
Vm1:Measured voltage ☑	12.218	12.218	12.218	6.08445	8.62204

Data

Figure 50 : Value of the output voltage of the Half-Bridge inverter

The converter's output, being a Half-bridge, is a square wave with a period of 1 µs, based on the 1 MHz switch driving frequency.

The square wave thus varies between 0 and the peak value, which in this case is 12.21 V. This result is obtained by substituting the peak voltage value imposed in the calculations, 5.5 V RMS, into formula (20), thereby getting the value of Vin.

The square waveform of the voltage has a first harmonic that can be approximated to that of the equivalent circuit, as seen from the Fourier decomposition in the Figure.
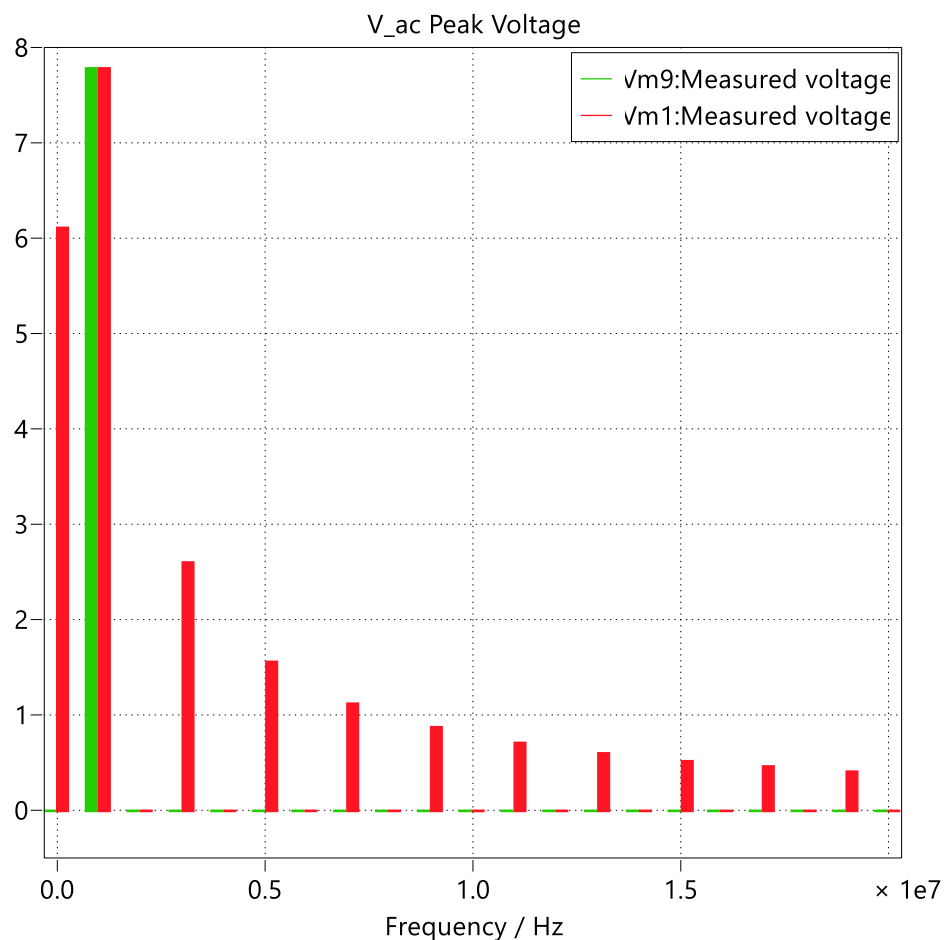
Figure 51 : Fourier spectrum of the voltage

Name			0	1	2	3	4
Frequency			0	1e+06	2e+06	3e+06	4e+06
∨ V_ac Peak Voltage		☑					
Vm9:Measured voltage	▥ ☑		-1.49773e-08	7.77815	3.50755e-08	7.50959e-08	3.06236e-08
Vm1:Measured voltage	▥ ☑		6.10898	7.7782	7.54441e-15	2.59273	2.14984e-15

Figure 52 : Comparison between the value of the voltage provided by the generator and the inverter

52

As can be observed, at a frequency of 1 MHz, the voltage value is the same, reaching 7.77 V peak. This indicates that even for the complete circuit, the resonance condition given by the series between L1 and C1 is being achieved. Specifically, 1 MHz and subsequent frequencies are the resonant frequencies at which the desired power transfer occurs.

This resonance condition isn't the only one valid in the circuit; in fact, there exists a resonance (and thus a frequency) for which maximum power transfer occurs. To achieve this, the total equivalent impedance of the circuit, including the converters, would need to be considered.

For this reason, a simplified circuit was chosen for a simpler and more precise computation, considering a power to be transmitted that's applicable to the type of device being designed.

From the circuit simulation, we can observe voltages and currents of interest and compare them with the equivalent circuit. The first result we'll look at is the voltage across the inductor and the current it's subjected to.
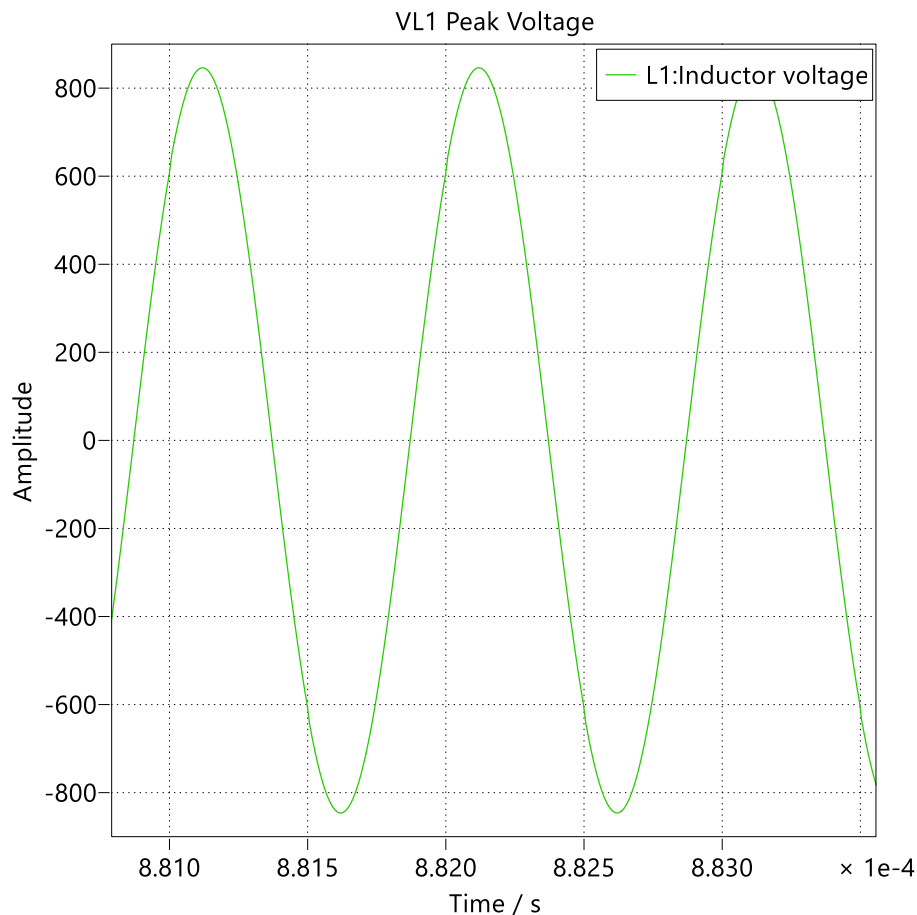
Figure 53 : Peak Voltage on L$_1$ with inverter on the primary side

Name		Cursor 1	Cursor 2	Delta	Max	RMS
Time		0.00184312	0.00184412	9.97e-07	🔒	
⌄ VL1 Peak Voltage	☑					
L1:Inductor voltage ⌃	☑	845.303	845.386	0.0832874	845.386	596.172

Figure 54 : Value of the Peak Voltage on L_1 with inverter on the primary side

The voltage value, as seen in the Figure, is 845.38 V. This is very close to the value obtained in the theoretical calculation and in the circuit without a converter. Another value to consider is the current.
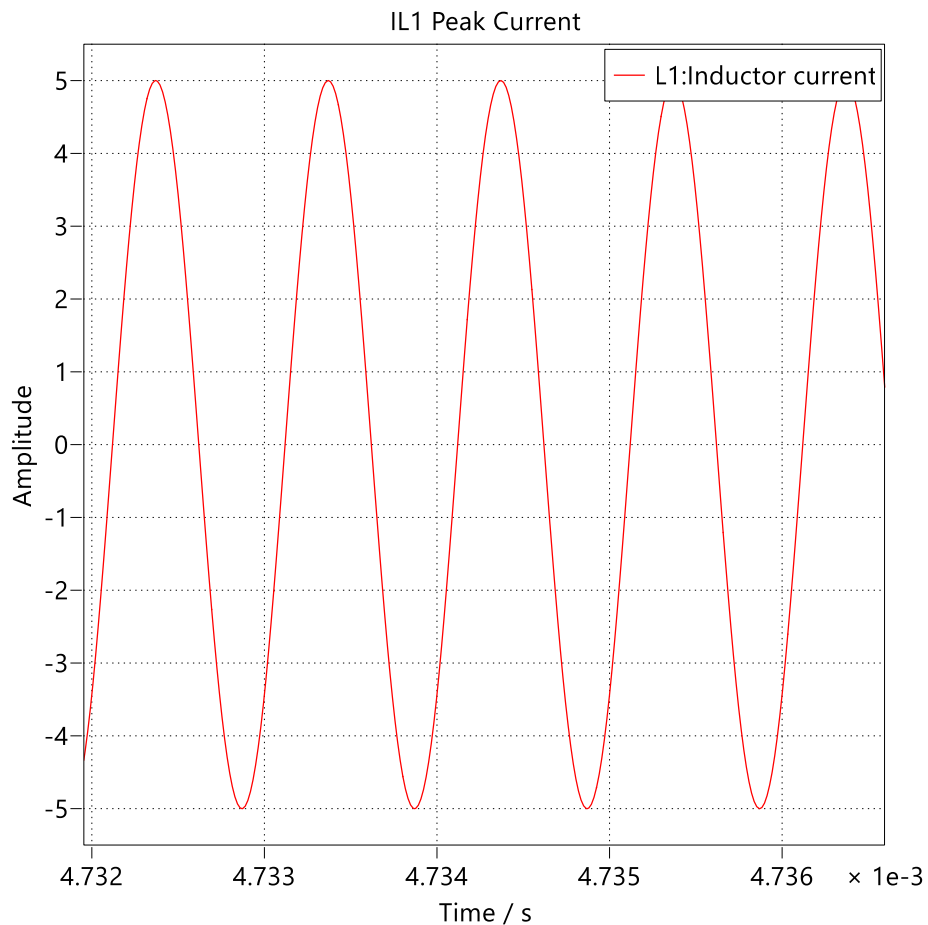
Figure 55 : Peak Current on L_1 with inverter on the primary side

Data

Name		Cursor 1	Cursor 2	Delta	Max	RMS	
Time		0.0047335	0.00473505	1.547e-06	🔒		
∨ IL1 Peak Current	☑						
L1:Inductor current ∿	☑	3.43538	-2.21561	-5.65099	5.0003	3.52061	

Figure 55 : Value of the Peak Current on L_1 with inverter on the primary side

The current flowing through the inductor has a peak value of 5 Amperes. This data is fundamentally important for choosing the right type of inductor to use. If an inductor wound with ferromagnetic material were chosen for this current value, it would lead to excessive overheating, damaging the component itself and the circuit. Furthermore, there would be increased losses due to parasitic currents and dissipation, making the component unsuitable for achieving resonance conditions and thus power transfer.

The voltage and current values are largely the same across capacitor C_1, as shown in the following Figures.
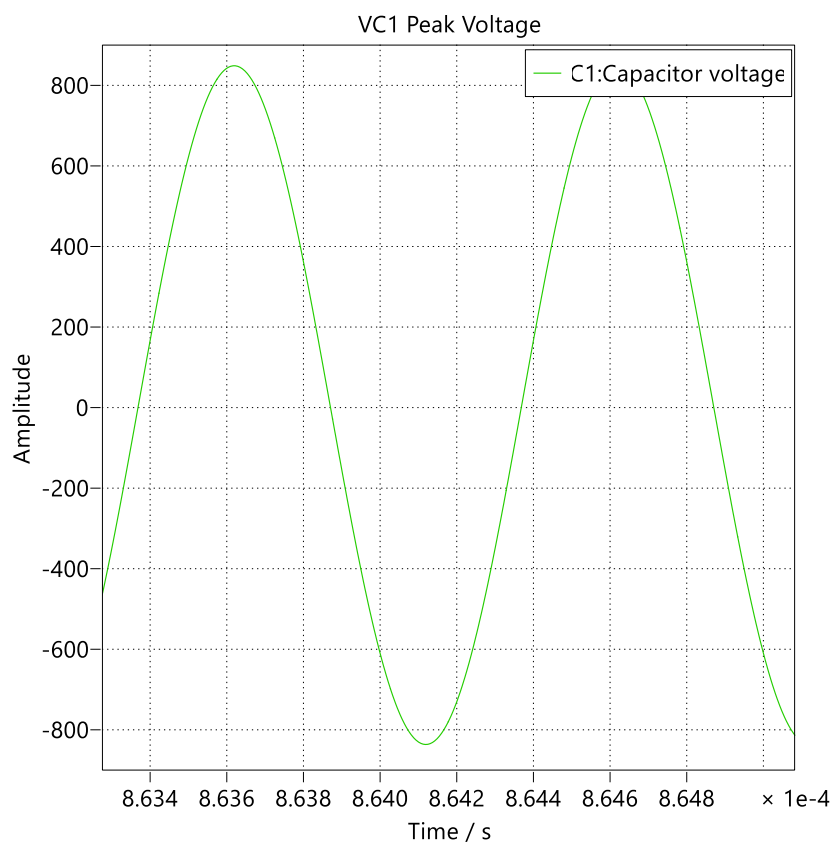
Figure 56 : Peak Voltage on C_1 with inverter on the primary side

Data					
Name	Cursor 1	Cursor 2	Delta	Max	RMS
∨ VC1 Peak Voltage ■					
C1:Capacitor voltage ✓ 848.696		848.518	-0.178073	848.696	595.944
C1:Capacitor current ☐					

Figure 57 : Value of the Peak Voltage on C_1 with inverter on the primary side

In this case as well, the capacitor will need to be selected based on the voltage value across its terminals, considering its characteristic equation. For instance, an electrolytic capacitor wouldn't withstand such a high voltage differential, which is why ceramic or polyester capacitors will be the focus of the research.
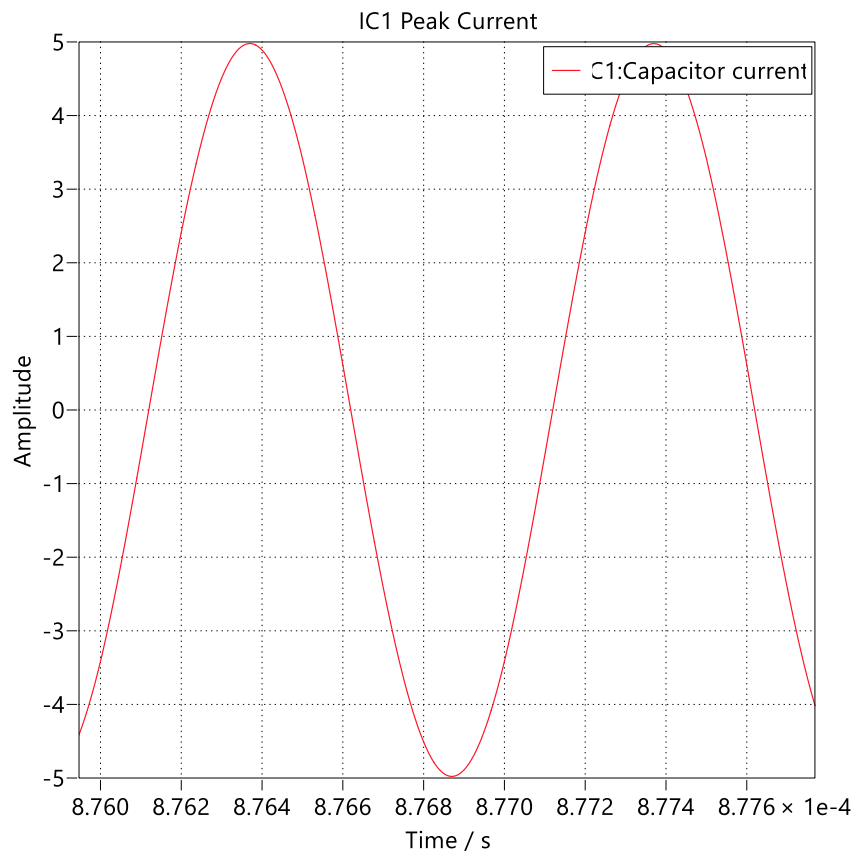
Figure 58 : Peak current on C_1 with inverter on the primary side

Data					
Name	Cursor 1	Cursor 2	Delta	Max	RMS
∨ IC1 Peak Current ■					
C1:Capacitor voltage ∿ ☐					
C1:Capacitor current ∿ ☑	-4.98155	3.84336	8.82492	4.9881	3.72934

Figure 59 : Value of the Peak current on C_1 with inverter on the primary side

The frequency for which these results were obtained is always the working frequency of 1MHz.

As previously mentioned, the same frequency provides the pulses for the switching, and these too have voltage and current limitations. In particular, the simulation shows the current values they are subjected to respect the alternating voltage due to the impulse for commutation.
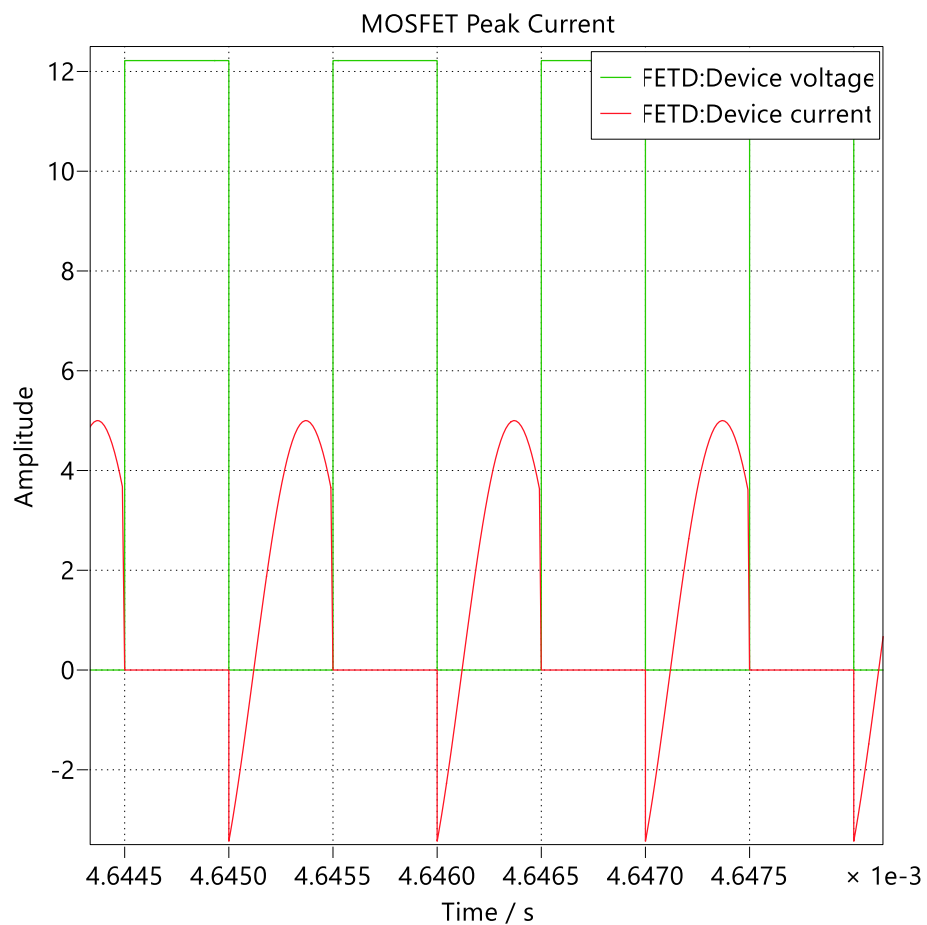
Figure 60 : Commutation current of the MOSFET

Name		Cursor 1	Cursor 2	Delta	Max	RMS
Time		0.00464537	0.00464687	1.498e-06	🔒	
∨ MOSFET Peak Current	☑					
FETD:Device voltage	∿ ☑	0	12.218	12.218	12.218	9.32183
FETD:Device current	∿ ☑	4.99877	0	-4.99877	5.00033	2.42169

Figure 61 : Value of Commutation current of the MOSFET

The image shows a current waveform with positive peaks followed by negative peaks, interspersed with periods where the current is almost zero. This behavior is typical of a MOSFET operating in a converter as a switch, in this case a half-bridge, within a resonant circuit.

Conduction Phase (positive/negative peak): when the device turns on, it allows current to flow through a part of the resonant circuit. The shape of the peak (more or less sinusoidal or bell-shaped) suggests that the current is responding to a resonant condition. Depending on the phase in which the device turns on relative to the circuit's resonance, the current can be positive or negative.

Positive Peaks: correspond to a conduction in one direction, often when it is charging an inductor or discharging a capacitor in a certain direction.

Negative Peaks: indicate that the current is flowing in the opposite direction. This can occur if the circuit is a bridge converter (where MOSFETs work in pairs to alternate the current direction in the resonant load) or if there are body diodes to conduct the return current.

Periods of zero (or near-zero) current: between a positive peak and a negative peak, the current drops almost to zero. This indicates the period when the device is "off." During this interval, the energy in the resonant circuit might be stored in the reactive components (L and C) or redirected through other paths (such as body diodes of other MOSFETs in a full bridge). In a resonant circuit, the 1 MHz control allows for control of the current and voltage phase to maximize power transfer or minimize losses.

Considering the secondary side circuit, the relevant parameters are the voltage and current values on the load, as well as the transmitted power. The full-bridge rectifier, thanks to the conduction and blocking of the diodes as the input voltage varies, will provide a rectified wave at its output, as shown in the Figure.
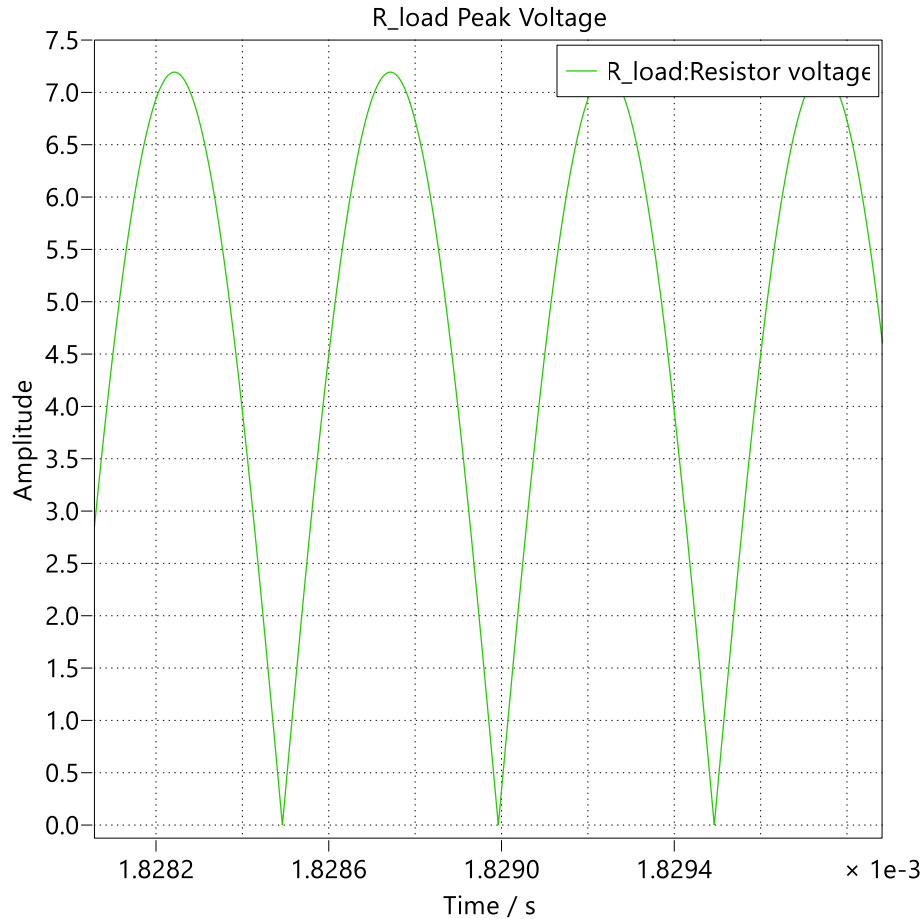
Figure 62 : Rectified voltage on the load

To achieve a more leveled voltage, approximated to a DC voltage, a capacitor is used in parallel with the load to function as a filter.

The filter capacitor, being connected in parallel to the rectifier's output, charges to the peak value of the rectified voltage. When the voltage at the rectifier's output begins to drop (between peaks), the capacitor slowly discharges through the load, maintaining the output voltage relatively constant. When the rectifier conducts again, the input voltage surpasses the capacitor's voltage and recharges it to the next peak. The chosen capacitance value is 100μF, and the resulting voltage is:
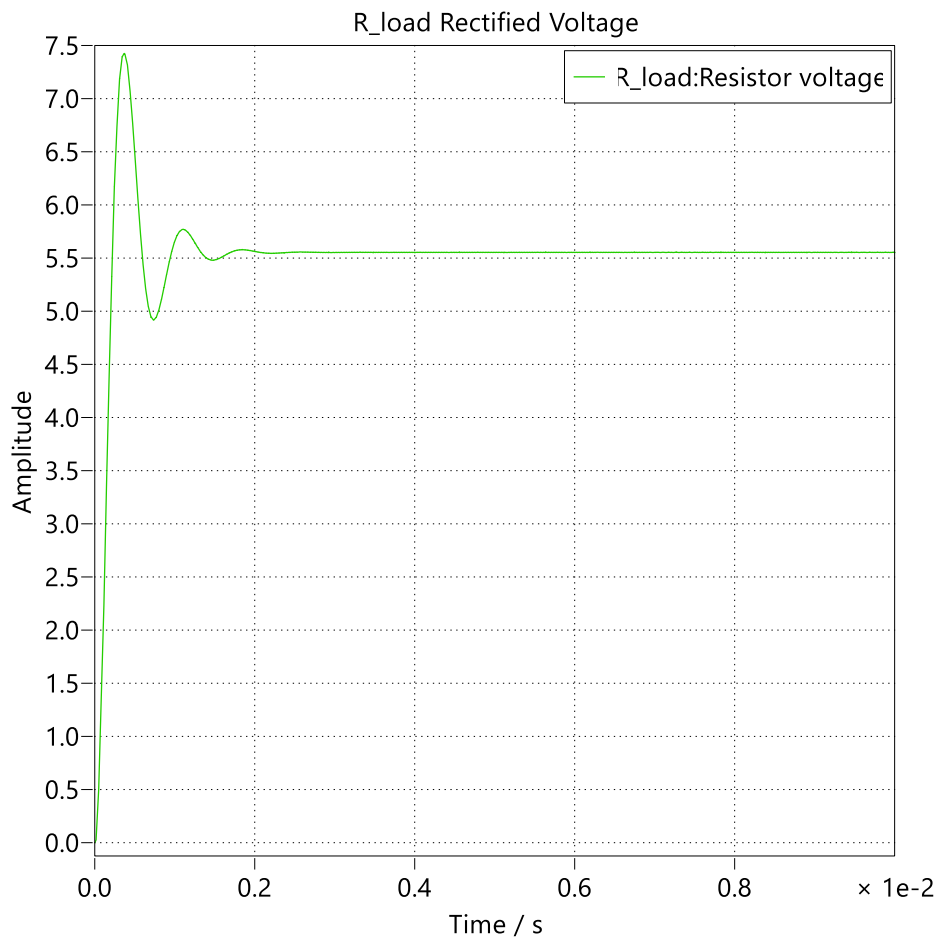
Figure 63 : Rectified voltage on the load with filter capacitance

Figure 64 : Rectified voltage on the load with filter capacitance

From the Figure 63 it can be seen how the voltage after a small transient stabilizes at a value of 5.55 V DC, which reflects what was established at the design level.

The current that flows in the load is :
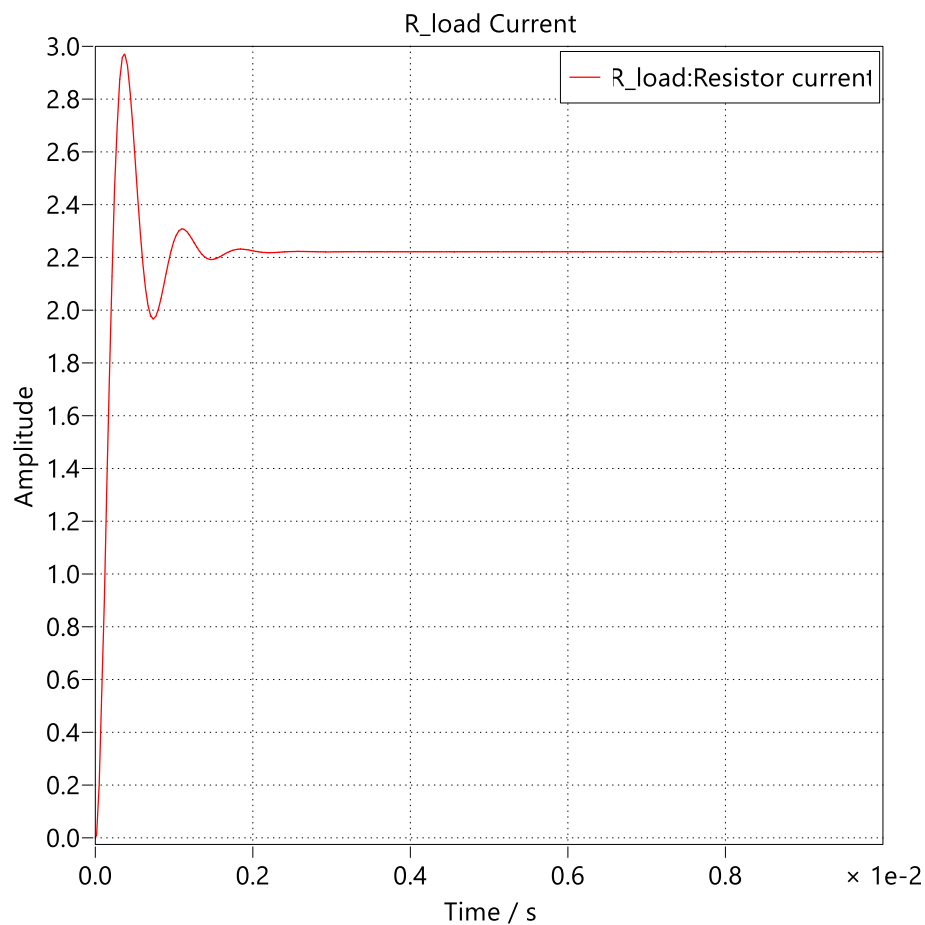
Figure 65 : Current in the load with rectification and filter capacitance

Data					
Name		Cursor 1	Cursor 2	Delta	Max
Time		0.00333333	0.00666667	0.00333333 🔒	
∨ R_load Current	☑				
R_load:Resistor curr... ∿	☑	2.22195	2.22108	-0.000871218	2.22202

Figure 66 : Value of current in the load with rectification and filter capacitance

The current value of 2.22 A corresponds to what can be calculated by applying a simple inverse Ohm's law, considering the load resistance to be 2.5 Ω and the previous voltage of 5.5 V.

As anticipated, the resonance condition achieved is not the only possible condition, nor is it the one for maximum power transfer; rather, it's the one useful for the design purpose. Indeed, from the circuit simulation, a power transfer of 12.33 Watt is observed, as seen in the Figures.
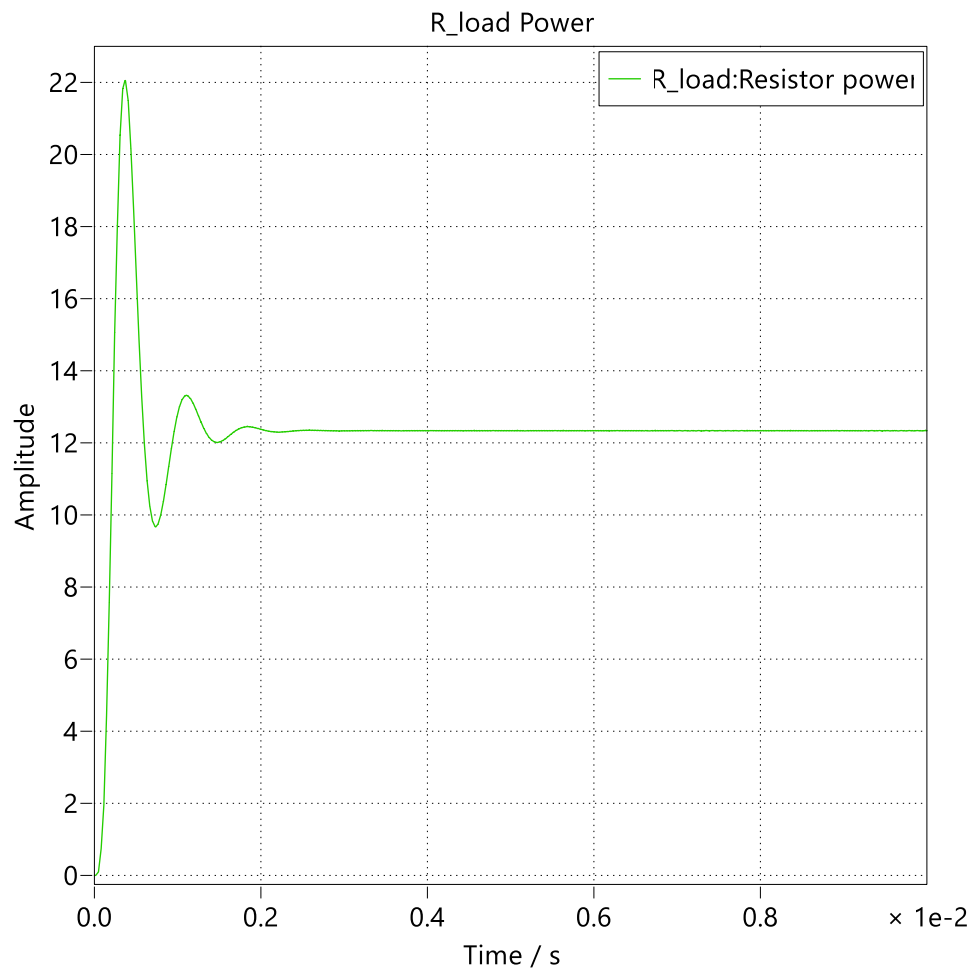
Figure 67 : Power transferred in the completed circuit

Data					
Name		Cursor 1	Cursor 2	Delta	Max
Time		0.00483181	0.00483784	6.025e-06	🔒
⌄ R_load Power	☑				
R_load:Resistor ... ⌄ ☑		12.3404	12.3413	0.00090143	12.342

Figure 68: Value of Power transferred in the completed circuit

It can be noted that the power value corresponds to the average value obtained on the load with the equivalent circuit.
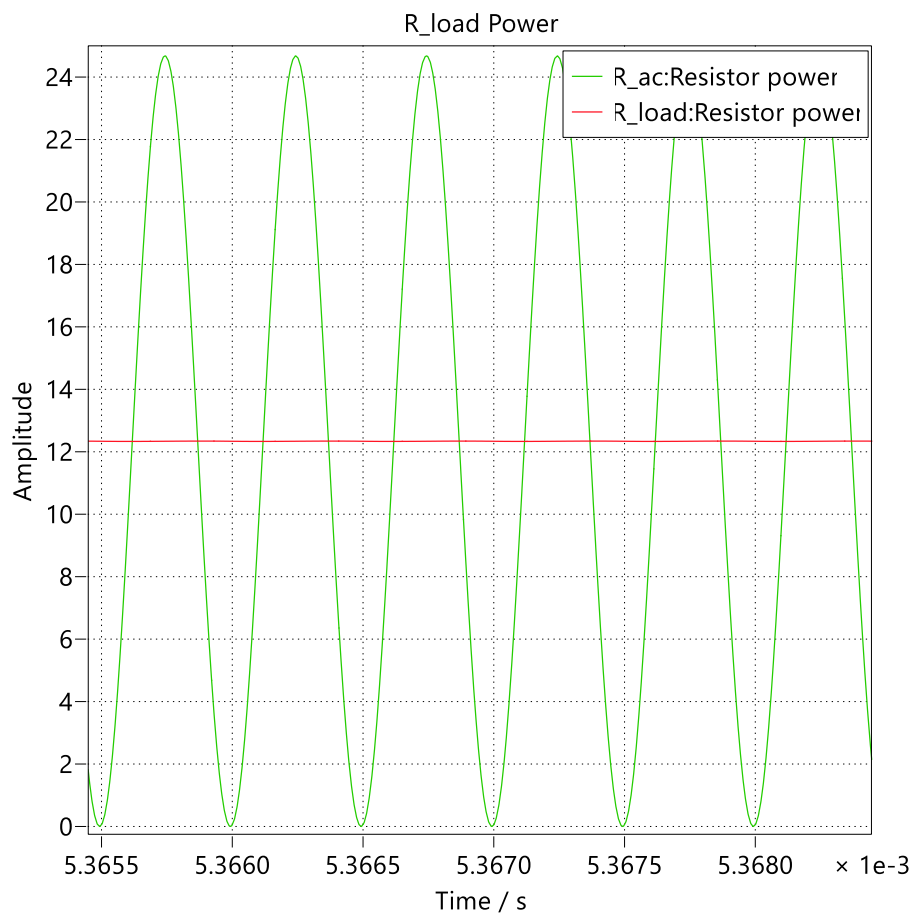
Figure 69: Comparison of the power of the equivalent circuit and the complete one

Name			Cursor 1	Cursor 2	Delta	Max	Mean
Time			0.00536674	0.00536724	5e-07	🔒	
∨ R_load Power		☑					
R_ac:Resistor power	∿	☑	24.6764	24.6764	9.62785e-13	24.6779	12.339
R_load:Resistor power	∿	☑	12.3369	12.3369	1.72455e-08	12.342	12.3368

Figure 70: Comparison of the power values of the equivalent circuit and the complete one

Chapter 5

Research of commercially available components and circuit adaptation with new simulations

Up to this point, the circuit analysis has been purely theoretical, from calculating component values to simulating effects and results concerning quantities of interest, such as the power transmitted from the charger side to the load side. It has been observed that starting from design assumptions, these have been respected throughout the discussion.

As a final step, it is necessary to conduct a search for components such as capacitors, inductors, MOSFETs, and diodes that are actually usable, meaning commercially available. This involves comparing their characteristics with simulation results and adapting the number of components to achieve their determined value. For example, if we consider the 943.43pF capacitance in the compensation circuit for the circuit's operation at a frequency of 1MHz, it might be necessary to connect multiple commercially available capacitors with a specific value to reach the theoretical one. The same applies to inductors.

Based on the voltage and current values found during the simulation phase, it is possible to conduct a search and selection of components from catalogs. In particular, for each frequency value considered, attention was paid to the value of the two quantities for each device involved. The results are reported in the following Table 2.

F(MHz)	V_{L1} [V]	V_{C1} [V]	I_{L1} [A]	I_{C1} [A]	I_FET [A]	I_D [A]	V_FET [V]	V_D [V]	P [W]
1	1474.1 845.44	1472.34 845.95	8.71 5.08	8.67 4.96	8.72 5	9.97 3.46	12.21	-7.04 -5.5	12.34
2	1438.19 601.95	1438.71 601.91	11.94 4.97	11.91 4.94	11.94 4.97	11.62 3.46	12.21	-7.54 -5.58	12.33
3	1432.6 493.17	1427.43 493.17	14.40 4.96	14.33 4.9	14.38 4.9	14.20 3.5	12.21	-7.38 -5.55	12.33
4	1418.38 429.34	1417.38 429.33	16.5 4.95	16.46 4.93	16.5 4.99	16.26 3.5	12.21	-7.51 -5.55	12.35
5	1407 385.33	1406 385.33	18.14 4.96	18.07 4.89	18.15 4.96	17.90 3.49	12.21	-7.37 -5.55	12.35
6	1402.3 353.01	1402.3 353.01	19.47 4.89	19.43 4.82	19.47 4.89	19.19 3.48	12.21	-6.72 -5.55	12.32
6.68	1350.98 334.89	1352.04 334.88	20.54 5.08	20.52 5	20.55 5.08	19.86 3.48	12.21	-6.65 -5.55	12.33

Table 2 : Values of Voltage and current on each component

In Table 2, two values are indicated for each component: the upper value shows the voltage and current at startup, i.e., at the beginning of the transients that occur, especially concerning capacitances and inductances, while the second value indicates the steady-state value during normal circuit operation.

Regarding the design purpose, the values for which a choice is made are those at the operating frequency of 1MHz.

As previously mentioned concerning the magnitudes involved during the discussion, electrolytic capacitors are a priori excluded for the selection of capacitances in the resonant circuit. This is because, even if they offer higher capacitances for the same volume, they are not polarizable. Applying a reverse voltage, even for a short period, can permanently damage them, cause a short circuit, overheating, or even explosions.

The choice therefore falls on ceramic or film capacitors. Ceramic capacitors, for example, possess exceptional temperature stability, have no polarity, which simplifies mounting on the PCB and makes them suitable for AC applications or where the voltage can reverse polarity. Furthermore, they are available in a wide range of nominal voltages, from a few Volt to thousands of Volt, making them suitable for various applications also thanks to their robustness and reliability.

In particular, in addition to choosing ceramic types, SMD capacitors are also considered. These are capacitors that feature very small dimensions, promoting greater compactness and high component density when the PCB is manufactured.

For the capacitor selection, the most relevant factor is the voltage it is subjected to.

Analyzing Tables 1 and 2, it is observed that at a frequency of 1MHz, the capacitance value is 943.43pF with a voltage drop across it of 845.95 V.

From the research conducted in the Mouser Electronics catalog, 4 capacitors were chosen: 3 with a value of 300pF and one with a value of 43pF. This choice is justified by their parallel connection, where their values sum up to obtain a total capacitance equal to the theoretical one. Since the voltage across them remains the same in parallel, capacitors suitable for the considered voltages were sought.

The choice therefore fell on the KEMET High Voltage, High Temperature 150 °C series SMD multilayer ceramic capacitors (MLCC), with X8G dielectric.

The datasheet from the Mouser Electronics catalog is as follows:

Surface Mount Multilayer Ceramic Chip Capacitors (SMD MLCCs)

High Voltage, High Temperature 150°C, X8G Dielectric, 500 – 2,000 VDC (Commercial & Automotive Grade)

YAGEO GROUP
KEMET

RoHS Lead-free REACH COMPLIANT

Overview

KEMET's X8G HV Class I dielectric features a 150°C maximum operating temperature, offering the latest in high temperature dielectric technology and reliability for extreme temperature applications and under the hood applications. X8G exhibits no change in capacitance with respect to voltage and boasts a minimal change in capacitance with reference to ambient temperature. It is a suitable replacement for higher capacitance and larger footprint devices that fail to offer capacitance stability. Capacitance change is limited to ±30ppm/°C from −55°C to +150°C.

Driven by the demand for a more robust and reliable component, X8G dielectric capacitors were developed for critical applications where reliability and capacitance stability at higher operating temperatures are a concern.

These capacitors are widely used in automotive for under the hood and harsh environment as well as general high temperature applications.

In addition to commercial grade, automotive grade devices are available and meet Automotive Electronics Council's AEC-Q200 qualification requirements. Also available with flexible termination technology which inhibits the transfer of board stress to the rigid ceramic body, therefore mitigating flex cracks which can result in low IR or short circuit failures.

Benefits

- Operating temperature range of −55°C to +150°C
- Capacitance offerings ranging from 1.0pF to 0.10μF
- EIA 0603, 0805, 1206, 1210, 1812 and 2220 case sizes
- DC voltage ratings of 500V, 630V, 1 KV, 1.5 KV and 2 KV
- Extremely low ESR and ESL
- High thermal stability
- High ripple current capability
- No capacitance shift with voltage
- Negligible capacitance shift with respect to temperature
- No piezoelectric noise
- Lead (Pb)-Free, RoHS and REACH compliant

Applications

- High frequency power converters
- Wide bandgap (WBG), silicon carbide (SiC) and gallium nitride (GaN) systems
- Snubber (high dV/dT)
- Resonant circuits (LLC, Wireless Charging, etc.)
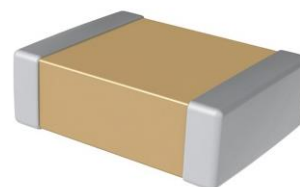- Timing
- Filtering

Built Into Tomorrow

© KEMET Electronics Corporation • One East Broward Boulevard Fort Lauderdale, FL 33301 USA • 954-766-2800 • www.kemet.com

C1112_X8G_HV_HT_SMD • 2/25/2025   1

Figure 71 : Capacitor Datasheet

Table 1A – Standard Termination Capacitance Range/Selection Waterfall (0603 – 2220 Case Sizes)

Product Availability and Chip Thickness Codes — See Table 2 for Chip Thickness Dimensions

Rated Voltage (VDC): C0603C / C0805C = 500 (C), 630 (B), 1,000 (D); C1206C / C1210C / C1812C / C2220C = 500 (C), 630 (B), 1,000 (D), 1,500 (F), 2,000 (G)

Capacitance	Cap Code	Tolerance	C0603C C	C0603C B	C0603C D	C0805C C	C0805C B	C0805C D	C1206C C	C1206C B	C1206C D	C1206C F	C1206C G	C1210C C	C1210C B	C1210C D	C1210C F	C1210C G	C1812C C	C1812C B	C1812C D	C1812C F	C1812C G	C2220C C	C2220C B	C2220C D	C2220C F	C2220C G
1.0 - 9.1 pF*	109 - 919*	B C D				DG	DG	DG	ED	ED	ED	ED	ED	FM	FM	FM	FM	FM	GB	GB	GB	GB	GB	JK	JK	JK	JK	JK
10 pF - 47pF*	100 - 470*	F G J K M				DG	DG	DG	ED	ED	ED	ED	ED	FM	FM	FM	FM	FM	GB	GB	GB	GB	GB	JK	JK	JK	JK	JK
11 pF	110	F G J K M				DG	DG	DG	ED	ED	ED	ED	ED	FM	FM	FM	FM	FM	GB	GB	GB	GB	GB	JK	JK	JK	JK	JK
12 pF	120	F G J K M				DG	DG	DG	ED	ED	ED	ED	ED	FM	FM	FM	FM	FM	GB	GB	GB	GB	GB	JK	JK	JK	JK	JK
13 pF	130	F G J K M				DG	DG	DG	ED	ED	ED	ED	ED	FM	FM	FM	FM	FM	GB	GB	GB	GB	GB	JK	JK	JK	JK	JK
15 pF	150	F G J K M				DG	DG	DG	ED	ED	ED	ED	ED	FM	FM	FM	FM	FM	GB	GB	GB	GB	GB	JK	JK	JK	JK	JK
16 pF	160	F G J K M				DG	DG	DG	ED	ED	ED	ED	ED	FM	FM	FM	FM	FM	GB	GB	GB	GB	GB	JK	JK	JK	JK	JK
18 pF	180	F G J K M				DG	DG	DG	ED	ED	ED	ED	ED	FM	FM	FM	FM	FM	GB	GB	GB	GB	GB	JK	JK	JK	JK	JK
20 pF	200	F G J K M				DG	DG	DG	ED	ED	ED	ED	ED	FM	FM	FM	FM	FM	GB	GB	GB	GB	GB	JK	JK	JK	JK	JK
22 pF	220	F G J K M				DG	DG	DG	ED	ED	ED	ED	ED	FM	FM	FM	FM	FM	GB	GB	GB	GB	GB	JK	JK	JK	JK	JK
24 pF	240	F G J K M				DG	DG	DG	ED	ED	ED	ED	ED	FM	FM	FM	FM	FM	GB	GB	GB	GB	GB	JK	JK	JK	JK	JK
27 pF	270	F G J K M				DG	DG	DG	ED	ED	ED	ED	ED	FM	FM	FM	FM	FM	GB	GB	GB	GB	GB	JK	JK	JK	JK	JK
30 pF	300	F G J K M				DG	DG	DG	ED	ED	ED	ED	ED	FM	FM	FM	FM	FM	GB	GB	GB	GB	GB	JK	JK	JK	JK	JK
33 pF	330	F G J K M				DG	DG	DG	ED	ED	ED	ED	ED	FM	FM	FM	FM	FM	GB	GB	GB	GB	GB	JK	JK	JK	JK	JK
36 pF	360	F G J K M				DG	DG	DG	ED	ED	ED	ED	ED	FM	FM	FM	FM	FM	GB	GB	GB	GB	GB	JK	JK	JK	JK	JK
39 pF	390	F G J K M				DG	DG	DG	ED	ED	ED	ED	ED	FM	FM	FM	FM	FM	GB	GB	GB	GB	GB	JK	JK	JK	JK	JK
43 pF	430	F G J K M				DG	DG	DG	ED	ED	ED	ED	ED	FM	FM	FM	FM	FM	GB	GB	GB	GB	GB	JK	JK	JK	JK	JK
47 pF	470	F G J K M				DG	DG	DG	ED	ED	ED	ED	ED	FM	FM	FM	FM	FM	GB	GB	GB	GB	GB	JK	JK	JK	JK	JK
51 pF	510	F G J K M				DG	DG	DG	ED	ED	ED	ED	ED	FM	FM	FM	FM	FM	GB	GB	GB	GB	GB	JK	JK	JK	JK	JK
56 pF	560	F G J K M				DG	DG	DG	ED	ED	ED	ED	ED	FM	FM	FM	FM	FM	GB	GB	GB	GB	GB	JK	JK	JK	JK	JK
62 pF	620	F G J K M				DG	DG	DG	ED	ED	ED	ED	ED	FM	FM	FM	FM	FM	GB	GB	GB	GB	GB	JK	JK	JK	JK	JK
68 pF	680	F G J K M				DG	DG	DG	ED	ED	ED	ED	ED	FM	FM	FM	FM	FM	GB	GB	GB	GB	GB	JK	JK	JK	JK	JK
75 pF	750	F G J K M				DG	DG	DG	ED	ED	ED	ED	EF	FM	FM	FM	FM	FM	GB	GB	GB	GB	GB	JK	JK	JK	JK	JK
82 pF	820	F G J K M				DG	DG	DG	ED	ED	ED	ED	EF	FM	FM	FM	FM	FM	GB	GB	GB	GB	GB	JK	JK	JK	JK	JK
91 pF	910	F G J K M				DG	DG	DG	ED	ED	ED	ED	EF	FM	FM	FM	FM	FM	GD	GD	GD	GD	GD	JK	JK	JK	JK	JK
100 pF	101	F G J K M	CG	CG	CG	DG	DG	DG	ED	ED	ED	ED	EF	FM	FM	FM	FM	FM	GD	GD	GD	GD	GD	JK	JK	JK	JK	JK
110 pF	111	F G J K M	CG	CG	CG	DG	DG	DG	ED	ED	ED	ED	EG	FM	FM	FM	FM	FM	GD	GD	GD	GD	GD	JK	JK	JK	JK	JK
120 pF	121	F G J K M	CG	CG	CG	DG	DG	DG	ED	ED	ED	EF	EG	FG	FG	FG	FM	FM	GD	GD	GD	GD	GD	JK	JK	JK	JK	JK
130 pF	131	F G J K M	CG	CG	CG	DG	DG	DG	ED	ED	ED	EF	EG	FG	FG	FG	FM	FM	GD	GD	GD	GD	GD	JK	JK	JK	JK	JK
150 pF	151	F G J K M	CG	CG	CG	DG	DG	DG	ED	ED	ED	EF	EG	FG	FG	FG	FM	FM	GD	GD	GD	GD	GD	JK	JK	JK	JK	JK
160 pF	161	F G J K M	CG	CG	CG	DG	DG	DG	ED	ED	ED	EF	EG	FG	FG	FG	FM	FM	GD	GD	GD	GD	GD	JK	JK	JK	JK	JK
180 pF	181	F G J K M	CG	CG	CG	DG	DG	DG	ED	ED	ED	EF	EG	FG	FG	FG	FM	FM	GD	GD	GD	GD	GD	JK	JK	JK	JK	JK
200 pF	201	F G J K M	CG	CG	CG	DG	DG	DG	ED	ED	ED	EF	FM	FG	FG	FG	FM	FM	GD	GD	GD	GD	GD	JK	JK	JK	JK	JK
220 pF	221	F G J K M	CG	CG		DG	DG	DG	ED	ED	ED	EG	EG	FG	FG	FG	FM	FM	GB	GB	GB	GB	GB	JK	JK	JK	JK	JK
240 pF	241	F G J K M	CG	CG		DG	DG	DG	ED	ED	ED	EG	EG	FG	FG	FG	FM	FM	GB	GB	GB	GB	GD	JK	JK	JK	JK	JK
270 pF	271	F G J K M	CG	CG		DG	DG	DG	ED	ED	ED	EG	EG	FG	FG	FG	FK	FK	GB	GB	GB	GB	GB	JK	JK	JK	JK	JK
300 pF	301	F G J K M	CG	CG		DG	DG	DN	ED	ED	EF			FG	FG	FG	FK	FK	GB	GB	GB	GB	GB	JK	JK	JK	JK	JK
330 pF	331	F G J K M	CG	CG		DG	DG	DN	ED	ED	EF	EG		FG	FG	FG	FK	FS	GB	GB	GB	GB	GB	JE	JE	JE	JE	JE
360 pF	361	F G J K M	CG	CG		DG	DG	DN	ED	ED	EF	EG		FG	FG	FG	FK	FS	GB	GB	GB	GB	GD	JE	JE	JE	JE	JE
390 pF	391	F G J K M	CG	CG		DG	DG	DN	ED	ED	EF	EG		FG	FG	FG	FK	FS	GB	GB	GB	GB	GD	JE	JE	JE	JE	JE
430 pF	431	F G J K M	CG	CG		DG	DG	DP	ED	ED	EF	EG		FG	FM	FM	FS	FS	GB	GB	GB	GB	GD	JE	JE	JE	JE	JE
470 pF	471	F G J K M	CG	CG		DG	DG	DP	ED	ED	EG	EG		FG	FM	FM	FS	FS	GB	GB	GB	GB	GD	JE	JE	JE	JE	JE
510 pF	511	F G J K M	CG	CG		DG	DG	DG	ED	ED	EG	EG		FG	FM	FM	FS	FS	GB	GB	GB	GD	GH	JK	JK	JK	JK	JK
560 pF	561	F G J K M	CG	CG		DG	DG	DG	ED	ED	EG	EG		FG	FM	FM	FS	FS	GB	GB	GB	GD	GH	JK	JK	JK	JK	JK
620 pF	621	F G J K M				DG	DG	DG	ED	ED	EG			FG	FM	FM	FS		GB	GB	GB	GD	GH	JK	JK	JK	JK	JK
680 pF	681	F G J K M	CG	CG		DG	DG	DG	ED	ED	EG			FG	FM	FM	FS	FS	GB	GB	GB	GD	GH	JE	JE	JE	JE	JK
750 pF	751	F G J K M				DG	DG	DG	ED	EF	EG			FG	FM	FM	FM		GB	GB	GB	GD	GK	JE	JE	JE	JE	JK
820 pF	821	F G J K M				DG	DG	DG	ED	EF	EG			FG	FM	FM	FM		GB	GB	GB	GD	GK	JE	JK	JK	JK	JK
910 pF	911	F G J K M				DN	DN		ED	EF	EG			FM	FM	FM	FY		GB	GB	GB	GH	GM	JE	JK	JK	JK	JK
1,000 pF	102	F G J K M				DN	DN		ED	EF	EG			FM	FM	FM	FY		GB	GB	GB	GH	GM	JE	JK	JK	JK	JK
1,100 pF	112	F G J K M				DN	DN		EF	EG	ED			FM	FK	FK	FS		GB	GB	GB	GH	GO	JE	JK	JK	JK	JK
1,200 pF	122	F G J K M				DN	DN		EF	EG	ED			FM	FK	FK	FS		GB	GB	GB	GH	GO	JE	JK	JK	JK	JK

Figure 72 : Capacitor Voltage Datasheet

The KEMET X8G dielectric was selected for its exceptional properties. This Class 1 ceramic type guarantees remarkable thermal stability, with a capacitance variation limited to ±30 ppm/∘C across a wide range from −55∘C to +150∘C. Even more importantly for a high-voltage resonant circuit, capacitors with X8G dielectric show no significant change in capacitance with varying applied voltage. This characteristic is fundamental for maintaining the circuit's resonant frequency stable and predictable, even in the presence of large voltage oscillations across the capacitor.

From Figure 71, it can be seen how this capacitor model can support voltages from 500 up to 2 Kilovolts. In particular, Figure 72 shows how for a capacitance of 300pF and 43pF, the allowable voltages are 1.5 KV and 2KV respectively, values significantly higher than the circuit voltage of 845.95V. The parallel connection, furthermore, in addition to achieving the desired capacitance value, limits the current flowing into the single capacitor.

The same research was conducted for inductors. In this case, what needs to be considered is no longer a voltage but rather the current to which the inductor is subjected.

Regarding this aspect, the material from which the inductor is made must be considered. At a frequency of 1 MHz, the losses associated with traditional ferromagnetic materials become considerable. These losses are primarily due to hysteresis and eddy currents. Both increase drastically with frequency. An inductor with an unsuitable core would overheat intolerably, drastically reducing efficiency and potentially destroying the component. For a simulated current of 5 Amperes, a ferromagnetic core could easily reach saturation, especially if the required inductance is significant. Saturation causes the inductance to drop sharply and increases losses.

To overcome these problems, the choice can fall on air-core inductors or those with a ferrite core. In the first case, regardless of the current, there will be no saturation and thus no core losses for good efficiency at high frequencies, also maintaining a tight resonance at the expense of a larger physical size of the component. In the second case, the ferrite core allows for high-frequency application with much lower losses and saturation risk, also considering reduced dimensions.

Therefore, for an accurate component selection that respects the design specifications, what needs to be observed is the saturation current and its behavior at the considered frequency. In particular, an evaluation is expressed regarding the Q-factor.

The Q-factor is a fundamental metric for describing the performance of a reactive component (inductor or capacitor) or a resonant circuit. It indicates how "efficient" a component or circuit is at storing energy compared to how much it dissipates in one cycle. A higher Q-factor (50-100) means lower losses and a "sharper" or more selective resonance.

For a real inductor, the Q-factor is defined as the ratio of its inductive reactance to its equivalent series resistance (ESR).

$$Q_L = \frac{2 \cdot \pi \cdot f \cdot L}{R_S} \qquad (24)$$

Where the resistance RS is the inductor's series resistance, which includes both the DC resistance of the windings and the AC losses converted into an equivalent resistance, which is why it increases with increasing frequency.

From Table 2, we observe a current in the inductor of 5.08 Amperes for an inductance value of 26.8µH.

The choice fell on ferromagnetic core SMD inductors, specifically the IHLP-5050FD-5A series (Vishay Dale). These inductors are characterized by a composite metal alloy core and are designed for high-current power applications, offering an ultra-low profile and excellent magnetic shielding.

Given that a single commercial inductor would hardly have provided exactly the theoretical value of 26.84 µH, a series combination of five commercially available inductors was chosen: four inductor IHLP-5050FD-5A of 5.6 µH and an IHLP-5050FD-5A of 4.7 µH. The sum of the nominal inductances of these five components offers a combined value of 27.1 µH, a little bit more to the required theoretical value.

This choice of using 5 inductors in series was made to distribute the voltage almost uniformly on each of them and to have a drop that the components can bear.

With this total inductance value it will be necessary to observe whether the resonance condition will still be respected. If not, it will be necessary to recalculate and adjust the working frequency to ensure that there is the same power transfer.

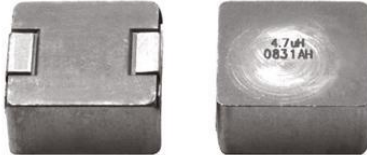The datasheet from the Mouser Electronics catalog is as follows:

IHLP® Automotive Inductors, High Temperature (155 °C) Series

LINKS TO ADDITIONAL RESOURCES

3D Models   Design Tools

FEATURES

- High temperature, up to 155 °C
- Shielded construction
- Excellent DC/DC energy storage up to 1 MHz to 2 MHz. Filter inductor applications up the SRF (see Standard Electrical Specifications table).
- Lowest DCR/µH, in this package size
- Handles high transient current spikes without saturation
- Ultra low buzz noise, due to composite construction
- AEC-Q200 qualified
- IHLP design; PATENT(S): www.vishay.com/patents
- Material categorization: for definitions of compliance please see www.vishay.com/doc?99912

AUTOMOTIVE GRADE
Pb-free
RoHS COMPLIANT
HALOGEN FREE
GREEN (5-2008)

APPLICATIONS

- Engine and transmission control units
- Diesel injection drivers
- DC/DC converters for entertainment / navigation systems
- Noise suppression for motors: windshield wipers / power seats / power mirrors / heating and ventilation blower / HID lighting
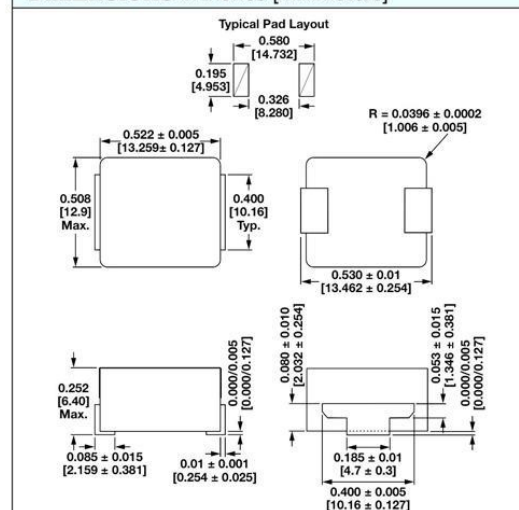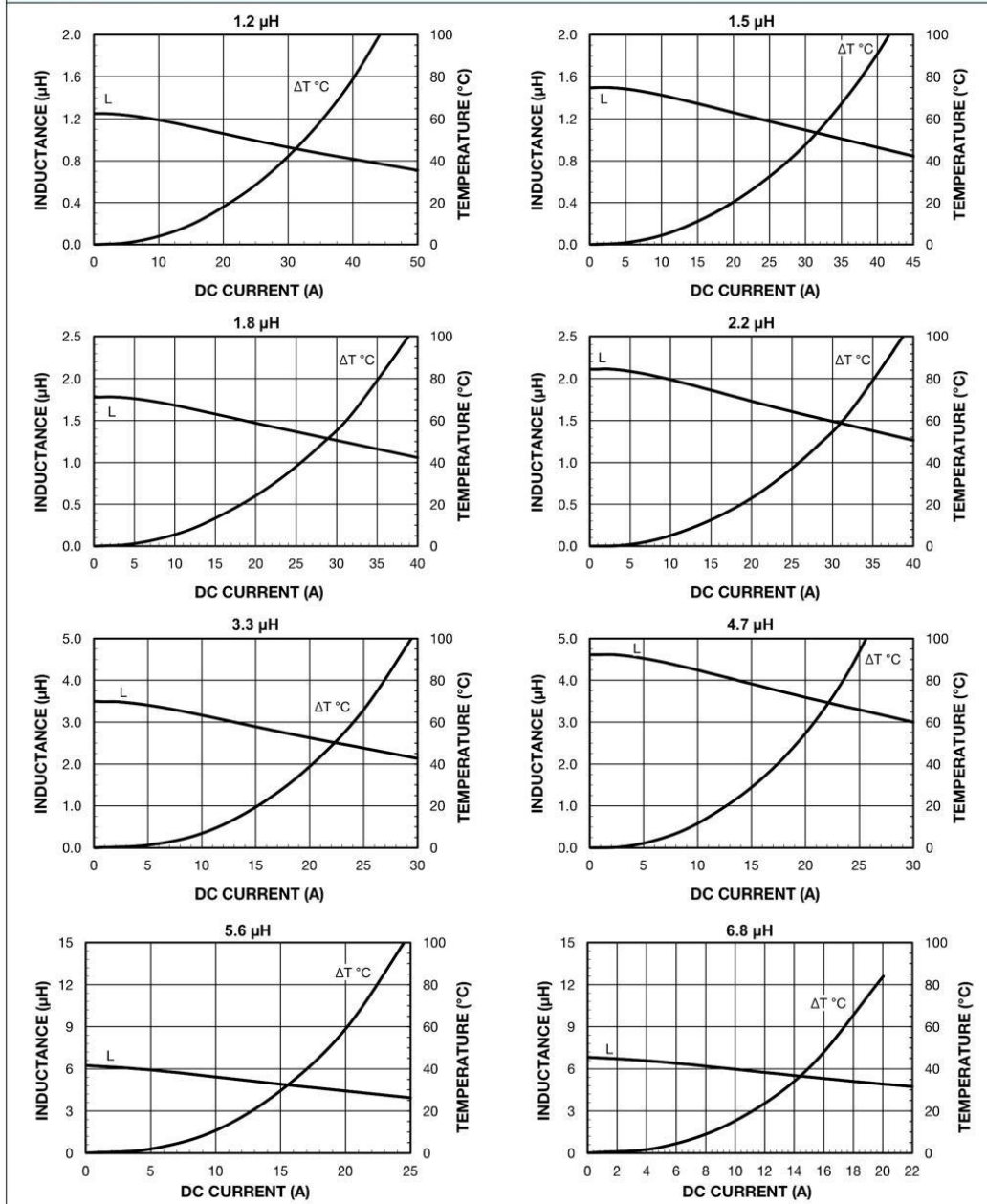- LED drivers

STANDARD ELECTRICAL SPECIFICATIONS

L₀ INDUCTANCE ± 20 % AT 100 kHz, 0.25 V, 0 A (µH)	DCR TYP. 25 °C (mΩ)	DCR MAX. 25 °C (mΩ)	HEAT RATING CURRENT DC TYP. (A) [1]	SATURATION CURRENT DC TYP. (A) [2]	SRF TYP. (MHz)
0.22	0.73	0.81	66	68	113
0.33	0.83	0.92	62	44	79.9
0.47	1.05	1.16	54	42	65.6
0.56	1.24	1.33	50	32	63.1
0.68	1.33	1.42	40	29	48.1
1.0	1.65	1.77	40	26	33.4
1.2	1.98	2.12	29	24.5	32.0
1.5	2.4	2.57	27.5	23.5	29.2
1.8	2.75	2.94	26	22.5	25.9
2.2	3.43	3.67	25.5	21.5	23.3
3.3	5.08	5.44	20.2	16.7	17.8
4.7	7.41	7.93	19.7	18.5	15.8
5.6	8.51	9.11	16.8	14.2	12.3
6.8	11.3	12.09	14.9	14.1	13.4
7.8	12.6	13.48	13.5	8.5	13.4
8.2	13.2	14.12	13.2	7.6	10.3
10	16.60	17.76	12.1	7.8	10.7
12	19.00	20.33	11.4	7.9	9.5
15	24.00	25.68	10.1	7.7	8.8
22	31.30	33.49	9.0	6.3	6.6
33	46.03	49.25	6.9	6.2	5.5
47	77.00	79.60	5.6	4.5	3.9
82	141.10	150.98	3.7	3.7	3.0
100	175.00	187.0	3.1	4.3	2.8

Notes
- All test data is referenced to 25 °C ambient
- Operating temperature range -55 °C to +155 °C
- The part temperature (ambient + temp. rise) should not exceed 155 °C under worst case operating conditions. Circuit design, component placement, PWB trace size and thickness, airflow and other cooling provisions all affect the part temperature. Part temperature should be verified in the end application
- Rated operating voltage (across inductor) = 75 V
- [1] DC current (A) that will cause an approximate ΔT of 40 °C
- [2] DC current (A) that will cause L₀ to drop approximately 20 %

DIMENSIONS in inches [millimeters]

Typical Pad Layout
0.580 [14.732]
0.195 [4.953]
0.326 [8.280]
R = 0.0396 ± 0.0002 [1.006 ± 0.005]
0.522 ± 0.005 [13.259± 0.127]
0.508 [12.9] Max.
0.400 [10.16] Typ.
0.530 ± 0.01 [13.462 ± 0.254]
0.080 ± 0.010 [2.032 ± 0.254]
0.053 ± 0.015 [1.346 ± 0.381]
0.000/0.005 [0.000/0.127]
0.000/0.005 [0.000/0.127]
0.252 [6.40] Max.
0.085 ± 0.015 [2.159 ± 0.381]
0.01 ± 0.001 [0.254 ± 0.025]
0.185 ± 0.01 [4.7 ± 0.3]
0.400 ± 0.005 [10.16 ± 0.127]

Figure 72 : Inductor Datasheet

70

PERFORMANCE GRAPHS

Figure 72 : Inductor Datasheet, Current Vs Inductance

71

PERFORMANCE GRAPHS: INDUCTANCE AND Q VS. FREQUENCY
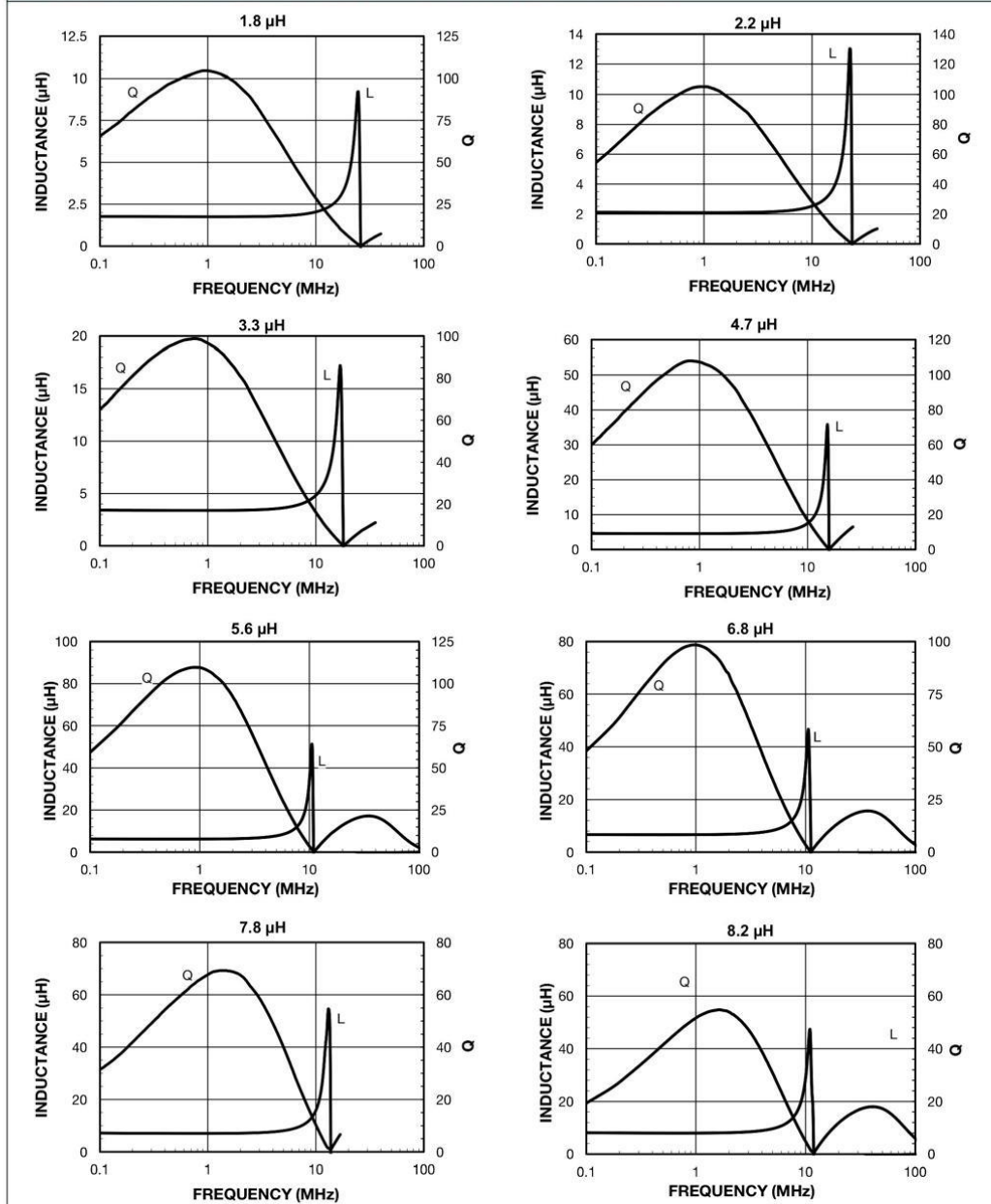
Figure 73 : Inductor Datasheet, Q-factor Vs Frequency

72

The analysis of the technical specifications of both inductors confirmed their suitability. Regarding the peak current of 5 Amperes expected in the circuit, the 5.6 µH inductor has a saturation current of 14.2 A, while the 4.7 µH inductor has a saturation current of 18.5 A, as shown in Figure 72. Since the circuit's peak current is below the saturation limits of both components, it is ensured that the overall inductance will not undergo significant reductions due to core saturation, preserving the linearity of operation, as shown in the graphs in Figure 73.

Regarding the quality factor Q, from consulting the specific graphs provided in the datasheet of the IHLP-5050FD-5A, it was possible to estimate the Q-factor of each inductor at the operating frequency of 1 MHz the 5.6 µH inductor has an approximate Q-factor of 110, also the 4.7 µH inductor shows a Q-factor of about 100-110 at 1 MHz When inductors are connected in series, the Q-factor of the combined system will be dominated by the component with the lowest Q-factor and the sum of their equivalent resistances. In this case the values are all the same indicating that energy losses within the inductors will be contained, contributing significantly to the overall efficiency of the resonant circuit.

Another component choice concerns the MOSFETs for conversion on the charger side. As seen in the simulation, to obtain an output frequency of 1MHz from the Half-Bridge inverter, the driving clock for switching the MOSFETs on and off is also the same. At this frequency, from Table 2, the current flowing through them is 5 A with a voltage of 12.21 V.

The choice of devices falls on components that allow for the correct resonance and provide the appropriate voltage to the circuit in question for the desired power transmission. As explained in Chapter 2, there are devices with high switching speeds, low losses, and maximum efficiencies for power circuits. These devices are the GaN transistors, power semiconductors made with Gallium Nitride instead of the more common Silicon (Si). Among the advantages obtained from their use in applications like the one under study are:

Low Gate Charge: They require less charge to turn on and off, which reduces losses in the gate drive circuit and allows for much higher switching speeds.

Minimal Parasitic Capacitances: They have much smaller intrinsic capacitances compared to silicon MOSFETs, reducing capacitive losses during switching.

Absence of Body Diode Reverse Recovery: This is a huge advantage in many power converter topologies, such as the Half-Bridge. Silicon MOSFETs have an intrinsic diode (body diode) with a significant reverse recovery charge. When this diode conducts and then turns off, an energy loss occurs (and often voltage/current spikes) due to the removal of this stored charge. GaN FETs, by not having a comparable body diode in terms of recovery behavior (or by having a "loss-less" recovery behavior), virtually eliminate this source of loss, drastically improving efficiency and allowing for much shorter dead times.

They are also excellent in terms of:

Breakdown Voltage: GaN has a much higher critical electric field for breakdown than silicon, which means it can withstand higher voltages per unit material thickness. This leads to more compact devices for a given nominal voltage.

High Temperature Resistance: Although the device you have chosen has a maximum junction temperature of 175°C, GaN as a material can intrinsically operate at higher temperatures than silicon, although package limitations may affect this.

Robustness: Many commercial GaN FETs are "normally-off," meaning they are off in the absence of gate voltage, a preferred safety feature for most power applications.

With respect to the design purposes, the search for commercially available GaN FETs ended with the choice of being able to use an evaluation board in which the half-bridge converter connection is already implemented.

These evaluation boards are in a monolithic half bridge topology with onboard gate drives, featuring the EPC2103 eGaNIC (Enhancementmode Gallium Nitride Integrated Circuits). The purpose of these evaluation boards is to simplify the evaluation process of these monolithically integrated eGaN FETs by including all the critical components on a single board that can be easily connected into any existing converter. The evaluation board is 2" x 2" and contains one eGaNIC in half bridge configuration using the Texas Instruments LM5113 gate driver, supply and bypass capacitors. The board contains all critical components and layout for optimal switching performance and has additional area to add buck output filter components on board. There are also various probe points to facilitate simple waveform measurement and efficiency calculation. A complete block diagram of the circuit is given in Figure 74 [13].
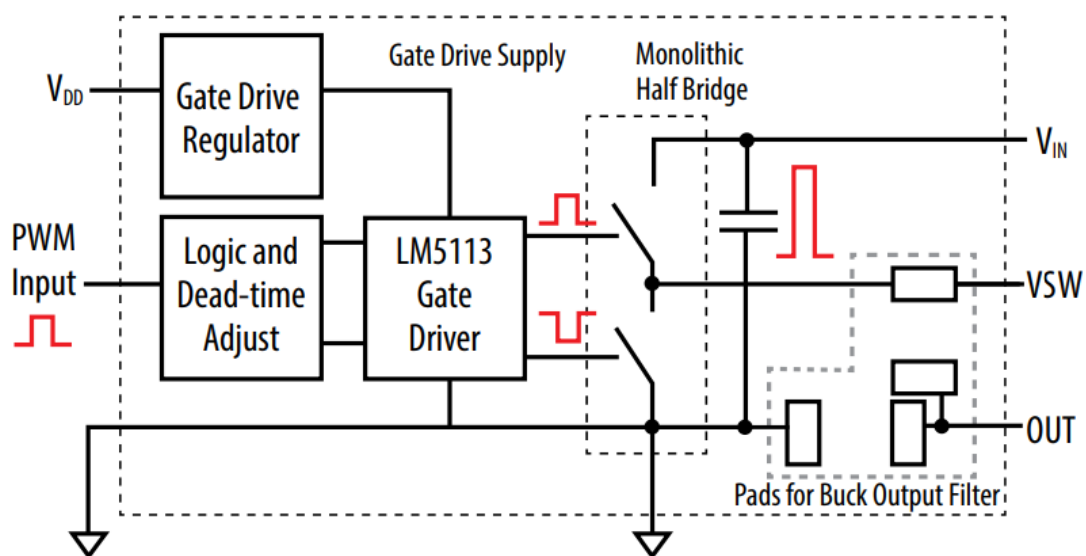

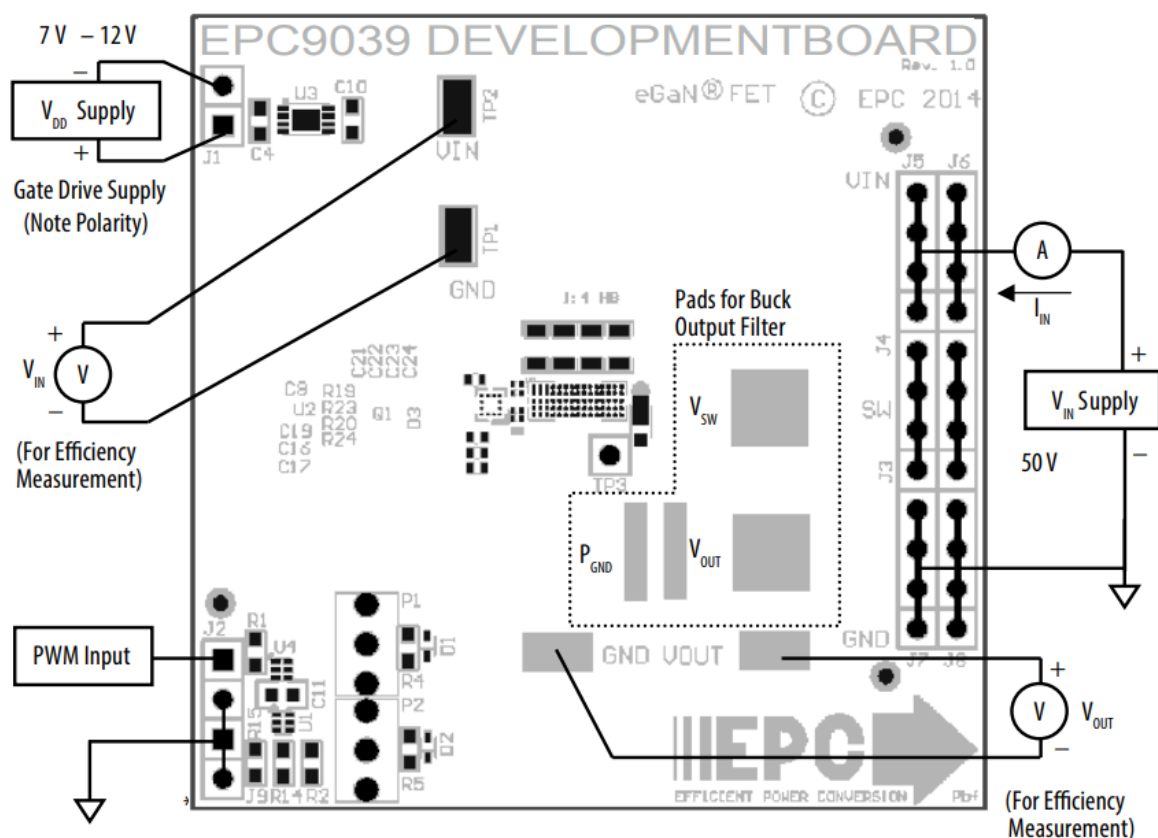Figure 74 : Block Diagram of Evaluation Board

Figure 75 : Proper Connection and Measurement Setup

The voltage and current level references on the board devices are given in Table 3.

Symbol	Parameter	Conditions	Min	Max	Units
V_{DD}	Gate Drive Input Supply Range		7	12	V
V_{IN}	Bus Input Voltage Range			64*	V
V_{OUT}	Switch Node Output Voltage			80	V
I_{OUT}	Switch Node Output Current			17*	A
V_{PWM}	PWM Logic Input Voltage Threshold	Input 'High'	3.5	6	V
		Input 'Low'	0	1.5	V
	Minimum 'High' State Input Pulse Width	V_{PWM} rise and fall time < 10ns	50		ns
	Minimum 'Low' State Input Pulse Width	V_{PWM} rise and fall time < 10ns	100#		ns

Table 3 : Voltage and current of the evaluation board

As can be seen from Table 3, the board provides a voltage of 80 V on the FET and a current that can flow through it of 17 A. These values are significantly higher than those predicted in the circuit simulations and reported in Table 2.

The last component selection made is for the diodes in the rectifier on the secondary side of the circuit. From Table 2, it is seen that during conduction, the diodes are traversed by a current of approximately 3.5 A, while during the off-state, the peak voltage they must withstand to block the current is a negative value of 5.5 V.

A possible type of diode capable of meeting these conditions is the Schottky diode. Compared to a classic semiconductor diode, the Schottky diode exhibits no recovery losses, which allows for much faster switching and thus makes it suitable for frequencies like those considered in this discussion. Furthermore, they possess a lower forward voltage (0.3 – 0.6 V), which reduces conduction losses and improves conversion efficiency.

From the consultation of the MOUSER catalog, the component's datasheet is obtained, which shows a forward current of 4A and a minimum reverse voltage of 20 V, both sufficient for the design purposes.

VISHAY.

Surface-Mount Schottky Barrier Rectifier

SMC (DO-214AB)

Cathode ○———▷|———○ Anode

LINKS TO ADDITIONAL RESOURCES

3D
3D Models

FEATURES

- Low profile package
- Ideal for automated placement
- Guardring for overvoltage protection
- Low power losses, high efficiency
- Very low forward voltage drop
- High surge capability
- Meets MSL level 1, per J-STD-020, LF maximum peak of 260 °C
- AEC-Q101 qualified available
  - Automotive ordering code: base P/NHE3 or P/NHM3
- Material categorization: for definitions of compliance please see www.vishay.com/doc?99912

AUTOMOTIVE GRADE
Available

RoHS
COMPLIANT

HALOGEN
FREE
Available

TYPICAL APPLICATIONS

For use in low voltage high frequency inverters, freewheeling, DC/DC converters, and polarity protection applications.

MECHANICAL DATA

Case: SMC (DO-214AB)
Molding compound meets UL 94 V-0 flammability rating
Base P/N-E3 - RoHS-compliant, commercial grade
Base P/N-M3 - halogen-free, RoHS-compliant, commercial grade
Base P/NHE3_X - RoHS-compliant and AEC-Q101 qualified
Base P/NHM3_X - halogen-free, RoHS-compliant, and AEC-Q101 qualified
("_X" denotes revision code e.g. A, B, ...)

Terminals: matte tin plated leads, solderable per J-STD-002 and JESD 22-B102
E3, M3, HE3, and HM3 suffix meets JESD 201 class 2 whisker test

Polarity: color band denotes the cathode end

PRIMARY CHARACTERISTICS	
$I_{F(AV)}$	4.0 A
V_{RRM}	20 V, 30 V, 40 V
I_{FSM}	150 A
V_F	0.31 V, 0.35 V
T_J max.	125 °C
Package	SMC (DO-214AB)
Circuit configuration	Single

MAXIMUM RATINGS (T_A = 25 °C unless otherwise noted)

PARAMETER	SYMBOL	SL42	SL43	SL44	UNIT
Device marking code		SL2	SL3	SL4	
Maximum repetitive peak reverse voltage	V_{RRM}	20	30	40	V
Maximum RMS voltage	V_{RMS}	14	21	28	V
Maximum DC blocking voltage	V_{DC}	20	30	40	V
Maximum average forward rectified current [1] at T_L (fig. 1)	$I_{F(AV)}$	4.0			A
		8.0			
Peak forward surge current 8.3 ms single half sine-wave superimposed on rated load	I_{FSM}	150			A
Operating junction temperature range	T_J	-55 to +125			°C
Storage temperature range	T_{STG}	-55 to +150			°C

Note
[1] PCB mounted 0.55" x 0.55" (14 mm x 14 mm) copper pad areas, T_L = 90 °C

Figure 76 : Schottky diode datasheet

77

Once the search for commercially available components is concluded, and after making the necessary considerations regarding their number and arrangement to satisfy the design specifications concerning the voltages and currents involved, it is appropriate to simulate the circuit's behavior with respect to these choices.

Primarily, it is recalled the use of 5 inductors in series and 4 capacitors in parallel for the resonant circuit.

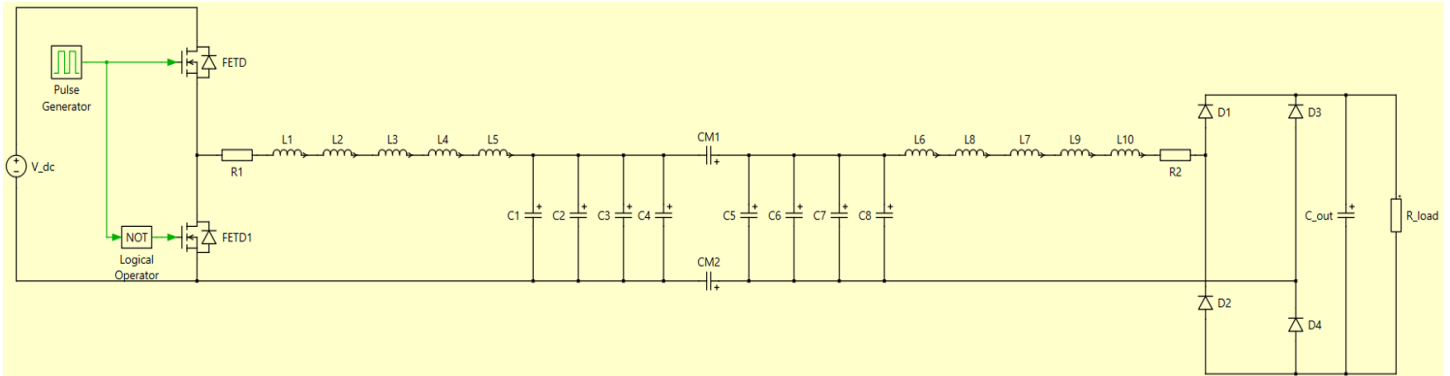The simulations are therefore performed for the following circuit shown in Figure 77.

Figure 77 : Circuit scheme with the series and parallel of inductors and capacitors with commercial value

During the simulation phase with this new configuration, the focus must be on whether the resonance condition continues to be met with the new total inductance and capacitance values. In particular, with a series inductance value of 27.1μH, it is observed that this condition is no longer met, resulting in a failure to transfer power. It is therefore necessary to adjust the circuit's operating frequency by recalculating it, considering the new values.

The latter is derived by inverting formula (11), obtaining the new operating frequency and thus the new resonance condition. Obviously, the same frequency is necessary for the MOSFETs' commutation.

The value is:

Fsw = 0.9956 MHz = 955.6 KHz

The following results are obtained from the simulation starting from the electrical quantities on the inductors.

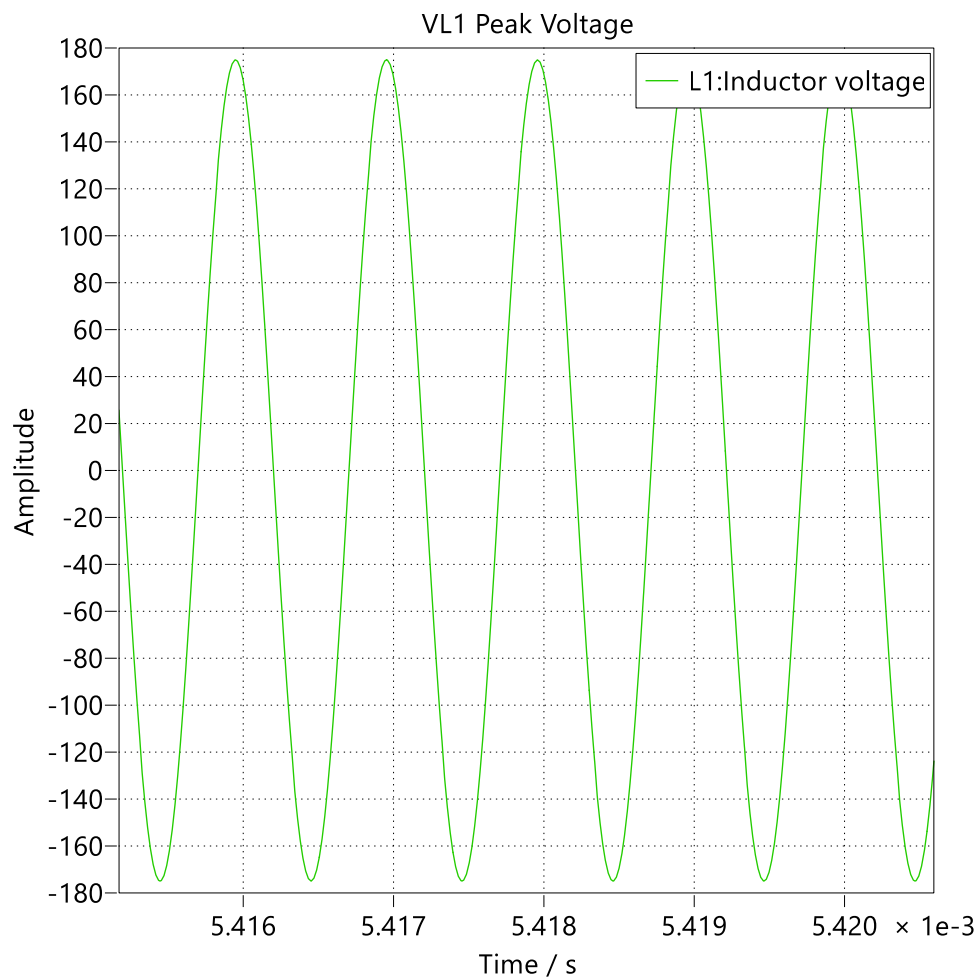Figure 78 : Peak Voltage on the first inductor of the series

Figure 79 : Value of the Peak Voltage on the first of the series

As can be seen from Figures 78 and 79, the voltage value is much lower compared to that of the previous circuit. This is because with the series connection, the voltage is distributed across each inductor, and in this case, it is divided approximately by 5, having 4 equal values and one very close. This avoids excessively high dissipation relative to the current flowing through them. Indeed, the peak current remains at 4.98A, unchanged from the previous one, as visible in Figures 80 and 81.
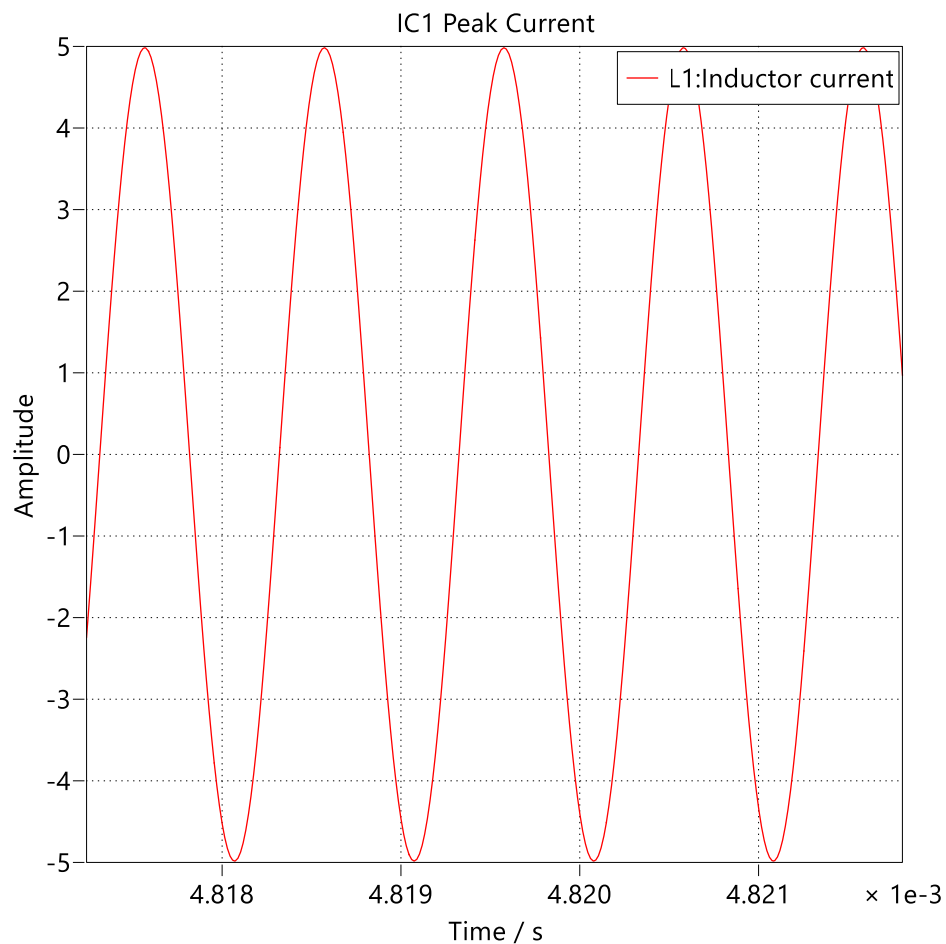

Figure 80 : Peak Current on the first inductor of the series

Data					
Name	Cursor 1	Cursor 2	Delta	Max	RMS
Time	0.00278563	0.00278663	1.00542e-06		
∨ IC1 Peak Current ☑					
L1:Inductor current ⌃ ☑	4.98132	4.98098	-0.000347352	4.98147	3.52753

Figure 81 : Value of the Peak Current on the first of the series

The same happens for capacitors in parallel. In this case, however, the current is distributed between the branches, assuming lower values visible in Figures 82 and 83.
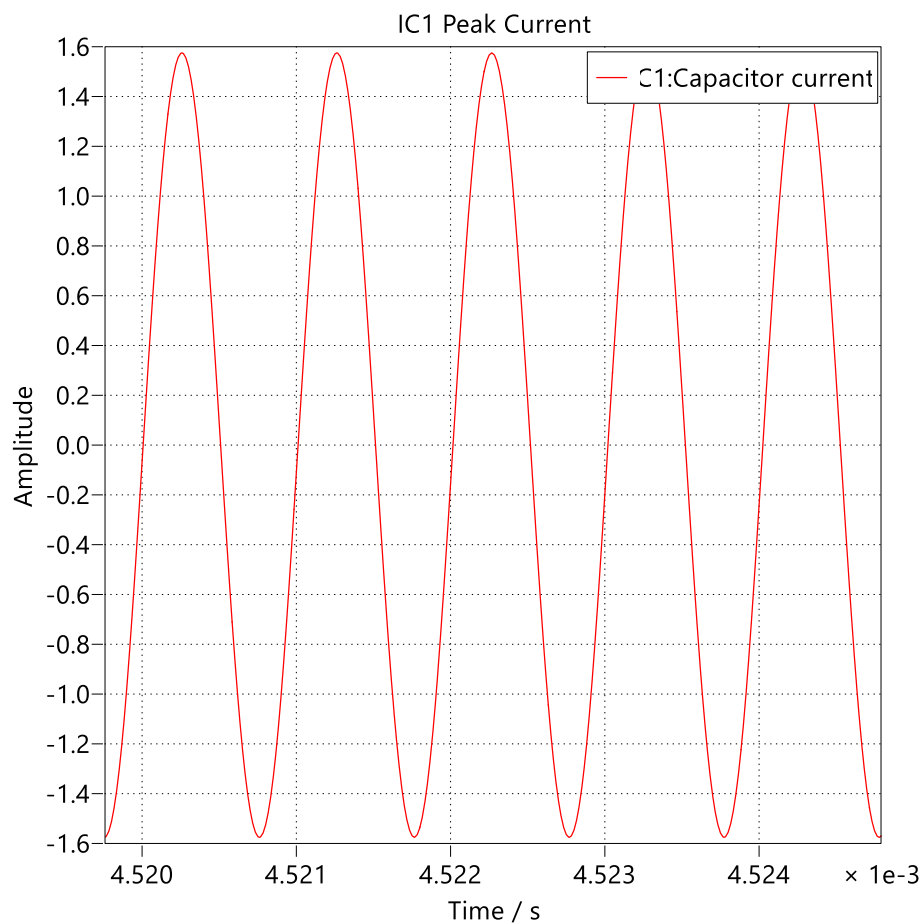

Figure 82 : Peak Current on the first capacitor of the parallel

Name	Cursor 1	Cursor 2	Delta	Max	RMS
Time	0.00541696	0.00541796	1.00442e-06		
∨ VC1 Peak Current					
C1:Capacitor current	0.0164815	0.0164815	-1.30451e-09	1.57533	1.11497

Figure 83 : Value of the Peak Current on the first of the parallel

It can be seen how the current is distributed and takes on a value approximately three times smaller since the current on the last capacitance of lower value is almost negligible.

81

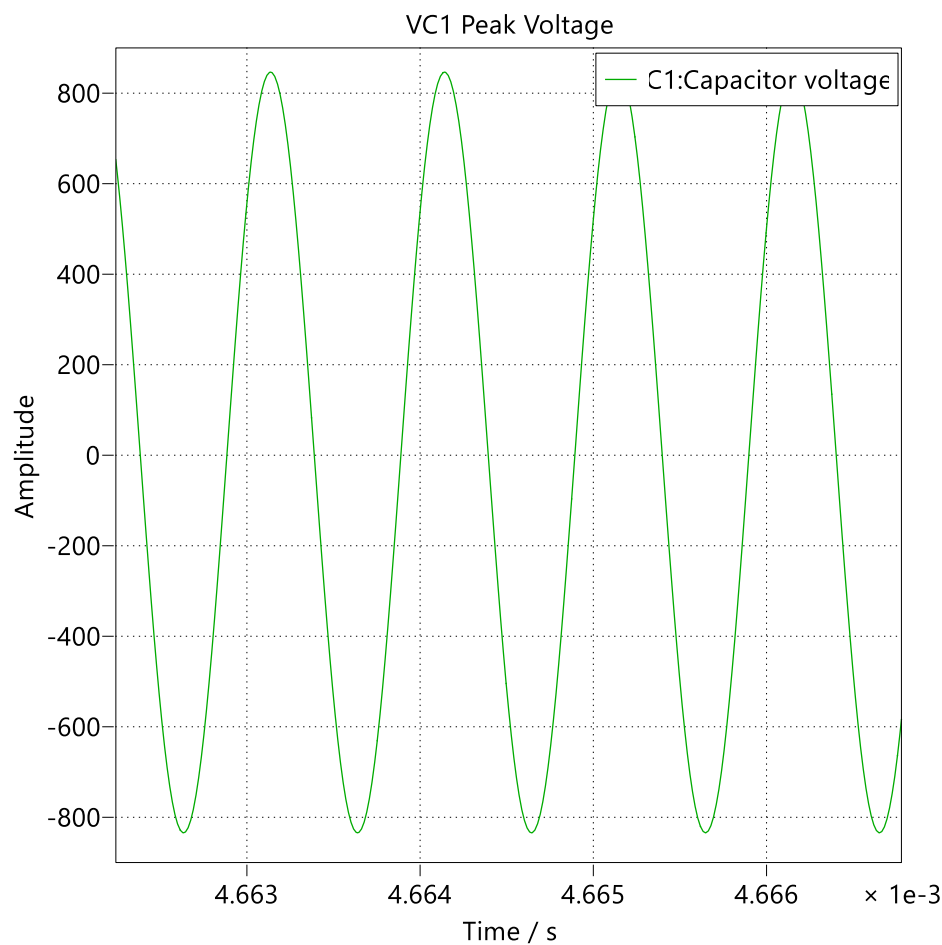The voltage on the parallel is equal to 846.28 V as previously simulated.

Figure 84 : Peak Voltage on the first capacitor of the parallel

Figure 85 : Value of the Peak Voltage on the first of the parallel

The magnitudes are therefore consistent with previous simulations, even having established a new resonance condition. Furthermore, the circuit's efficiency has been improved in terms of dissipation and component operation with the decrease of voltage and current on inductors and capacitors, respectively.

What needs to be observed, therefore, is the power transfer with this new circuit configuration and resonance condition. The result is visible in Figure 86.

Figure 86 : Transmitted Power on the resistor load

Figure 87 : Value of the Transmitted Power on the resistor load

The transmitted power value is the same as in the previous simulation, considering the theoretical component values. It can therefore be concluded that the selection made from the catalog and the circuit arrangement provides an excellent result based on the theoretical and design specifications.

Once the key components of the resonant circuit (the 5 series inductors and 4 parallel capacitors) have been defined and selected, a preliminary estimation of the physical dimensions that the PCB dedicated to this section of the circuit might take can be made. This phase is crucial not only for space planning but also for anticipating challenges related to high-frequency layout.

For the resonant circuit, the arrangement of components on the PCB is dictated by the need to minimize parasitic inductances and capacitances, which become critical at a frequency of 1 MHz. The five inductors can be arranged in a linear configuration, as close as possible to each other to minimize the length of the interconnecting traces and, consequently, the resistance and total parasitic inductance of the series. Between one inductor and the next, a minimum space for solder pads and vias would be foreseen, estimated at approximately 1-2 mm. [13]

The four capacitors, operating in parallel, can be placed close to each other and near the inductor chain, forming a "capacitive bank." This grouping minimizes the current loop and the parasitic inductances associated with the parallel connection.

From the component datasheets, the following dimensions are obtained: Inductor 13.462 mm x 12.9 mm x 6.4 mm, Capacitor 3.20 mm x 1.6 mm x 1.6 mm.

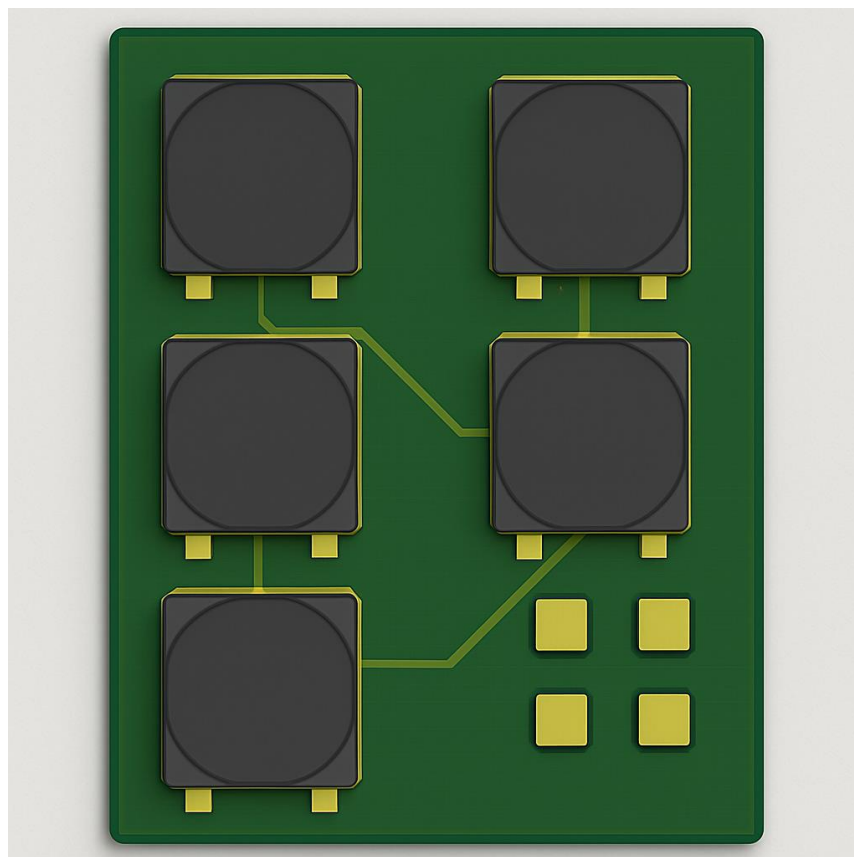A possible configuration is indicated in the following Figure 88.

Figure 88 : Possible configuration of the resonant circuit on the board

The largest footprint is given by the inductors. Therefore, the presumed dimensions of the board can be calculated based on the established configuration.

Length = 3 x 13.462 mm = 40.38 mm

Width = 2 x 13.462 mm = 26.924 mm

The 4 capacitors, being smaller in size, fit within the space created by the inductors. Allowing for minimal space for connections between components and for the addition of connectors, for example, for the converter, the total board dimensions can reach approximately 50 mm x 50 mm.

In terms of height, the dimensions are also dictated by the inductors, with a measurement of 6.4 mm.

This dimensional estimate is only the starting point. For optimal operation at 1 MHz, the PCB's realization will require careful layout design.

The traces carrying the resonant currents, in fact, (approximately 5 A peak) will need to be as short and wide as possible to minimize their resistance and parasitic inductance, thereby reducing losses and voltage drops.

The use of a solid ground plane on one layer of the PCB (ideally a multi-layer PCB) will be fundamental to provide a low-impedance current return path and to shield the circuit from electromagnetic interference (EMI).

Despite the components being chosen for low losses, the dissipated power, especially in the inductors and capacitors, will require adequate copper area for heat dissipation.

This preliminary estimate provides a solid basis for the next design phase, which will involve the realization of a complete PCB layout using dedicated software (e.g., KiCad, Altium Designer). This process will include the precise definition of footprints, trace routing, the addition of connections between layers, the management of ground/power planes, and integration with other system components (such as the inverter's GaNFET's, their gate drivers, the secondary rectifier, and connectors). The PCB design phase will be crucial for translating simulated performance into an efficiently functioning physical prototype.

Chapter 6

Conclusions and future developments

The present work discussed in the preceding chapters addressed the design, conceptual implementation, and evaluation of a Capacitive Wireless Power Transfer (CPT) system, with the specific aim of developing an innovative solution for wireless charging with high efficiency and compactness. The project is situated within the broader context of the evolution of Wireless Power Transfer (WPT), recognizing CPT as a promising and versatile alternative, capable of overcoming some of the intrinsic limitations of traditional wired charging systems and Inductive Power Transfer (IPT).

The research journey began with a theoretical analysis of the fundamental principles of WPT, providing the necessary conceptual foundations for subsequent design and thoroughly examining the essential functional blocks of the system.

The focus then shifted to the basic study of a capacitive power transmission circuit, proceeding to examine, calculate, and simulate the components and quantities involved for each individual part. The main aspect was to move from initial design hypotheses, such as the size of the charging device and the transmitted power, to the validation of operation through existing market components during the simulation phase. Starting from the calculation of the coupling capacitance to achieve a specific transmitted power value, the conversion circuits on both sides were dimensioned, in addition to, the resonant LC circuits.

For the transmitter-side conversion, the choice of a Half-bridge inverter with Gallium Nitride transistors was motivated by the exceptional properties of these semiconductors, such as the high switching speed necessary to operate at frequencies in the MHz range (target 1 MHz), low conduction losses, and, in particular, the absence of body diode reverse recovery phenomena. These characteristics proved fundamental for effective high-frequency operation, minimizing switching losses and maximizing the efficiency of the input converter.

A crucial aspect of the project was the careful dimensioning and selection of components for the resonant LC circuit and for the secondary-side rectifier. For the resonant circuit, thorough research into commercial components led to the selection of 5 series inductors (with a footprint of 13.462 mm x 12.9 mm) and 4 parallel capacitors. This configuration allowed not only to achieve the desired resonant values but also to distribute the voltage and current among the individual components. In particular, it was observed that the voltage is divided across each inductor and the current across the capacitors, significantly reducing the stress on individual elements compared to a solution with single components. The peak current was maintained at 4.98 A, consistent with design requirements, avoiding excessive dissipation.

For the secondary-side rectifier, the use of Schottky diodes proved to be a winning choice. Simulations confirmed their suitability, showing that they are traversed by a peak current of approximately 3.5 A and withstand a peak inverse voltage of only 5.5 V. This condition, combined with their low forward voltage drop and, above all, their almost zero reverse recovery time, guaranteed negligible switching losses and high efficiency in AC/DC conversion at 1 MHz. This allowed for power transmission slightly above the set design value of 10 Watts.

The simulations conducted with real components and the adapted configuration robustly validated the design choices. Despite the need to slightly recalculate the resonant frequency due to component tolerances and commercial specifications, it was demonstrated that the circuit is capable of operating effectively with the new resonance condition. The most significant result was the unaltered maintenance of the transmitted power value compared to the initial theoretical predictions, confirming that the choice of catalog components and the circuit arrangement provide an excellent result based on the project specifications.

Finally, the preliminary estimation of the PCB dimensions for the resonant circuit section highlighted the feasibility of a compact design. Considering the footprint of the inductors as the predominant factor, the total board dimension was estimated to be approximately 50 mm x 50 mm, with a maximum height of 6.4 mm dictated by the inductors.

The work carried out in this thesis lays solid foundations for further research and development in the field of CPT, proposing several promising directions. The next step will be the fabrication of a physical prototype of the system. This will allow for the validation of simulated performance under real operating conditions, measurement of actual efficiencies, and addressing practical challenges such as electromagnetic interference and unforeseen parasitic couplings. To improve performance, the implementation of an active control system, based on microcontrollers, could also be a subject of study. This would allow for dynamic regulation of the inverter's frequency, phase, or duty cycle. This would improve the system's robustness against load variations, capacitive coupler misalignments, and environmental fluctuations, maximizing efficiency in real-time.

In conclusion, this thesis work demonstrated the feasibility of an innovative approach to CPT, leveraging the potential of GaN semiconductors and a sound selection of resonant components to operate at high frequencies and achieve high levels of efficiency. The obtained results pave the way for the realization of more compact, efficient, and versatile wireless charging systems, contributing to the advancement of a technology that promises to transform how devices and vehicles are powered.

References

[1] *https://www.strategicmp.it/2024/09/10/wireless-power-transmission-strategic-report/*

[2] *https://www.agendadigitale.eu/infrastrutture/wireless-power-transmission-rivoluzione-energetica-senza-fili-in-arrivo/*

[3] *"A Comprehensive Review on Wireless Capacitive Power Transfer Technology: Fundamentals and Applications"*

IEEEXPLORE.IEEE.ORG

[4] *"30 W Capacitive Wireless Power Transfer System with 5.8 pF Coupling Capacitance"*

IEEEXPLORE.IEEE.ORG

[5] *https://elettricomagazine.it/emobility/ricarica-elettrica-wireless-auto-elettrica-pieno-senza-fili/*

[6] *Wireless Power Transfer—A Review*

Kalina Detka and Krzysztof Górecki

[7] *C95.1-2005 - IEEE Standard for Safety Levels with Respect to Human Exposure to Radio Frequency Electromagnetic Fields, 3 kHz to 300 GHz*

[8] *Modern Trends in Inductive Power Transfer for Transportation Applications*

Publisher: IEEE

[9] *Design issues of a core-less transformer for a contact-less application*

Publisher: IEEE

[10] *https://www.sciencedirect.com/topics/engineering/full-bridge-inverter*

[11] *Wide Band Gap Devices and Their Application in Power Electronics*

[12] *A Review on the Recent Development of Capacitive*

Wireless Power Transfer Technology.

Fei Lu Hua Zang and Chris Mi

[13] *https://epc-co.com/epc/products/evaluation-boards/epc9039*

Appendix A

Matlab Code

```matlab
clear all
close all
clc

format shortEng

% Transmitted Power
Po = 10;
% Output Voltage load side
Vo = 5;
% Equivalent resistance on the rectifier side
RL_DC = Vo^2/Po
% Current in the equivalent resistance
Io = Vo/RL_DC;
% Charger side voltage
V_in=5.5;
% Distance between the plates
d=1e-3;

% Calculating the coupling capacity with 5x5 cm plate dimensions
l=5e-2;
% Cm sizing with correction factor
Cm = 0.5*(8.875e-12*l^2/d*(1+2.34*(d/l)^0.891))
% Determination of resonant capacity
C1_aux=linspace(0.6e-9,4e-9,100);
% Working frequency
fsw_aux= 1e6;
```

```matlab
out_3 = [];
out_4 = [];
out_5 = [];
out_6 = [];
out_7 = [];
% Circuit parameter calculation
for m=1:length(fsw_aux)
    fsw = fsw_aux(m)
    omega=2*pi*fsw;
    out_1 = [];
    out_2 = [];
    aux_5 = [];
    aux_6 = [];
    aux_7 = [];


    for k=1:length(C1_aux)
        C1=C1_aux(k);
        C2=C1;
        R=0.1;
        R_c=1e-3;
        R1=R;
        R2=R;
% Calculate the equivalent resistance on the rectifier side
        R_ac=8*RL_DC/(pi^2)
% Calculating inductances in a compensation circuit

        L1 = 1/(omega^2*C1)
        L2 = L1;
```

```matlab
% Capacitive reactance calculation
        Zc2 = -i/omega/C2;
        Zc1 = -i/omega/C1;
        Zcm = -i/omega/Cm;
% Inductive reactance calculation
        Zl1=omega*i*L1;
        Zl2=omega*i*L2;
% Circuit impedance calculation
        Z_A=R2+R_ac+Zl2;
        Z_B=(Z_A*Zc2)/(Z_A+Zc2);
        Z_D=Zcm+Z_B;
        Z_E=(Zc1*Z_D)/(Zc1+Z_D);
        Z_eq1=R1+Zl1+Z_E;

        R_eq=real(Z_eq1);
        X_eq=imag(Z_eq1);
% Calculation of circuit currents
        I_in=V_in/Z_eq1;
        I_c=I_in*Zc1/(Zc1+Z_D);
        I_cp=I_in*Z_D/(Zc1+Z_D);
        I_l=I_c*Zc2/(Zc2+Z_A);

        V_l=R_ac*I_l;

        out_1(end+1)=abs(V_l)/Vo;
        out_2(end+1)=abs(Zl1*I_in)*sqrt(2);
        aux_5(end+1)=abs(Zc1*I_cp)*sqrt(2)
        aux_6(end+1)=abs(0.5*Zcm*I_c)*sqrt(2)
        aux_7(end+1)=L1;

    end
```

```matlab
figure
    hold on
    yyaxis left
    plot(C1_aux,out_1,'b*')
    yyaxis right
    plot(C1_aux,out_2,'r*')
    ylim([0,3000])

    [a,b]=min(out_2)
    C1_aux(b)
    a
    out_3(end+1) = C1_aux(b);
    out_4(end+1) = a;
    out_5(end+1) = aux_5(b);
    out_6(end+1) = aux_6(b);
    out_7(end+1) = aux_7(b)

end
figure
hold on
scatter(fsw_aux/1e6,out_3/1e-12,100,out_4,'filled')
cb = colorbar;
colormap turbo
axis square
xlabel('f_{sw} (MHz)')
ylabel('C_{1} (pF)')
ylabel(cb, 'Voltage stress on L_1, peak value (V)')
title('5 cm x 5 cm plates')
```